Universität Rostock Traditio et Innovatio

Katalysis LIKAT Leibniz-Institut für Katalyse e.V.

CO_2 capture using Amino Acid-based ionic liquids and subsequent hydrogenation to Formate and Methanol

Dissertation

zur Erlangung des akademischen Grades

Doctor rerum naturalium (Dr. rer. nat.)

der Mathematisch-Naturwissenschaftlichen Fakultät

der Universität Rostock

vorgelegt von

Ayeshe Moazezbarabadi

Geboren am 04.02.1991 im Iran

Rostock, den 12.11.2025

https://doi.org/10.18453/rosdok_id00005926

Die vorliegende Arbeit entstand in der Zeit von Mai 2021 bis November 2025 am Leibniz-Institut für Katalyse e.V. unter der Betreuung von Prof. Dr. Matthias Beller.

Gutachter 1: Prof. Matthias Beller, Leibniz-Institut für Katalyse

Gutachter 2: Prof. Martin Nielsen, Technical University of Denmark

Datum der Einreichung: 11/2025

Datum der Verteidigung: 04/2026

Erklärung

Hiermit versichere ich an Eides statt, dass ich die vorliegende Arbeit selbständig angefertigt und ohne fremde Hilfe verfasst habe. Dazu habe ich keine außer den von mir angegebenen Hilfsmitteln und Quellen verwendet. Die aus den benutzten Werken inhaltlich und wörtlich entnommenen Stellen sind als solche kenntlich gemacht.

_____

Ayeshe Moazezbarabadi

Rostock, den 12.11.2025

Acknowledgments

I would like to begin by expressing my heartfelt gratitude to Professor Matthias Beller for giving me the opportunity to work on this project and for his valuable guidance throughout my PhD. His support and feedback have been important in shaping this research. I am incredibly fortunate to have been part of your group, where I learned not only about the science but also about the passion and curiosity that drive great research.

A special thanks to Dr. Henrik Junge for his unwavering support, mentorship, and encouragement over the past three years. Your thoughtful feedback, insightful suggestions, and your ability to create an inclusive and collegial atmosphere within the group have made a significant impact on both my scientific and personal development. I am truly grateful for your patience and guidance throughout this journey.

I would also like to acknowledge the Analytical Department for their support with the analytical techniques required for my research. Their help in providing reliable data and assisting with instrumentation was essential for the success of this project.

I also want to express my appreciation to Hendrik Kempf, Hilario Diego Huerta Zerón, Dr. Duo Wei, Dr. Elisabetta Alberico, Dr. Yong Peng, Dr. Guangxin Xue, Carolin Stein, and Anja Kammer. You have all played an important role in my personal and professional development, and I am thankful for the numerous insightful discussions and collaborations we've had over the years.

Finally, to my husband, Mohammad Asadpour, my deepest thanks for your love, support, and understanding. Thank you for your patience, your unwavering belief in me, and for being a constant source of strength. I truly could not have done this without you.

Abstract – Zusammenfassung

This thesis presents an exploration of amino acid-based ionic liquids (AAILs) as innovative and sustainable alternatives to traditional amine-based systems for carbon dioxide (CO_2) capture and conversion, addressing the urgent need for climate change mitigation and carbon neutrality. As CO_2 levels continue to rise, driving global warming, the development of technologies that integrate CO_2 capture, even from dilute sources such as air, with its conversion into valuable chemicals is essential for achieving a circular carbon economy. Unlike conventional amines, which are volatile, energy-intensive, and environmentally problematic, amino acid-based ILs offer unique advantages such as negligible volatility, high thermal stability, and tunable properties, making them ideal candidates for CO_2 capture and catalytic conversion processes.

In the first part of this thesis, a series of alkyl ammonium and imidazolium-based ILs, incorporating various amino acids as counter ions, were synthesized and evaluated for their CO_2 capture capacity. Among these, tetrabutylammonium L-argininate ([TBA][Arg]) demonstrated exceptional CO_2 absorption, with a capacity of up to 1.94 mmol CO_2 per mmol of absorbent. The captured CO_2 was then efficiently hydrogenated to formate using the commercially available Ru-MACHO-BH catalyst, achieving a turnover number (TON) of 959 under optimized conditions. The system exhibited excellent scalability and catalyst reusability, maintaining high activity over five consecutive runs with an overall TON of 12,741. Importantly, the system was also effective in capturing CO_2 directly from air, achieving a TON of 305 for formate production, demonstrating its potential for direct air capture (DAC) applications. These results highlight the potential of amino acid-based ILs as effective and sustainable alternatives to amine-based systems for CO_2 capture and conversion, even from low-concentration sources.

Building on these findings, the second part of the thesis focused on the hydrogenation of CO_2 to methanol, a valuable chemical feedstock and fuel. By modifying the reaction conditions, the combination of [TBA][Arg] with the Ru-MACHO-BH catalyst led to significant yields of methanol, with a TON of up to 700. Optimization of reaction parameters, including temperature, solvent, and CO_2/H_2 pressure, revealed that the [TBA][Arg] IL promotes an efficient hydrogenation pathway leading to methanol formation.

Overall, this thesis demonstrates the potential of amino acid-based ILs as sustainable alternatives to amines in CO_2 valorization, offering a green and efficient approach to mitigating carbon emissions while producing valuable chemicals. The ability to capture CO_2 from air and convert it into useful products further enhances the system's relevance for addressing climate change. The findings contribute to the development

of integrated CO_2 capture and conversion technologies, paving the way for a circular carbon economy and advancing efforts toward a more sustainable future.

Diese Dissertation beinhaltet Untersuchungen von aminosäurebasierten ionischen Flüssigkeiten (AAILs) als innovative und nachhaltige Alternativen zu traditionellen aminbasierten Systemen zur Kohlendioxidabscheidung und -umwandlung, wobei die dringende Notwendigkeit zur Minderung des Klimawandels und zur Erreichung der Kohlenstoffneutralität adressiert wird. Da der CO_2-Gehalt in der Atmosphäre weiterhin steigt und die globale Erwärmung vorantreibt, ist die Entwicklung von Technologien, die die CO_2-Abscheidung, insbesondere auch aus verdünnten Quellen wie der Luft, mit der Umwandlung in wertvolle Chemikalien verbinden, von entscheidender Bedeutung für die Erreichung einer Kohlenstoff-Kreislaufwirtschaft. Im Gegensatz zu herkömmlichen Aminen, die flüchtig, energieintensiv und umweltproblematisch sind, bieten aminosäurebasierte ILs einzigartige Vorteile wie nahezu keine Flüchtigkeit, hohe thermische Stabilität und anpassbare Eigenschaften, die sie zu idealen Kandidaten für CO_2-Abscheidungs- und katalytische Umwandlungsprozesse machen.

Im ersten Teil dieser Arbeit wurden eine Reihe von alkylammonium- und imidazolium-basierten ILs, die verschiedene Aminosäuren als Gegenionen enthalten, synthetisiert und auf ihre CO_2-Bindungskapazität hin untersucht. Unter diesen zeigte Tetrabutylammonium L-Argininat ([TBA][Arg]) eine außergewöhnlich hohe CO_2-Absorption mit einer Kapazität von bis zu 1,94 mmol CO_2 pro mmol Absorber. Das gebundene CO_2 wurde dann effizient zu Formiat hydriert, wobei der kommerziell verfügbare Ru-MACHO-BH-Katalysator verwendet wurde und eine Umsatzzahl (TON) von 959 unter optimierten Bedingungen erreicht wurde. Das System zeigte ausgezeichnete Skalierbarkeit und Katalysatorwiederverwendbarkeit und behielt eine hohe Aktivität über fünf aufeinanderfolgende Zyklen hinweg bei, mit einer Gesamt-TON von 12.741. Besonders wichtig war, dass das System auch effektiv CO_2 direkt aus der Luft absorbierte und eine TON von 305 für die Formiatproduktion erzielte, was sein Potenzial für Anwendungen in der direkten Absorption von CO_2 aus der Luft (Direct Air Capture, DAC) unterstreicht. Diese Ergebnisse verdeutlichen das Potenzial von aminosäurebasierten ILs als effektive und nachhaltige Alternativen zu aminbasierten Systemen für die CO_2-Abscheidung und -Umwandlung, selbst aus Quellen mit niedriger Konzentration.

Aufbauend auf diesen Ergebnissen konzentrierte sich der zweite Teil der Forschung auf die Hydrierung von CO_2 zu Methanol, einem wertvollen chemischen Rohstoff und Brennstoff. Durch Modifikation der Reaktionsbedingungen wurden mit der Kombination von TBA-Arg mit dem Ru-MACHO-BH-Katalysator signifikante Methanol-Ausbeuten erzielt, mit einer TON von bis zu 700. Eine systematische Optimierung der Reaktionsparameter, einschließlich Temperatur, Lösungsmittel und CO_2/H_2-Druck,

zeigte, dass das [TBA][Arg] IL einen effizienten Hydrierungsweg fördert, der zur Methanolbildung führt.

Insgesamt zeigt diese Dissertation das Potenzial von aminosäurebasierten ILs als nachhaltige Alternative zu Aminen in der CO_2-Wertschöpfung und bietet einen grünen und effizienten Ansatz zur Minderung von Kohlenstoffemissionen bei gleichzeitigem Erzeugen wertvoller Chemikalien. Die Fähigkeit, CO_2 aus der Luft zu absorbieren und in nützliche Produkte umzuwandeln, erhöht die Relevanz des Systems zur Bekämpfung des Klimawandels. Die Ergebnisse tragen zur Entwicklung integrierter CO_2-Abscheidungs- und Umwandlungstechnologien bei und ebnen den Weg für eine Kohlenstoff-Kreislaufwirtschaft, wodurch die Bemühungen um eine nachhaltigere Zukunft vorangetrieben werden.

List of abbreviations

AAILs	Amino acid-based ionic liquids	DBU	1,8-diazabicyclo(5.4.0)undec-7-ene
CCS	Carbon capture and storage	DABCO	1,4-diazabicyclo[2.2.2]octane
CCU	Carbon capture and utilization	PEHA	Pentaethylenehexamine
DAC	Direct air capture	BMIM	Butyl methyl imidazolium
FA	Formic acid	MIBC	4-Methyl-2-pentanol
$HCOO^-$	Formate	MF	Methyl formate
Lys	Lysine	CPME	Cyclopentyl methyl ether
HCOOH	Formic Acid	THF	Tetrahydrofuran
CO_2	Carbon dioxide	$NaOCH_3$	Sodium methoxide
$NaHCO_3$	Sodium bicarbonate	$ScCO_2$	Supercritical CO_2
NH_3	Ammonia	PEI	Polyethyleneimine
ppm	Parts per million	DME	Dimethyl ether
MeCN	Acetonitrile	DMFCs	Direct methanol fuel cells
MeOH	Methanol	His	Histidine
DMF	*N,N*-dimethylformamide	CHO	choline
CO	Carbon monoxide	MTG	Methanol-to-gasoline
Pro	Proline	PMDTA	Pentamethyldiethylenetriamine
Gly	Glycine	MTP	Methanol-to-propylene
TEOA	Triethanolamine	AA	Amino acid
MEA	Monoethanolamine	DEA	Diethanolamine
Arg	Arginine	MDEA	N-methyl diethanolamine
TEA	Triethylamine	ASN	Asparagine
TOF	Turnover frequency	GLN	Glutamine
TON	Turnover number	GLU	Glutamic acid
WGSR	Water-gas shift reaction	TMG	Tetramethylguanidine
Ala	Alanine	TBA	Tetrabutylammonium
ILs	Ionic liquids	Leu	Leucine
ASU	6-azonia-spiro[5.5]undecane	TMA	Tetramethylammonium
MTO	Methanol-to-olefins	TBP	Tetrabuthylphosphonium
BTMA	Benzyltrimethylammonium		

Contents

1. Introduction 1
   1.1. CO_2 challenges and circular economy 1
   1.2. Carbon Capture and Utilization (CCU): Towards carbon neutrality 3
   1.3. CO_2 Capture Technologies and Absorbents 4
   1.4. Integrated CO_2 capture and catalytic hydrogenation 6
   1.5. Formic Acid and formate: 7
      1.5.1. Properties and applications 7
      1.5.2. Current production 9
      1.5.3. CO_2 hydrogenation to FA/ formate 10
      1.5.4. Integrated CO_2 capture and hydrogenation to formate: 16
   1.6. Methanol: A Fundamental Chemical 24
      1.6.1. Background: Properties and applications of methanol 24
      1.6.2. Methanol production from syn gas 24
2. Objectives 31
3. Experimental part 32
   3.1. Materials and methods 32
   3.2. Synthesis of Ionic Liquids 33
      3.2.1. Tetrabutylammonium L-Arginine ([TBA][Arg]) 33
      3.2.2. Benzyltrimethylammonium L-arginine ([BTMA][Arg]) 33
      3.2.3. *N*,*N*,*N*-trimethyl-1-adamantylammonium L-arginine ([TMAA][Arg]) 34
      3.2.4. 6-Azonia-spiro[5.5]undecane Hydroxide ([ASU][OH]) 35
      3.2.5. 6-azonia-spiro[5.5]undecane L-Arginine ([ASU][Arg]) 36
      3.2.6. Tetrabutylammonium L-norleucine ([TBA][Nor]) 36
      3.2.7. Tetrabutylammonium 4-guanidinobutirrate ([TBA][GB]) 37
   3.3. CO_2 Capture experiments 37
      3.3.1. CO_2 capture for formate production (aqueous system) 37
      3.3.2. CO_2 capture procedure for methanol production (organic media) 38
   3.4. Catalytic Hydrogenation of CO_2 to Formate 39
      3.4.1. Procedure for the hydrogenation of gaseous CO_2 39
      3.4.2. Procedure for the hydrogenation of captured CO_2 39
   3.5. Catalytic Hydrogenation of CO_2 to Methanol 40
      3.5.1. Procedure for the hydrogenation of gaseous CO_2 40
      3.5.2. Procedure for the hydrogenation of captured CO_2 40
      3.5.3. Post-Reaction Analysis 40
   3.6. Synthesis of reaction intermediates: 41
4. Results and Discussion 44

4.1. CO_2 capture using amino acid based-Ionic liquids and subsequent catalytic hydrogenation to formate ... 44
4.1.1. Evaluation of ionic liquids for CO_2 capture ... **44**
4.1.2. Hydrogenation of gaseous CO_2 to formate catalyzed by Ru-MACHO-BH **48**
4.1.3. Integrated CO_2 capture and subsequent conversion to formate ... **53**
4.1.4. Summary ... **55**
4.2. CO_2 hydrogenation to methanol ... 56
4.2.1. Screening of Amino Acid–Based Ionic Liquids ... **56**
4.2.2. Effect of Reaction Parameters ... **61**
4.2.3. CO_2 capture from air and subsequent hydrogenation to methanol ... **71**
4.2.4. Structural and Functional Characteristics of [TBA][Arg] in CO_2 Hydrogenation to Methanol ... **72**
4.2.5. Summary ... **75**
5. Outlook and final remarks ... 77
6. References ... 79
7. Appendix ... I
8. Publications ... XXIV
9. Curriculum Vitae ... XXV

1. Introduction

1.1. CO_2 challenges and circular economy

Carbon dioxide (CO_2) is one of the most critical greenhouse gases driving global warming and climate change. Its contribution to the climate crisis stems from its ability to trap heat in the Earth's atmosphere through the greenhouse effect. In this process, CO_2 absorbs infrared radiation emitted by the Earth's surface, preventing it from escaping into space and thereby warming the planet.[1, 2] Historically, CO_2 concentrations were relatively stable, hovering around 280 parts per million (ppm) during pre-industrial times.[3] However, since the onset of industrialization, human activities—especially the burning of fossil fuels—have caused a dramatic increase in CO_2 levels, reaching 422.8 ppm in 2024[4] (**Figure 1**). This surge is a primary driver of the current climate crisis.

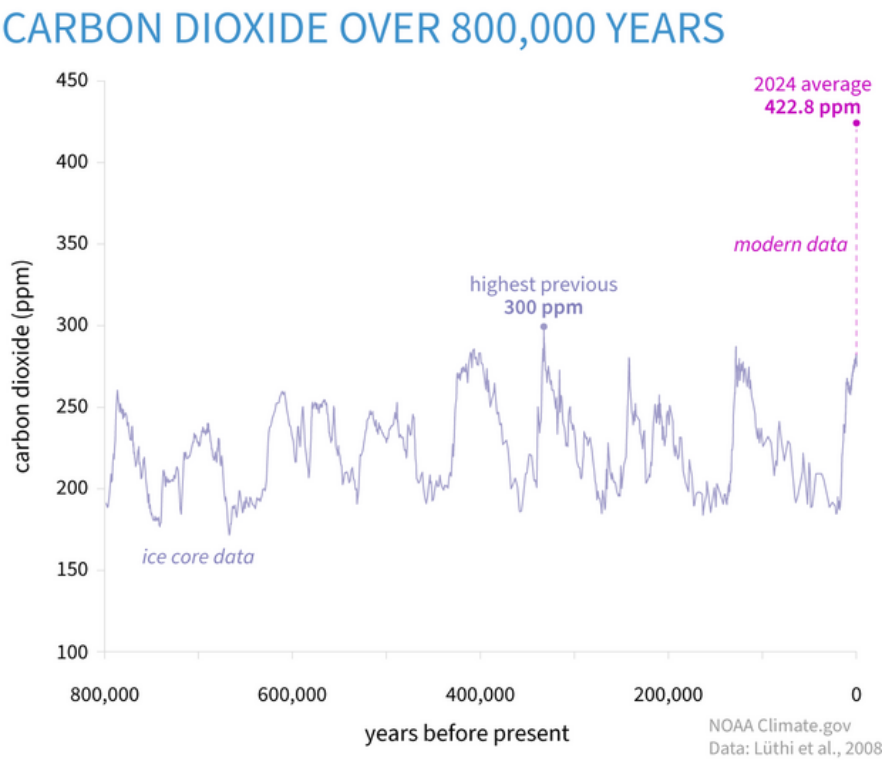


Figure1. Atmospheric CO_2 in parts per million (ppm) for the past 800,000 years. [4]

The majority of global CO_2 emissions originate from the energy sector. In 2023, fossil fuels - namely coal, oil, and natural gas - continued to be the primary energy sources worldwide, making up around 82% of total energy consumption.[5, 6] This heavy reliance

on carbon-intensive energy is central to the rise in CO_2 concentrations. If global energy demand continues to grow rapidly and is met predominantly with fossil fuels, annual human-induced CO_2 emissions could exceed 75 billion tons by the end of the century. This could raise atmospheric CO_2 concentrations to 800 parts per million or higher - levels not observed on Earth for nearly 50 million years.[7]

Beyond energy production, land-use changes such as deforestation and soil degradation also release significant amounts of CO_2 stored in vegetation and soils.[8, 9] Additionally, industrial processes like cement production contribute to the problem. The heating of limestone to produce lime - a key component of cement - releases CO_2 as a byproduct, further adding to the atmospheric burden.[10]

The consequences of elevated CO_2 levels are profound and far-reaching. As a potent greenhouse gas, CO_2 traps heat in the atmosphere, leading to a rise in global temperatures. This warming fuels more extreme and frequent weather events, including heatwaves, hurricanes, wildfires, and droughts, all of which have devastating economic and social impacts.[11, 12] For example, warmer ocean temperatures are intensifying tropical storms, while shifting rainfall patterns are threatening global food security by disrupting agricultural production. Rising temperatures also contribute to the melting of glaciers and ice caps, which is causing sea levels to rise. This poses an existential threat to low-lying coastal areas and island nations, where millions of people live in vulnerable conditions.[13]

Elevated CO_2 concentrations are also causing ocean acidification. When CO_2 is absorbed by seawater, it reacts to form carbonic acid, which lowers the pH of oceans. This acidification has severe implications for marine ecosystems, particularly for organisms that rely on calcium carbonate to build shells and skeletons, such as corals and shellfish.[14]

Mitigating the impact of increasing CO_2 levels has become a key focus of international climate agreements, including the 2015 Paris Agreement. Achieving the target of limiting global warming to 1.5°C above pre-industrial levels requires a significant reduction in CO_2 emissions.[15] To achieve this, a shift toward renewable energy - including wind, solar, and hydropower - is crucial, alongside the adoption of carbon capture and storage (CCS) technologies to actively remove CO_2 from the atmosphere.[16, 17] Furthermore, protecting and restoration of forests, which act as

carbon sinks, is crucial for mitigating CO_2 emissions.[18] In addition to reducing emissions, enhancing the efficiency of energy use and adopting sustainable land-use practices are essential strategies for limiting the rise of CO_2 concentrations. The global transition to a circular economy, which aims to minimize waste and resource consumption through recycling, reuse, and sustainable production, can significantly contribute to lowering CO_2 emissions by reducing reliance on resource extraction and energy-intensive manufacturing.[19, 20] Within the framework of CO_2 emissions, the circular economy aims to establish systems that lower carbon footprints, enable carbon recycling, and transform waste CO_2 into useful products. A fundamental element of this strategy is carbon capture and utilization (CCU).[21, 22]

1.2. Carbon Capture and Utilization (CCU): Towards carbon neutrality

CCU offers an innovative approach tackling climate change by converting CO_2, either captured from industrial emissions or directly from the atmosphere through technologies such as Direct Air Capture (DAC),into valuable products such as fuels, chemicals, and plastics.[23, 24] In contrast to CCS, which stores CO_2 underground, CCU repurposes it as a resource, establishing a sustainable, closed-loop system that contributes to carbon neutrality, where CO_2 emissions are offset by the amount captured and utilized.[25, 26]

Therewith, CO_2 is going to become an attractive renewable raw material due to its abundance, non-toxic nature, and low cost. It functions as a valuable alternative to hazardous industrial chemicals, such as phosgene, providing a safer and more sustainable option for chemical production.[27] Additionally, utilization of CO_2 as a feedstock for the production of valuable chemicals and energy carriers enables an effective circular economic model. The energy required for CO_2 conversion can be derived from renewable sources, such as wind or solar power, contributing to an overall carbon-neutral cycle and facilitating successful renewable energy storage.[28, 29]

While CCS focuses on long-term storage to prevent atmospheric emissions, CCU can be more cost-effective by avoiding energy-intensive steps such as CO_2 compression and desorption. Instead, it converts captured CO_2 directly into useful products, making the process more efficient and financially sustainable.[30] This approach is essential for transitioning industrial systems toward carbon neutrality by substituting fossil-derived

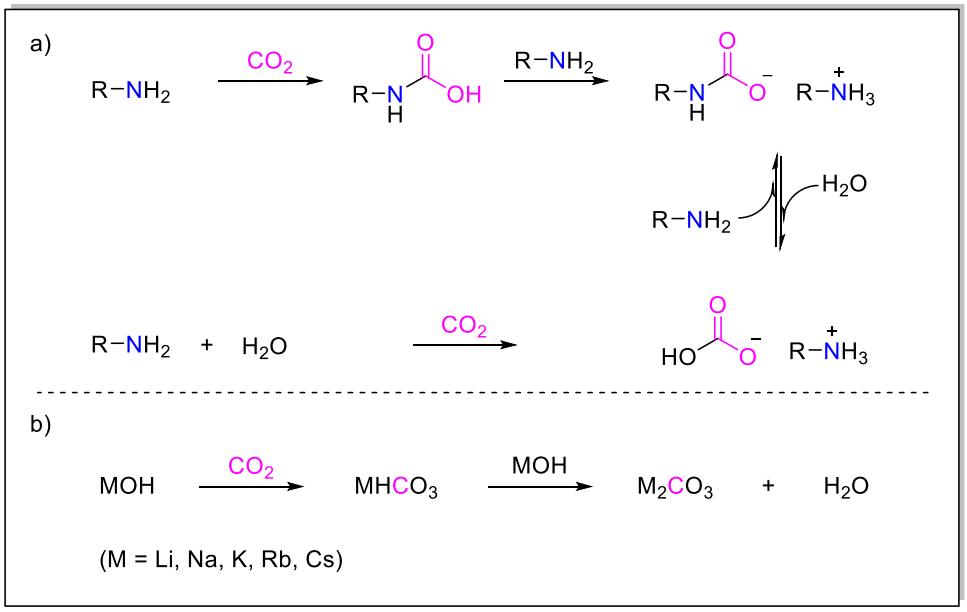
materials with CO_2-based alternatives, thereby helping to offset emissions and advance climate goals.[31, 32]

The challenges faced by CCS, such as high capital and operational expenses, are well documented. For example, power plants using CCS may consume 10–40% of their energy output solely for CO_2 capture and compression, which limits large-scale implementation.[33, 34] In contrast, CCU offers the dual advantage of mitigating CO_2 emissions while producing valuable, carbon-neutral products. A notable example is the George Olah Renewable CO_2-to-Methanol Plant in Iceland, which uses locally sourced renewable energy to convert CO_2 into methanol, operating at an energy requirement of 9.5 MWh per ton and achieving an overall efficiency of 60%.[35]

1.3. CO_2 Capture Technologies and Absorbents

A variety of CO_2 capture technologies are currently employed, including physical adsorption, chemical absorption, membrane separation, and cryogenic separation.[36, 37] Among these, chemical absorption, particularly with alkanolamines like monoethanolamine (MEA), is the most common and effective method, particularly in the context of power generation facilities.[38] Amine-based absorbents chemically react with CO_2 to form ammonium carbamate and bicarbonate species (**Scheme 1a**). Despite their effectiveness, these systems are associated with high energy demands and limited CO_2 absorption capacities, thereby motivating the development of alternative approaches. The energy required for solvent regeneration (i.e., CO_2 desorption) ranges from 2.4 to 4.2 GJ per ton of CO_2, representing approximately 60–70% of the total capital investment in the capture process.[39, 40]

Alkali hydroxides, such as sodium hydroxide (NaOH) and potassium hydroxide (KOH), have also been investigated for CO_2 capture. These strong bases react with CO_2 to form stable carbonates (**scheme 1b**). The resulting carbonates can be regenerated via thermal or electrochemical methods, enabling the release of CO_2 and the recycling of the hydroxide absorbent. While effective, alkali hydroxide-based systems demand substantial energy input for regeneration, underscoring the need for the development of more energy efficient alternatives.[41, 42]



Scheme 1. CO_2 capture with a) conventional amines, b) alkali hydroxides.

Ionic liquids (ILs) have emerged as promising alternatives, providing enhanced energy efficiency and selectivity in CO_2 absorption.[43-44]

ILs have negligible vapor pressure and are thermally stable, making them "green solvents."[45] CO_2 absorption in non-functionalized ionic liquids occurs via physical absorption through weak Lewis acid–base interactions. Although the absorption rate and capacity are limited, these systems offer the advantage of low energy demand during regeneration. The physicochemical properties and CO_2 absorption capacity of ILs can be tailored by modifying the structure of their cations and/or anions.[46-53]Given that conventional amine solvents react strongly with CO_2, research on amine-functionalized ILs seeks to combine both physisorption and chemisorption mechanisms to enhance CO_2 solubility while maintaining high thermal stability.[53-57] In such systems, the incorporation of amine functionalities enables the same CO_2 chemical absorption mechanism observed in amine-based solvents, proceeding via the formation of carbamate and bicarbonate species. Bates et al. demonstrated that introducing an amine functional group to the imidazolium cation significantly enhanced CO_2 absorption.[58]

Within the class of functionalized ionic liquids, amino acid–based ionic liquids (AAILs) stand out due to their unique ability to combine the tunable physicochemical properties of ILs with the reactive functionality of amino acids (AAs). AAs are biodegradable, have negligible volatility, resist oxidative degradation, and exhibit low environmental impact.

[59, 60] Due to the ultra-dilute concentration of CO_2 in ambient air (approximately 400 ppm), direct air capture (DAC) technologies require absorbents with strong binding affinities—characterized by sharp uptake at low partial pressures—and high CO_2/N_2 selectivity.[61] This underscores the need for advanced materials specifically engineered for efficient atmospheric CO_2 capture, thereby enabling a viable and scalable DAC process. In this context, AAILs are particularly well-suited for DAC applications, owing to their strong interactions with CO_2 and environmentally benign characteristics.

To demonstrate the synergistic advantages of combining ILs structures with amino acid functionality, Li and co-workers (2015) investigated the CO_2 capture performance of an aqueous amino acid–based ionic liquid featuring hydroxyethyl methyl imidazole as the hydrophilic cation and Glycine [GLY) as the anion ([C_2OHmim][GLY]).[62] For comparison, aqueous solutions of monoethanolamine (MEA) and sodium glycinate at the same concentration (0.4 M) were examined. The measured CO_2 loadings were 0.457, 0.26, and 0.575 $mol_{CO_2}/mol_{Absorbent}$ for MEA, sodium glycinate, and [C_2OHmim][GLY], respectively, clearly demonstrating the superior absorption capacity of the AAIL. Furthermore, [C_2OHmim][GLY] exhibited higher oxidative stability during multiple regeneration cycles under high O_2 concentrations, highlighting its potential to overcome the drawbacks of conventional amine-based solvents.

1.4. Integrated CO_2 capture and catalytic hydrogenation

An innovative strategy for sustainable CO_2 utilization involves integrating CO_2 capture with *in situ* hydrogenation to produce energy-relevant chemicals such as formic acid (HCOOH), methanol (CH_3OH), amides, and other methylated compounds (**Figure 2**). This integrated approach contributes to closing the carbon cycle and supports the transition toward carbon neutrality.

A key advantage of this approach lies in its ability to capture CO_2 from low-concentration sources, such as ambient air, and convert it into value-added products. Green hydrogen (H_2) —generated from renewable energy sources via processes such as water electrolysis or photocatalysis—offers a markedly more sustainable alternative to conventional CO_2 fixation agents, including epoxides and alkenes.[63-65].

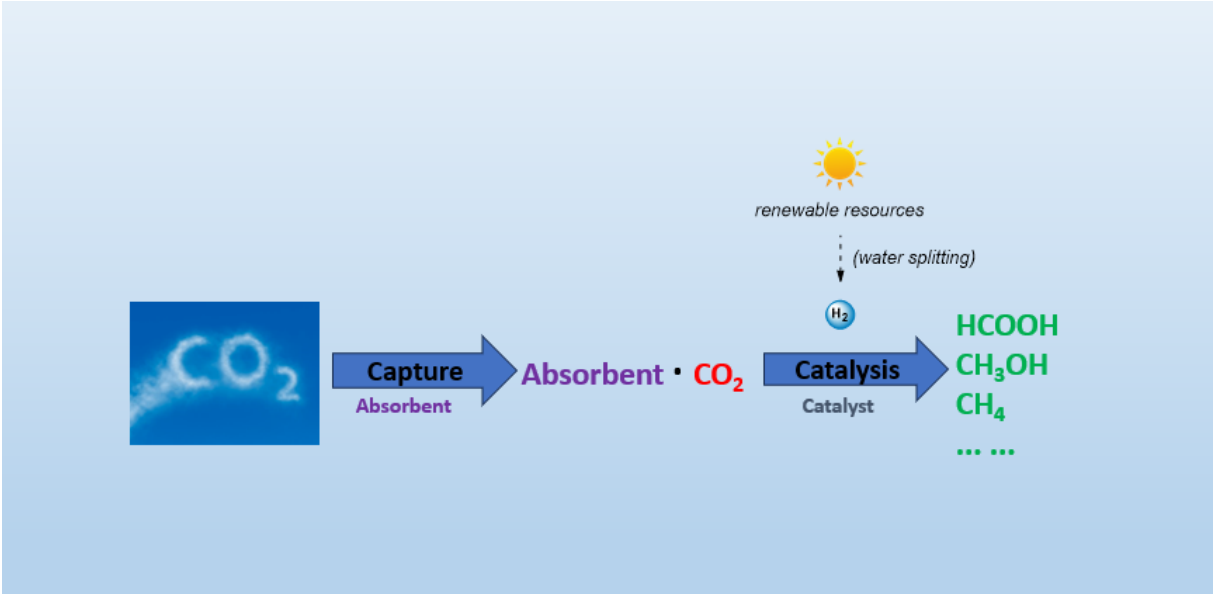


Figure 2. Concept of CO_2 capture and *in-situ* hydrogenation.

1.5. Formic Acid and formate:

1.5.1. Properties and applications

Formic acid (FA), the simplest carboxylic acid, is a colorless and highly corrosive liquid with a sharp, pungent odor at room temperature. It exhibits moderate acidity, as reflected by its pKa value of 3.75, and is volatile under standard conditions, with a melting point of 8.3 °C and a boiling point of 100.8 °C.[66-68] Despite being biodegradable and demonstrating low acute toxicity, FA presents considerable hazards due to its corrosive properties, particularly to the skin and mucous membranes.

Deprotonation of its carboxyl group yields formate ($HCOO^-$), the conjugate base of FA, which can participate in reactions with metals or organic groups to form salts and esters. Given its acidic and reducing capabilities, FA is extensively employed in various industrial processes. Its predominant application, particularly in Europe, is in silage preservation, where it facilitates lactic acid fermentation while suppressing butyric acid production.[69, 70] Global demand for this use continues to grow steadily. Furthermore, FA serves a critical function in emerging industrial applications, including steel pickling and wood pulping, where its acidic properties are indispensable.[70]

In leather and textile processing, FA is favored for its clean evaporation without residual buildup.[71] Within the rubber industry, it is commonly utilized as a coagulant. Roughly

10% of global formic acid production is directed toward the synthesis of organic compounds, including pharmaceutical intermediates, agrochemicals, and the artificial sweetener aspartame.[72] Moreover, it plays a significant role in organic synthesis, contributing to reactions such as Schiff base reduction, esterification, and formylation. It also functions as a carbon monoxide donor in the Koch reaction for carboxylic acid synthesis.[73]

Formate salts, derived from FA, are utilized in a wide range of applications across various industries. Aluminum and sodium formates are employed in the production of leather and textiles, while sodium and potassium formates are critical for deicing operations, particularly in airport settings.[74-76] Furthermore, sodium formate is used in the synthesis of sodium dithionite, electroplating processes, and photographic fixing baths.[69] Calcium formate serves as an additive in concrete production, and ammonium formate is employed in silage preservation and in chemical transformations such as the Leuckart reaction and transfer hydrogenation.[77]

FA has gained attention as a potential energy carrier, particularly in direct formic acid fuel cells (DFAFCs), which could power portable electronic devices.[78] It is also being explored as a hydrogen carrier, a concept that was first introduced in 1978.[79] Organometallic catalysts enable the hydrogenation of CO_2 to form FA/formate, which can then be reversed to release hydrogen and CO_2 on demand. This process avoids the generation of toxic carbon monoxide, making it a safer alternative for fuel cell technologies.[80]

Despite its relatively low hydrogen storage capacity (4.4 wt%), FA offers an advantage in its liquid state at room temperature, which simplifies transportation, storage, and refueling.[81] However, its corrosive properties necessitate the use of specialized storage materials, such as steel alloys and durable plastics like PTFE and PVDF.[70] The melting point of 8.3°C plays a crucial role in ensuring efficient transportation and storage under standard conditions.[70]

When concentrated, formic acid can decompose into carbon monoxide (CO) and water through decarbonylation/dehydration, with the rate of decomposition influenced by concentration and temperature.[70] Proper storage and ventilation are essential to prevent degradation. Notably, this decomposition reaction also opens up the possibility

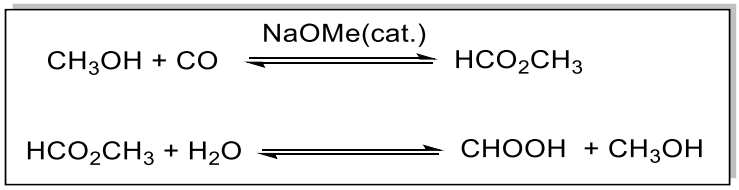
of using formic acid as a safer alternative for CO storage and transport. With a high CO_2 storage capacity (60.8 wt%), formic acid presents a less toxic method for storing and transporting carbon monoxide.[82] The decarbonylation process is catalyzed by substances such as mineral acids, zeolites, and aluminum oxide. Together with CO_2 hydrogenation to FA, the decarbonylation step forms an indirect reversed water-gas shift (rWGS) reaction, offering a safer and more manageable method for CO storage and transport.[70, 82]

1.5.2. Current production

Today, industrial production of FA involves several key methods, including:

1. Hydrolysis of methyl formate
2. Oxidation of hydrocarbons
3. Hydrolysis of formamide
4. Production of free FA from formates

The most commonly employed method for the industrial production of FA is the indirect carbonylation of methanol with CO. In this process, methanol reacts with CO in the presence of sodium methoxide ($NaOCH_3$) to generate methyl formate, which is subsequently hydrolyzed with excess water to yield FA and regenerate methanol (**Scheme 2**).[83, 84]



Scheme 2. FA production from CO and water via methyl formate

The global FA market reached approximately 750 kilotons in 2022, with BASF recognized as the leading producer worldwide.[85]

Environmental considerations play a critical role in ensuring the sustainability of FA acid production. Conventional methods that rely on CO are associated with substantial CO_2 emissions, estimated at approximately 3,076 kg of CO_2 per ton of FA produced. In contrast, hydrogenation of CO_2 represents a more environmentally benign

alternative, with the potential to reduce emissions to as little as 100 kg of CO_2 per ton.[86] This highlights the significant promise of CO_2-based production pathways in minimizing environmental impact and advancing greener manufacturing practices for FA.

1.5.3. CO_2 hydrogenation to FA/ formate

The hydrogenation of CO_2 to FA is considered a highly attractive process due to its 100% atom economy, wherein CO_2 reacts with hydrogen to produce FA without generating any by-products. This reaction is of considerable interest from both theoretical and practical standpoints, as it presents a sustainable strategy for CO_2 utilization. As a result, extensive research efforts have been directed toward the development of efficient catalytic systems to enable and optimize this transformation.

1.5.3.1. Thermodynamics, kinetics and mechanism of hydrogenation of CO_2 to FA and formate salts

Despite the potential of the direct hydrogenation of CO_2 to FA there exists major thermodynamic and kinetic challenges that require innovative solutions. Thermodynamic constraints are especially critical. The gas-phase reaction of CO_2 and H_2 to form FA is exothermic, but the process is strongly endergonic due to a substantial unfavorable entropic contribution.[87] This results in a positive Gibbs free energy change, as shown in Table 1, Eq. (1). The thermodynamic parameters highlight the challenges associated with achieving high yields under standard conditions.

Table 1. Thermodynamic data for the hydrogenation of CO_2 to FA.

	$\Delta H°$ (kJ mol^{-1})	$\Delta S°$ (J mol^{-1} K^{-1})	$\Delta G°$ (kJ mol^{-1})	Eq.
$CO_{2(g)} + H_{2(g)} \rightarrow HCOOH_{(l)}$	−31.2	−215	+32.9	(1)
$CO_{2(g)} + H_{2(g)} + NH_{3(aq)} \rightarrow HCO^-_{2(aq)} + NH^+_{4(aq)}$	−84.3	−250	−9.5	(2)
$CO_{2(aq)} + H_{2(aq)} + NH_{3(aq)} \rightarrow HCO^-_{2(aq)} + NH^+_{4(aq)}$	−59.8	−81	−35.4	(3)

To address these challenges, optimization strategies aim to reduce the entropy difference between reactants and products or to offset the entropic penalty through highly exothermic reactions. Critical factors influencing this process include the selection of base additives and solvents, both of which play essential roles in shifting the reaction equilibrium. For example, the introduction of a base such as ammonia

promotes the reaction by exothermically protonating ammonia with FA, thereby rendering the overall process thermodynamically favorable (Table 1, Eq. (2)).[87, 88]

Moreover, solvents affect both the thermodynamics and the reaction mechanism by solvating the reactants or disrupting the hydrogen-bonding network of FA. These interactions contribute to alleviating entropy penalties associated with the reaction (Table 1, Eq. (3)).[88] Polar solvents, in particular, can stabilize reaction intermediates within the catalytic cycle or intracting directly with metal catalysts, thereby enhancing catalytic activity.[89] To date, a variety of solvents—including organic solvents, ionic liquids, water, and supercritical carbon dioxide ($scCO_2$)—have been extensively investigated, each providing distinct advantages in enhancing reaction efficiency and addressing thermodynamic constraints.

In parallel to addressing thermodynamic barriers, developing effective catalysts is crucial for achieving efficient CO_2 hydrogenation. In the context of selectivity and catalyst designing, homogeneous catalysis can play pivotal roles. Homogeneously catalyzed reactions quite often operate under milder conditions resulting in better selectivity.

Additionally, experimental mechanistic understanding in solution may provide insight into choosing appropriate ligand-based complexes for the targeted task. For industrial applications, the focus is on developing efficient, easy-to-handle catalysts that are compatible with environmentally friendly solvents.

The reduction of CO_2 to FA/formate requires the insertion of the CO_2 molecule into a metal–hydride (M-H) bond. The corresponding mechanism is depicted in **Figure 3**, wherein CO_2 first coordinates to the metal center, followed by hydride transfer to the carbon atom via nucleophilic attack. In the case of coordinatively saturated metal complexes, the formation of a vacant coordination site—typically through the dissociation of an ancillary ligand—may be essential for enabling CO_2 coordination and subsequent insertion into the M–H bond. It is also noteworthy that an alternative mechanism has been proposed, involving direct nucleophilic attack by the hydride on CO_2 without prior coordination to the metal center. This pathway remains feasible even for coordinatively saturated complexe such as the Nozaki pyridine-based PNP-ligated iridium(III) trihydride .[90-93]

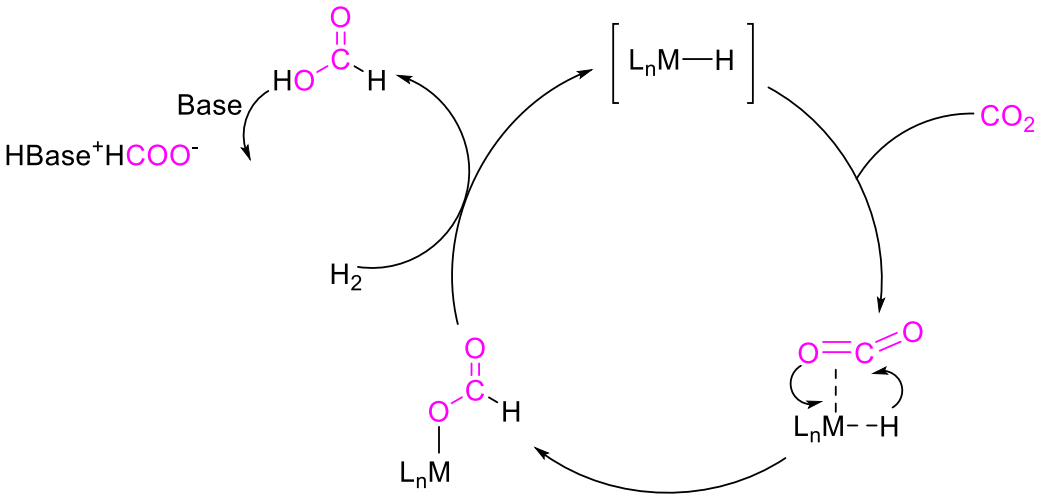


Figure 3. General pathway of CO_2 hydrogenation to FA via homogeneous catalysis. Reprint from ref.[94] with copyright permission.

1.5.3.2. State of the art of CO_2 hydrogenation to FA/formate

The groundbreaking study by Inoue et al. in 1976, which employed triphenylphosphine (PPh_3)-coordinated Pd, Fe, Co, Ni, Ru, Rh, and Ir complexes, pioneered the homogeneous catalytic hydrogenation of CO_2 to formic acid, establishing a new research direction in this field.[95] The reaction was carried out in benzene under 25 bar of CO_2 and 25 bar of H_2 at room temperature, in the presence of a small amount of water and an amine base, specifically triethylamine (NEt_3). Under these conditions, the catalyst $[RuH_2(PPh_3)_4]$ exhibited the highest activity, achieving a turnover number (TON) of 87 and a turnover frequency (TOF) of approximately 4.5 h^{-1} over a 20-hour reaction period.[96] Building upon this foundational work, extensive research efforts have investigated transition metal-based catalytic systems,, particularly utilizing iron,[97, 98] cobalt,[99-101] ruthenium,[102-104] iridium,[105-107] and rhodium complexes.[108] A major advancement was reported by Nozaki et al. in 2009, who developed Ir(III) complexes featuring alkylphosphine-based pincer ligands, which served as highly effective electron donors for the hydrogenation of CO_2. Notably, their PNP-pincer iridium complex, $[2,6\text{-}(PiPr_2)_2C_5H_3N]IrH_3$, achieved an exceptional TON of 3,500,000 and a TOF of up to 150,000 h^{-1} at 200 °C and 80 bar, in a H_2O/ tetrahydrofuran (THF) solvent system using KOH as the base. While these Ir(III) complexes demonstrated outstanding catalytic efficiency, it is important to note that such high performance was

obtained under highly dilute catalyst conditions and at relatively low substrate conversion.[92]

Peris et al. in 2010 reported the development of a water-soluble iridium complex, $IrI_2(AcO)$(bis-NHC), incorporating bis-NHC (N-heterocyclic carbene) ligands as strong electron donors. Under reaction conditions of 60 bar H_2/CO_2 (1:1) in 1 M KOH at 200 °C for 75 hours, the complex exhibited a high TON of 190,000.[109]

A highly efficient dinuclear Cp*Ir catalyst, incorporating 4,4',6,6'-tetrahydroxy-2,2'-bipyrimidine (thbpym) as a bridging ligand, was developed by Himeda and colleagues for CO_2 hydrogenation in aqueous media. Under conditions of 50 bar H_2/CO_2 in an aqueous KOH solution at 80 °C, the system achieved an impressive TON of 79,000 and a TOF of 53,800 h^{-1}.[110] In 2013, Linehan et al. reported the application of a cobalt complex, $Co(dmpe)_2H$ (where dmpe = 1,2-bis(dimethylphosphino)ethane), for the hydrogenation of CO_2 in THF. Upon the addition of Verkade's base (pK_a = 33.6), a very strong organic base, the system achieved a remarkable TON of 9,500 under 20 bar CO_2/H_2 (1:1) at 21 °C within 1 hour. Despite its high activity, a key limitation of this catalytic system is its reliance on Verkade's base for regeneration of the active catalyst.[101]

In 2014, Pidko et al. introduced a highly stable ruthenium-based catalytic system that employed N,N-dimethylformamide (DMF) as the solvent, 1,8-diazabicyclo[5.4.0]undec-7-ene (DBU) as the base, and a H_2/CO_2 ratio of 3:1 under 40 bar pressure at 120 °C. The Ru-PNP complex [RuH(Cl)(CO)(P_2)] demonstrated an exceptional TOF of 1,100,000 h^{-1} and a TON exceeding 200,000.[103] In 2016, Leitner et al. reported a ruthenium complex, [Ru(Acriphos)(PPh_3)(Cl)($PhCO_2$)] (acriphos = 4,5-bis(diphenylphosphino)acridine), for the hydrogenation of CO_2 to FA. Under reaction conditions involving sodium acetate in a dimethyl sulfoxide (DMSO)/H_2O mixture at 60 °C and 120 bar of H_2/CO_2 (2:1), the catalyst achieved an average TOF of 1,000 h^{-1} and a TON of 16,000.[107]

In 2015, Enthaler and Junge assessed a well-characterized nickel PCP pincer hydride complex for CO_2 hydrogenation. Although CO_2 could not be reduced, bicarbonate was successfully transformed into the corresponding formate salt under 55 bar H_2 pressure in methanol at 150 °C, achieving a TON greater than 3,000 (TOF = 150 h^{-1}).[111] Later,

Gonsalvi and colleagues reported the hydrogenation of CO_2 to formate using the manganese complex [Mn(PNPNMe-iPr)(H)$(CO)_2$]. The reaction was conducted in a THF/H_2O mixture at 100 °C under a CO_2/H_2 pressure of 80 bar, employing DBU as the base and Lithium trifluoromethanesulfonate (LiOTf) as a co-catalyst. This system achieved a high TON exceeding 30,000.[112]

In 2018, the Hazari and Bernskoetter groups developed a series of iron complexes based on the PNMeP ligand for the hydrogenation of CO_2 in THF. Using (iPrPNMeP)Fe(H)CO(BH_4) as the catalyst, the reaction achieved a TON of up to 60,000 after 24 hours at 80 °C. The process was carried out under 35 bar each of H_2 and CO_2 in THF, with DBU as the base and lithium triflate (LiOTf) as a co-catalyst.[113] In 2019, the Klankermayer group reported the hydrogenation of CO_2 using a nickel precursor, $Ni(BF_4)_2$, in combination with the $N(CH_2CH_2PPh_2)_3$ (NP_3) ligand to form the active catalyst. Remarkably, using only 0.002 µmol of catalyst and DBU as the base, the reaction was carried out in acetonitrile under 90 bar of a H_2/CO_2 mixture (2:1) at 120 °C for 20 hours, resulting in the formation of formate. An exceptional TON of 4,650,000 was achieved.[114]

Trivedi, Masram, and Rath in 2020 successfully hydrogenated CO_2 using the [CuI(dtbpf)] complex (dtbpf = 1,1′-bis(di-tert-butylphosphino)ferrocene). The reaction was performed in DMF with DBU as the base under a total pressure of 2 bar (1 bar H_2 and 1 bar CO_2). Using 0.002 mmol of the catalyst at 80 °C for 48 hours afforded a 98% yield of formate with a turnover number (TON) of 106,500.[115]

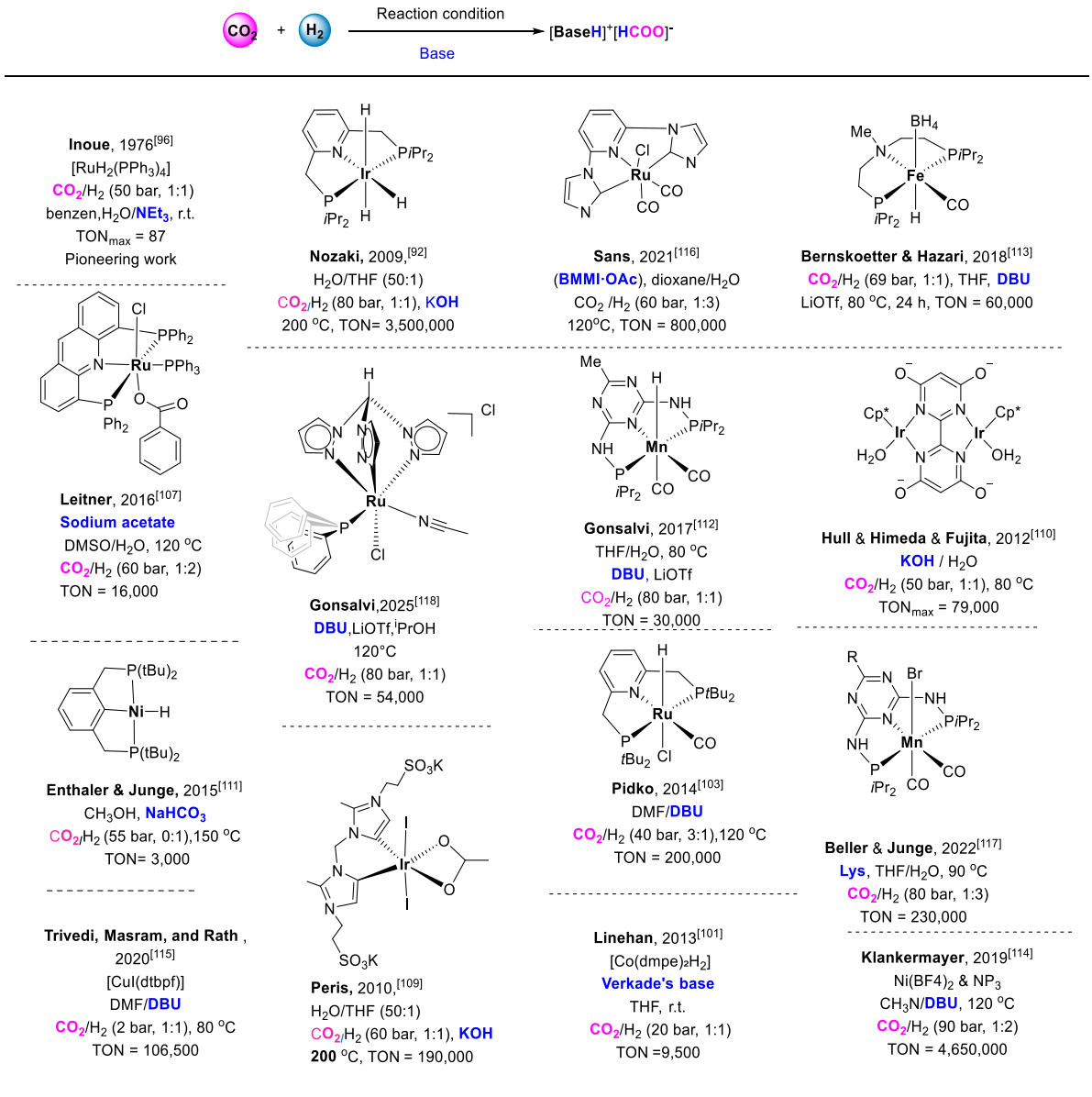


Figure 4. State-of-the-art catalytic systems for direct CO_2 hydrogenation to FA/formate.

In 2021, Sans and co-workers achieved exceptional productivity and catalytic activity in the hydrogenation of CO_2 to FA without salt formation. This was made possible by the rational design of a ruthenium bis-carbene pyridine CNC-pincer catalyst and the use of 1,2-dimethyl-3-butylimidazolium acetate (BMMI·OAc) as a basic ionic liquid. The reaction was carried out under optimized conditions: 120 °C in 6 mL of a 1,4-dioxane/H_2O mixture (5% v/v water), with 3.3 mmol BMMI·OAc, 20 mM $Sc(OTf)_3$, and a H_2/CO_2 gas mixture at 60 bar (3:1). In this system, BMMI·OAc promotes the conversion of CO_2 into bicarbonate, which is subsequently hydrogenated, while simultaneously buffering the solution. This shifts the equilibrium toward FA formation and prevents the pH from dropping low enough to protonate and deactivate the active

ruthenium hydride species. The system demonstrated remarkable catalytic performance, achieving TON exceeding 800,000 and TOF greater than 21,000 h^{-1}.[116]

Later, Beller and co-workers reported a manganese-based PNP pincer complex in combination with the naturally occurring α-amino acid lysine (Lys) for the hydrogenation of CO_2 to formate. This system achieved a formate yield of up to 92% with a TON of 230,000. Notably, the catalyst demonstrated excellent stability and could be reused multiple times, ultimately reaching a cumulative TON of up to 2,000,000.[117]

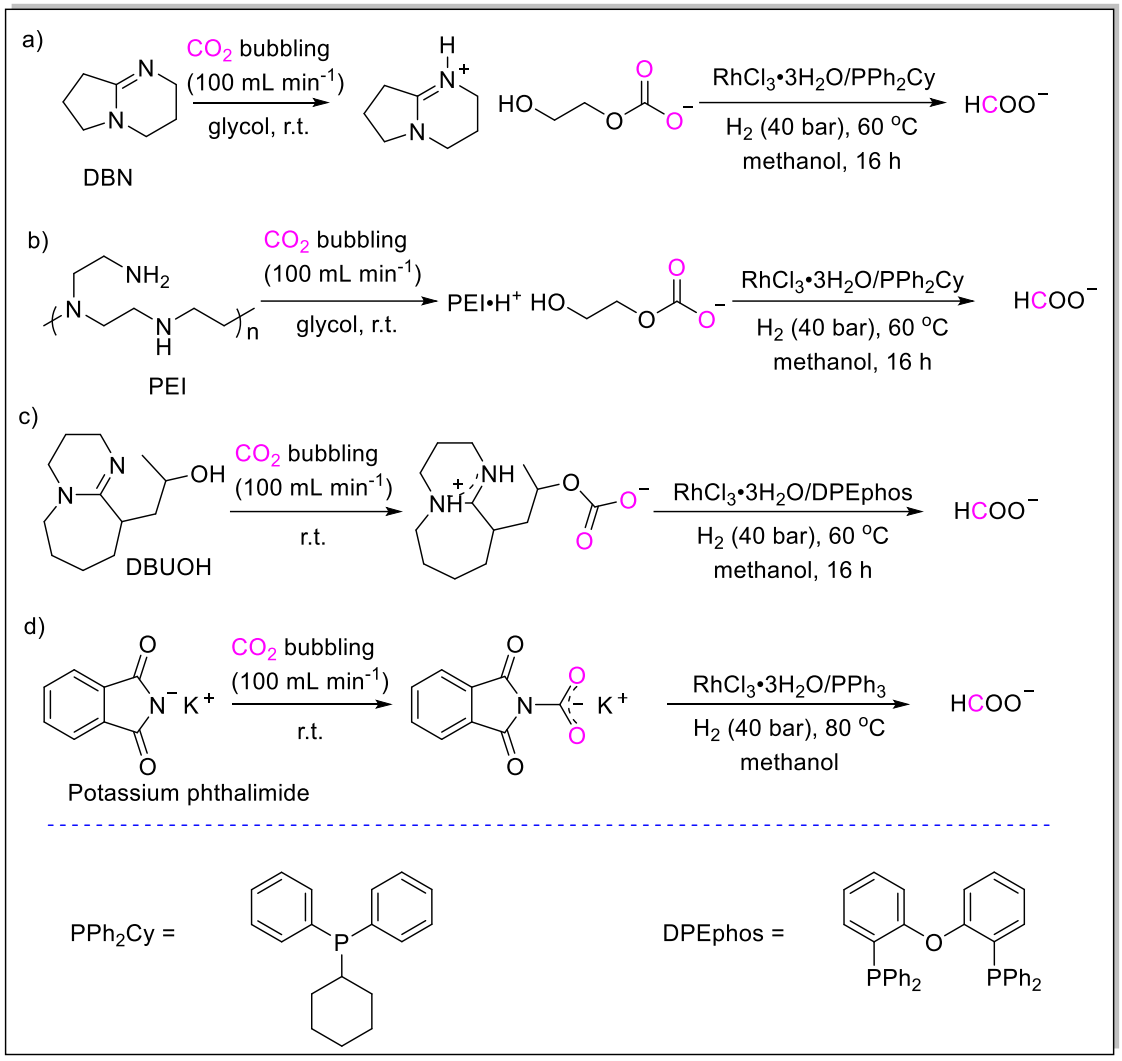
In 2025, Gonsalvi and co-workers developed an efficient homogeneous Ru(II) catalytic system featuring a tris(pyrazolyl)methane (tpm) ligand for the hydrogenation of CO_2 to formate. The optimized complex, [RuCl(κ³-tpm)(PPh_3)(CH_3CN)]Cl, operated under a total pressure of 80 bar (H_2/CO_2 = 1:1) at 120 °C, employing DBU as the base and LiOTf as a Lewis acid additive in isopropanol (iPrOH) as the solvent. Under these conditions, the system achieved a turnover number (TON) exceeding 54,000.[118] **Figure 4** provides an overview of the state of the art in CO_2 hydrogenation to formate/FA, summarizing the key catalytic systems, their performance (TON), and the conditions under which they operate. Despite these advancements, very few examples have been reported for converting low concentrations of CO_2 into formate. The next section will delve into recent developments in carbon capture from low-concentration CO_2 sources, such as air, and their catalytic conversion to formate.

1.5.4. Integrated CO_2 capture and hydrogenation to formate:

Several studies have investigated integrated approaches that combine CO_2 capture with hydrogenation, enabling the direct conversion of captured CO_2—including atmospheric CO_2—into value-added products such as formate and methanol (CH_3OH). This strategy eliminates the need for energy-intensive desorption and compression steps, enhancing overall process efficiency and sustainability. A key aspect of integrated CO_2 capture and conversion processes is the use of bases such as amines or alkali-metal hydroxides for capturing CO_2. These bases not only promote CO_2 absorption and activation but also enhance the hydrogenation step by increasing the activity of the employed homogeneous catalysts. While many studies have explored the transformation of CO_2 into formate salts using homogeneous and heterogeneous catalysts or other methods[119-122], the concept of integrated capture and

conversion to formate salts was not realized until 2013, when He and co-workers demonstrated this approach by employing polyamines and amidine bases for CO_2 capture in alcohol solvents, followed by successful hydrogenation of the captured products using a rhodium-based catalyst under mild conditions (40 bar H_2, 60 °C, 16 h), yielding alkylammonium formate salts.[108] The catalyst was prepared in situ using a metal precursor and a phosphine ligand. The most effective conversion of CO_2 to ammonium formate was achieved when CO_2 was captured with 1,5-diazabicyclo[4.3.0]non-5-ene (DBN) in glycol, forming a bicarbonate intermediate that was subsequently hydrogenated in the presence of $RhCl_3 \cdot 3H_2O$ and the phosphine ligand PPh_2Cy (Scheme 3a). This system delivered a maximum TON of 726, corresponding to a 55% yield of the formate product. The presence of glycol during the capture step was essential, as it helped stabilize the bicarbonate intermediate. Additionally, the absorbent played a dual role by enriching the CO_2 prior to hydrogenation and reacting with the formed FA, thereby shifting the reaction equilibrium toward formate formation. Notably, when polyethyleneimine (PEI, molecular weight 600) was used instead of DBN for CO_2 capture, interactions between the nitrogen atoms of PEI and the rhodium center were observed, indicating that PEI could function as a weakly coordinating ligand during catalysis. PEI_{600} demonstrated a high CO_2 absorption capacity of 7.20 mol CO_2/mol amine in ethylene glycol, leading to the formation of ammonium alkylcarbonate (Scheme 3b). CO_2 was captured by bubbling through the amine solution (0.1 L min^{-1}), followed by hydrogenation at 40 bar H_2 in an ethylene glycol/methanol mixture at 60 °C for 16 hours, resulting in a 37% conversion to formate (TON = 260). The following year, the same research group reported an improved integrated system using a tunable, ethoxy-functionalized amidine, DBUOH, which achieved significantly higher formate yields of up to 99% (Scheme 3c). DBUOH exhibited a CO_2 absorption capacity of 0.95 mol CO_2/mol amidine. CO_2 was again introduced by bubbling at a rate of 0.1 L min^{-1}. Importantly, the inclusion of a hydroxyl group on the amidine side chain eliminated the need for glycol as a capture solvent. Additionally, the ligand DPEphos was identified as a slightly more effective alternative to PPh_2Cy, delivering a TON of 516 compared to 480 under similar conditions.[123] Later, the same research group introduced a system in which CO_2 was captured as a carbamate using potassium phthalimide (Scheme 3d). The CO_2 absorption capacity of phthalimide was measured at 0.96 mol CO_2 per mol of phthalimide. The resulting carbamate was subsequently hydrogenated in methanol

using $RhCl_3 \cdot 3H_2O$ in combination with PPh_3 as the ligand under 80 bar of H_2 pressure, yielding formate with a TON of 60.[124]



Scheme 3. CO_2 capture and subsequent hydrogenation to formate catalyzed by $RhCl_3 \cdot 3H_2O$/phosphine ligands, as reported by He et al.

In 2014, Heldebrant and co-workers demonstrated the capture of CO_2 (1 atm) using DBU in methanol, resulting in the formation of methyl carbonate. This intermediate was subsequently hydrogenated to formates using $[RuCl_2(PPh_3)_3]$ as the catalyst (Table 2, entry 5). Under 20 bar of H_2, the [DBUH$^+$] methyl carbonate was converted into [DBUH$^+$] formate and methyl formate, achieving a TON of up to 5,100 after 40 hours at 140 °C. At reduced temperatures and in the presence of excess base, [DBUH$^+$] formate was the sole hydrogenation product, reaching 24% conversion and a TON of 510 after 16 hours at 110 °C.[125]

In the same year, McNamara and Hicks studied polyethyleneimine tethered iminophosphine/Ir catalyst for the one-pot CO_2 capture and conversion to formate.[126] In this bifunctional molecule, the highly branched PEI chain played a crucial role in both capturing CO_2 and stabilizing the resulting formate, while the iridium center functioned as the active catalytic site. However, achieving a satisfactory formate yield required elevated CO_2 pressure (20 bar), high temperature (120 °C), and an excess of base (4% NEt_3 in water). Under these conditions, the catalyst demonstrated a TON of 248, with the reaction carried out at a hydrogen pressure of 20 bar (Table 2, entry 6).

In 2016, Prakash and co-workers investigated the CO_2 capture efficiency of various amines in aqueous solutions, followed by hydrogenation of the captured CO_2 to formate using the Ru-MACHO-BH catalyst.[127] CO_2 was initially bubbled through aqueous amine solutions at room temperature, and to improve catalyst solubility for the subsequent hydrogenation, organic co-solvents such as THF or dioxane were added. Among the tested superbases, 1,1,3,3-tetramethylguanidine (TMG) and 1,4-diazabicyclo[2.2.2]octane (DABCO) showed the highest effectiveness. TMG achieved a CO_2 capture capacity of 0.92 mmol per mmol of base, primarily as bicarbonate/carbonate. Under optimized conditions - 17 mmol TMG in aqueous/dioxane, 20 µmol Ru-MACHO-BH, 50 bar H_2, 50 °C, and 15 hours - a high TON of 7,375 was reached, corresponding to a 95% yield of formate based on captured CO_2 (Table 2, entry 7). The study also introduced a biphasic water/Me-THF system for catalyst recovery and recycling, with optimization centered on DABCO as the absorbent and minimal Ru leaching into the aqueous phase (below 3 ppm).

In 2017, Franciò and Leitner reported a semicontinuous process for CO_2 capture and utilization, employing the cis-[$RuCl_2(dppm)_2$] complex (with dppm = 1,1-bis(diphenylphosphino)methane) as the catalyst and MEA as the CO_2-absorbing base.[128] In this setup, CO_2 was captured at 30 bar using water as the solvent for MEA-based absorption. The captured CO_2 was subsequently hydrogenated at 75 bar of H_2 and 70 °C, using 4-methyl-2-pentanol (MIBC) as the reaction solvent (Table 2, entry 8). Over the course of 11 reaction runs, the system achieved a remarkable total TON of approximately 150,000 moles of formic acid per mole of catalyst - though this high efficiency ultimately led to near-complete catalyst deactivation.

In 2018, Huang and co-workers developed a direct air capture system that utilized pentamethyldiethylenetriamine (PMDTA) to absorb CO_2 from the atmosphere.[129] The captured CO_2 was initially converted to ammonium bicarbonate and then to ammonium formate salts. Hydrogenation of the aqueous PMDTA solution was performed using a Ru-PN_3P pincer complex as the catalyst and 2-methyltetrahydrofuran (2-MTHF) as the solvent. Under reaction conditions of 130 °C and 100 bar H_2 for 12 hours, the system achieved a total TON of 700 (Table 2, entry 9).

In 2018, Prakash and colleagues reported a recyclable system for CO_2 capture and subsequent conversion to formate salts, utilizing aqueous inorganic hydroxide solutions for CO_2 absorption and homogeneous Ru- and Fe-based PNP catalysts for hydrogenation.[130] In this approach, CO_2 was captured from a 1 psi source into aqueous hydroxide solutions, forming metal carbonate or bicarbonate salts. These CO_2-loaded solutions were then directly hydrogenated at 80 °C under 50 bar of H_2, converting the metal salts into metal formate salts. The Ru-based catalyst achieved a turnover number (TON) of 2,560, while the Fe-based system reached a TON of 2,706 (Table 2, entries 10 and 11). To improve the sustainability of the process, a biphasic solvent system (2-MTHF/H_2O) was employed, allowing efficient recycling of both the catalyst and the organic solvent with minimal loss in TOF over five cycles. Screening of various alkali-metal hydroxides identified NaOH and KOH as effective CO_2 absorbents, each with a 1:1 molar CO_2 absorption capacity and comparable catalytic performance.

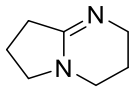
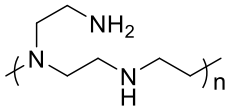
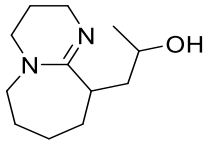
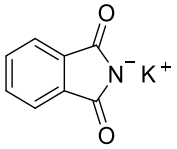
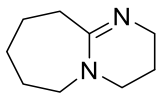
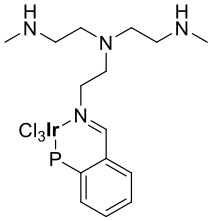
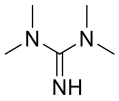
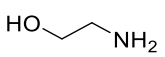
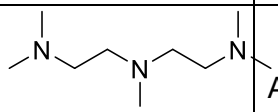
Choudhury and colleagues recently developed a fully aqueous system for direct air capture and hydrogenation to formate.[131] In this system, TMG served as the CO_2-capturing agent alongside a water-soluble iridium catalyst featuring a chelating N-heterocyclic carbene (NHC) ligand, thereby eliminating the need for organic co-solvents. Remarkably, the catalyst exhibited excellent air stability and could be handled in solution without strict air exclusion. In their experiments, 17 mmol of TMG in water captured 16 mmol of CO_2 directly from air. The captured CO_2 was then hydrogenated using 2.0 µmol of the iridium catalyst under 50 bar H_2 at 120 °C for 30 hours. This process yielded a TON of 6,142, corresponding to a 76% formate yield based on the captured CO_2 (Table 2, entry 12)

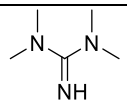
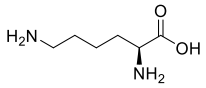
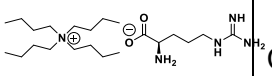
In 2021, Beller and Junge were the first to demonstrate the use of amino acids to integrate CO_2 capture with the direct hydrogenation of the resulting adducts into

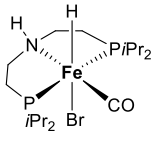
formate.[132] Initially the CO_2 capture efficiency of various amino acids was assessed in aqueous solutions. Among the tested amino acids, lysine (LYS)—featuring a basic side chain due to an extra amino group—demonstrated the highest CO_2 absorption capacity, reaching 0.48 mol CO_2 per mol of LYS. Remarkably, it enabled direct air capture of CO_2, converting up to 98% of the initial lysine into bicarbonate and carbamate species. Following capture, in-situ hydrogenation to formate was performed using Ru-MACHO-BH as the catalyst, achieving a TON of approximately 55,000 under the conditions of H_2O/THF (1:1), 80 bar H_2, 145 °C, and 12 hours. These findings underscore the potential of amino acids for direct air capture and CO_2 conversion. The use of tetrahydrofuran (THF), a water-miscible organic co-solvent, improved catalyst solubility and facilitated the reaction.

Building on these advances, in this thesis we developed and tested an aqueous amino-acid-based ionic liquid (AAIL) system for the integrated capture of CO_2 from low-pressure and ambient sources and its catalytic hydrogenation to formate, with tetrabutylammonium argininate ([TBA][Arg]) identified as the most effective absorbent among the tested AAILs. Under 2 bar of CO_2, [TBA][Arg] captured 1.94 mmol of CO_2 per mmol of absorbent in aqueous solution. In total, 9.70 mmol of CO_2 were captured and subsequently hydrogenated to 6.00 mmol of formate, achieving a TON of 600. The hydrogenation of captured CO_2 was performed at 80°C using the Ru-MACHO-BH catalyst, with high selectivity for formate (100% at 80°C).

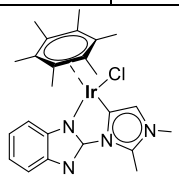
For DAC, the system successfully captured 5.61 mmol of CO_2 from ambient air over 5 days using an aqueous solution of [TBA][Arg]. This captured CO_2 was hydrogenated to 3.05 mmol of formate, with a TON of 305. When the DAC process was scaled up, the system captured 27.2 mmol of CO_2 over 10 days, producing 14.69 mmol of formate (TON = 293) in a mixture of THF/water and 12.90 mmol of formate (TON = 258) in pure water. The system demonstrated good scalability and reusability, with the catalyst being reused for multiple runs without significant loss of activity. These results highlight the potential of [TBA][Arg] for efficient CO_2 capture from both low-pressure CO_2 sources and ambient air in aqueous solutions, followed by catalytic conversion to formate, offering a promising approach for sustainable CCU technologies.[133]

Table 2. Overview of CO_2 capture in-situ conversion to formate.						
Entry	**Absorbent**	**CO_2 Source**	**Catalyst**	**Captured CO_2 /absorbent**	**TON**	**Ref**
1		CO_2 bubbling (0.1 L min−1)	$RhCl_3•3H_2O/PPh_2Cy$	1.1	726	[108]
2		CO_2 bubbling (0.1 L min−1)	$RhCl_3•3H_2O/PPh_2Cy$	7.20	260	[108]
3		CO_2 bubbling (0.1 L min−1)	$RhCl_3•3H_2O$/DPEphos	0.95	298	[123]
4		CO_2 bubbling (0.1 L min−1)	$RhCl_3•3H_2O/PPh_3$	0.96	60	[124]
5		CO_2 bubbling (0.1 L min−1)	$RuCl_2(PPh_3)_3$	n.m*	5,100	[125]
6		20 bar	The catalytic center was incorporated into the amine	n.m	6,142	[126]
7		CO_2 bubbling (85 mL min^{-1})	Ru-MACHO-BH	0.92	7,375	[127]
8		CO_2 (30 bar)	cis-$[RuCl_2(dppm)_2]$	n.m	150,000	[128]
9	 PMDTA	Air	Ru-PN_3P	n.m	700	[129]
10	NaOH	CO_2 (1 psi)	Ru-MACHO-BH	1.00	2,560	[130]

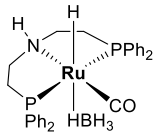
11	NaOH	CO_2 (1 psi)	FeHBrPNPiPr(CO)	1.00	2,706	[130]
12		Air	Ir(III)-NHC	1.06	6,142	[131]
13		Air	Ru-MACHO-BH	0.48	54,000	[132]
14		Air CO_2 (2 bar)	Ru-MACHO-BH	1.12 1.94	305 600	[133]



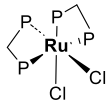
FeHBrPNPiPr(CO)



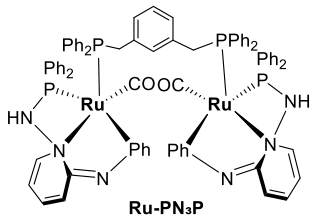
Ir(III)-NHC



Ru-MACHO-BH



***cis*-[$RuCl_2(dppm)_2$]**



Ru-PN_3P

1.6. Methanol: A Fundamental Chemical

1.6.1. Background: Properties and applications of methanol

Methanol (CH_3OH), also traditionally referred to as wood alcohol, methyl alcohol, or carbinol, is a colorless, neutral, and polar liquid at room temperature, with a boiling point of 64.6 °C and a freezing point of −97.6 °C.[134] Methanol was first identified by Robert Boyle in 1661 via the distillation of crude wood vinegar and became widely used as a heating fuel in Europe by the early 20th century. [135-137]

Nowadays, methanol serves as a key platform chemical for the production of a wide range of compounds and materials, including formaldehyde, methyl tert-butyl ether (MTBE), acetic acid, as well as numerous polymers, paints, adhesives, construction materials, pharmaceuticals, and more. [138] Industrially, methanol can also be catalytically converted into olefins and hydrocarbons via the methanol-to-olefin (MTO) and methanol-to-gasoline (MTG) processes.[139, 140] Fundamentally, many carbon-based chemicals and fuels currently derived from petroleum and natural gas can also be synthesized from methanol[141] When methanol is produced through CO_2 recycling, this approach - known as the methanol economy - holds significant promise for reducing our reliance on finite fossil fuel resources and enabling a more sustainable future.[140, 142]

In addition to its role as a chemical feedstock, methanol is an efficient and clean-burning fuel. It can be directly used in internal combustion engines (ICEs), gas turbines, cooking stoves, boilers, and direct methanol fuel cells (DMFC).[143-146] Owing to its high octane number, methanol is also commonly blended with gasoline as an additive..[147] Moreover, methanol possesses a substantial hydrogen storage capacity (12.6 wt% H_2), and hydrogen can be readily released via methanol reforming for use in hydrogen fuel cells - specifically, reformed methanol fuel cells (RMFC).[148-150] Hence, methanol is considered a promising liquid organic hydrogen carrier (LOHC).[151]

1.6.2. Methanol production from syn gas

The annual production of methanol is approximately 98 million tons, with the vast majority sourced from fossil fuels such as coal and natural gas.[152] The process begins by converting these carbon-based feedstocks into synthesis gas (syngas), a mixture

primarily composed of CO and H_2, along with minor amounts of methane (CH_4) and CO_2. This syngas is then purified and compositionally adjusted before entering a reactor, where it undergoes catalytic conversion to methanol. The reaction is facilitated by a copper-based catalyst ($Cu/ZnO/Al_2O_3$) at approximately 250 °C and pressures above 50 bar. However, due to thermodynamic equilibrium constraints, the conversion per pass is limited to about 30%. To maximize yield, the unreacted gases are continuously recycled, enabling near-complete conversion of the syngas to methanol.[152-154]

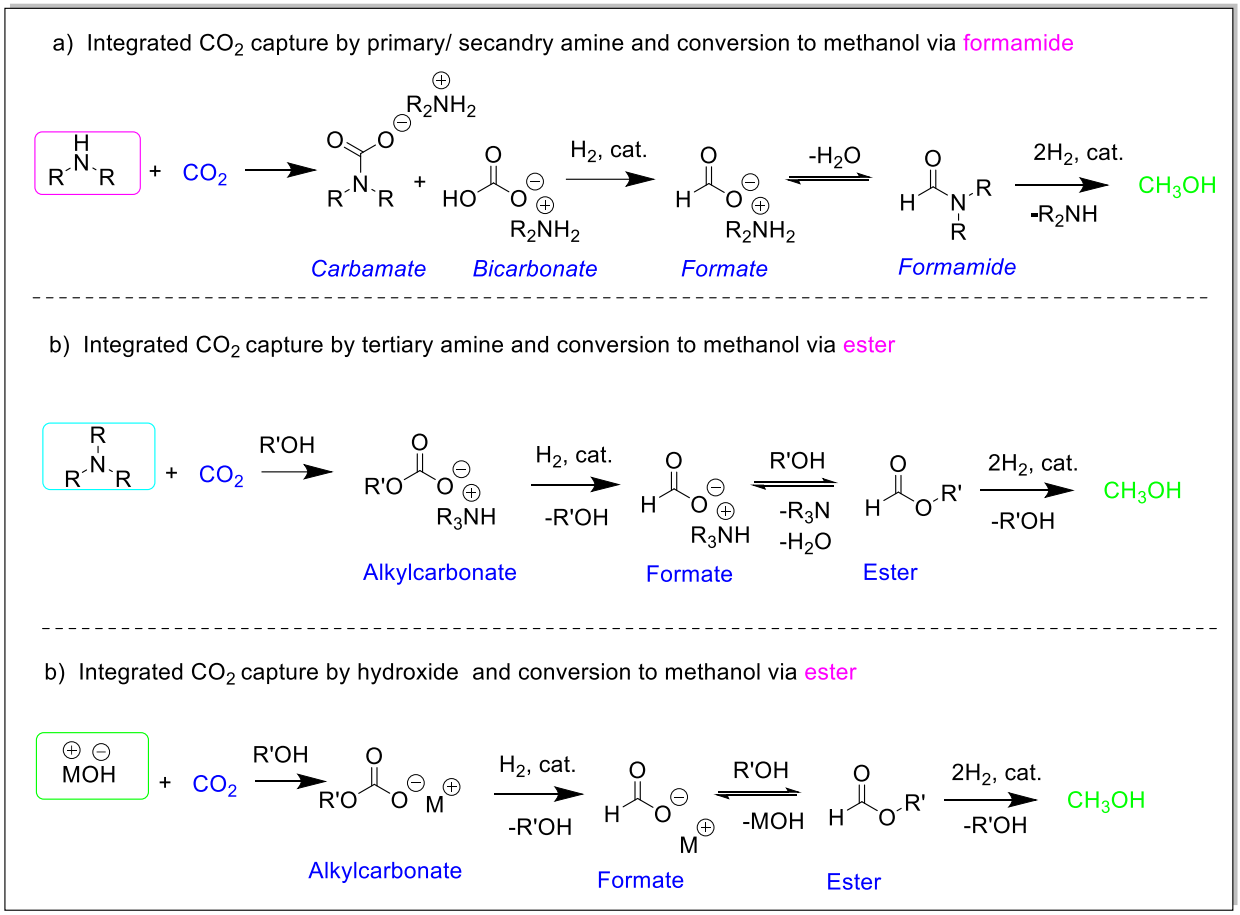
1.6.3. Methanol synthesis via CO_2 hydrogenation

As an alternative to producing methanol from fossil fuel-derived synthesis gas, it can also be synthesized via CO_2 hydrogenation - ideally using hydrogen generated through water splitting powered by renewable energy.

Over the past decade, several homogeneous catalytic systems, primarily based on ruthenium complexes, have been developed. Although these systems remain far from industrial implementation, they enable CO_2 hydrogenation to methanol under relatively mild conditions.[155, 156] These systems can generally be divided into two categories: those operating in neutral or slightly acidic media, and those functioning under basic conditions. In the former, CO_2 is first reduced to FA, which is then esterified with an alcohol to form a formic acid ester. Subsequent hydrogenation of the ester yields methanol - potentially CH_3OH itself - thus creating a self-propagating reaction cycle, with the assisting alcohol being regenerated in the process.[157, 158] Notable contributions in this field have come from the research groups of Sanford[159], Goldberg[160], Beller[161], Klankermayer[162], and Byer[163] who have reported alcohol-assisted CO_2 hydrogenation to methanol under neutral or slightly acidic conditions using Ru-, Ir-, and Co-based catalysts.

Catalysts compatible with basic media are considered more suitable for direct hydrogenation in the alkaline environments typically used to absorb CO_2 from flue gas or air. These catalysts have been more extensively investigated for integrated CO_2 capture and hydrogenation processes. The chemical species present in solution after CO_2 absorption - and the conditions required for its conversion to methanol - depend largely on the nature of the absorbent, which may be an inorganic base (e.g., alkali hydroxide) or an organic nitrogen-containing base, as well as on the choice of solvent.

Scheme 4 illustrates the various species formed in solution following CO_2 capture, along with the intermediates involved in CO_2 hydrogenation to methanol, organized by the type of base employed.



Scheme 4: Pathways for integrated CO_2 capture and hydrogenation to methanol, categorized by the type of absorbent used.

The majority of the reported systems for CO_2 hydrogenation to methanol are based on amine-assisted approaches. **Figure 5** shows an overview of homogeneous base-metal-catalyzed hydrogenation of CO_2 to methanol.

The first proof-of-concept demonstrating the sequential use of a secondary amine as a CO_2 capture agent and the Ru-MACHO-BH complex as a catalyst for converting the resulting carbamate to methanol via a formamide intermediate was published by Sanford in 2015.[164] In a water-lean organic solvent, CO_2 is initially chemisorbed by the amine in a 1:2 molar ratio, forming an ammonium carbamate. Ru-MACHO-BH then catalyzes the hydrogenation of this intermediate to ammonium formate, which undergoes thermal dehydration to yield formamide. The catalyst further facilitates the hydrogenation of formamide to methanol, while the amine is simultaneously

regenerated. The reaction was conducted using a temperature ramp from 95 to 155 °C. In the same year, Ding and co-workers developed a morpholine-mediated sequential pathway for the hydrogenation of CO_2 to methanol via formamide intermediates, employing the same class of ruthenium pincer catalysts.[165] During this period, Prakash & Olah also investigated methanol synthesis from CO_2 using Ru-MACHO-BH catalyst in combination with commercially available, high-boiling polyamines such as PEHA.[166]

Later, the groups of Wass and Kayaki independently reported notable advancements in amine-assisted CO_2 hydrogenation to methanol, also employing ruthenium-based catalysts.[167, 168] In the emerging field of homogeneous base-metal-catalyzed CO_2 hydrogenation to methanol, the Prakash group reported in 2017 the first system employing a manganese(I)–PNP complex, which operates via formamide intermediates in a sequential one-pot process.[169] In 2019, Hazari, Bernskötter, and co-workers reported a similar method employing iron PNP catalysts. [170]

Very recently, Prakash demonstrated that combining an ionic liquid such as 3-butyl-1-methylimidazolium acetate (BMIM.OAc) with PEHA enhances the Ru-MACHO-BH catalyzed hydrogenation of CO_2 to methanol.[171]The resulting yield, productivity, and catalytic activity surpass those achieved when using either the ionic liquid or the amine alone.

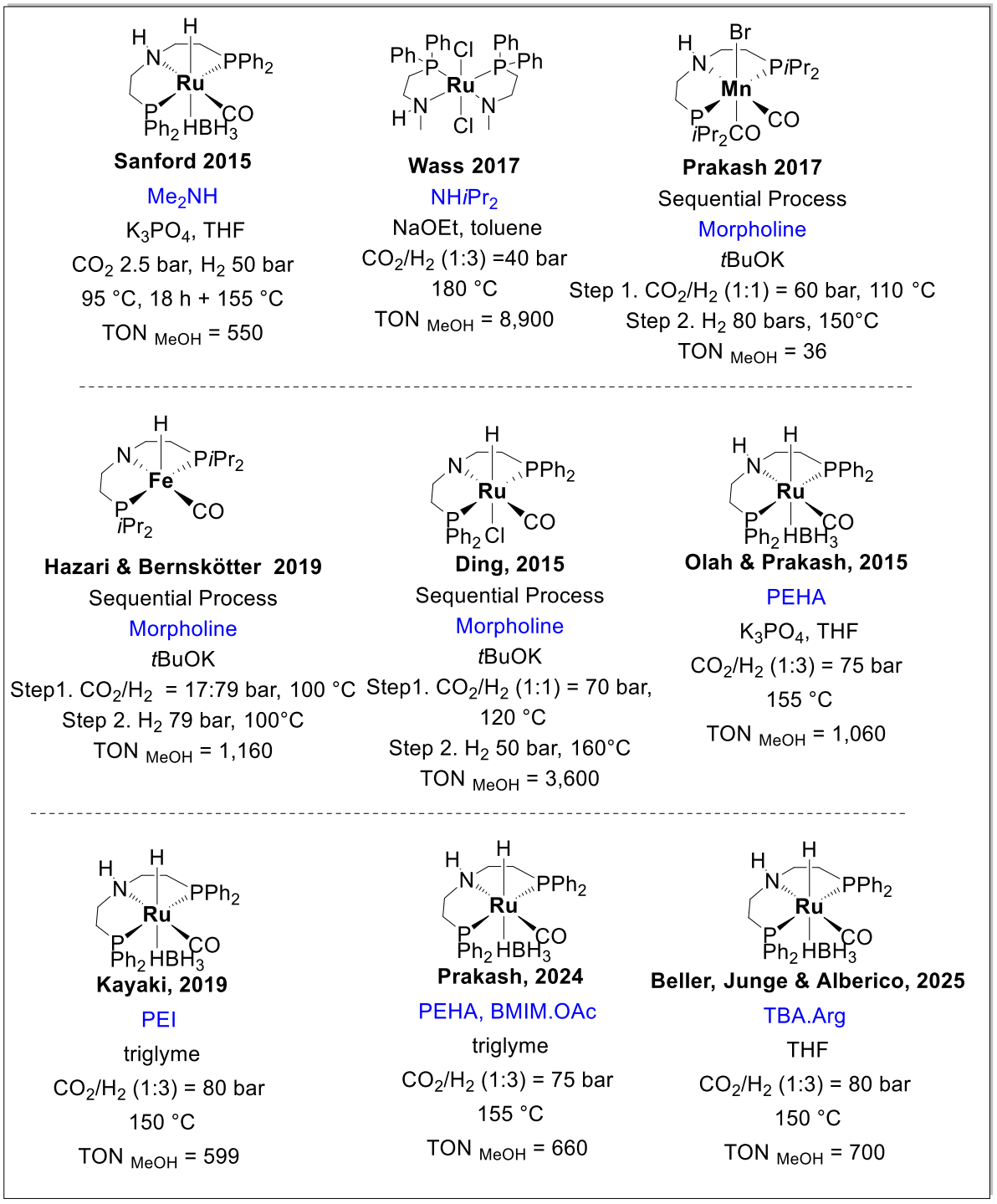
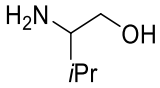
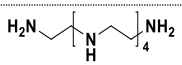
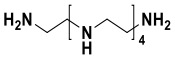
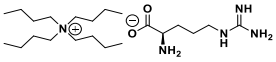
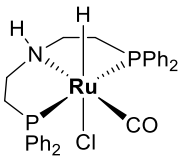
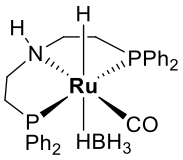
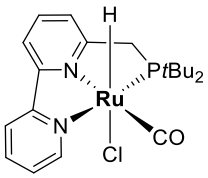
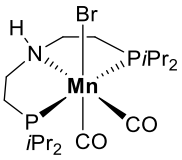


Figure 5. Overview of homogeneous base-metal-catalyzed hydrogenation of CO_2 to methanol.

Building on these developments, this thesis also investigates the use of amino acid-AAILs as a sustainable and efficient strategy for the catalytic hydrogenation of CO_2 to methanol. By combining tetrabutylammonium L-argininate ([TBA][Arg]) with the Ru-MACHO-BH catalyst, we achieved exceptional methanol yields, reaching a turnover number (TON) of up to 700. This underscores the significant role of AAILs in promoting

methanol synthesis. The reaction mechanism proceeds through the formation of formamide intermediates, which are then efficiently reduced to methanol. This approach not only demonstrates the potential of AAILs in enhancing catalytic performance but also highlights their promise as a greener alternative for CO_2 utilization. Direct CO_2 capture from air was also demonstrated, albeit with a captured CO_2/TBA·Arg ratio of 0.35, compared to 1.09 in water. This limitation arises from the poor solubility of [TBA][Arg] in 1,4-dioxane at room temperature. Under optimized conditions, the captured CO_2 was hydrogenated with 94% conversion and 80% selectivity toward methanol. An overview of CO_2 utilization from air or under low pressure (1–3 bar) and its conversion to methanol is summarized in Table 3. While most existing systems rely on amines, our work the advantages of AAILs over conventional amine-based CO_2 capture systems were also demonstrated.

Table 3. Overview of CO_2 capture with different absorbents and subsequent hydrogenation to methanol.

Entry	Absorbent	CO_2 Source	Catalyst	Captured * CO_2/ absorbent	TON	Ref
1		CO_2 (1 bar)	Ru-PNN/tBuOK	n.m	21	[172]
2	$NHMe_2$	CO_2 (2.5 bar)	Ru-MACHO-BH	n.m	550	[173]
3	KOH/ethylene glycol	CO_2 (1 psi)	Ru-MACHO-BH	1.00	480	[174]
4		CO_2 (30 bar)	Ru-MACHO	n.m	840	[175]
5		CO_2 (1 psi)	Ru-MACHO-BH	2.58	520	[176]
6		CO_2 (1 psi)	Mn-PNP	2.58	25	[176]
7		Air	Ru-MACHO-BH	0.35	-	[177]
	 **Ru-MACHO**	 **Ru-MACHO-BH**	 **Ru-PNN**	 **Mn-PNP**		

2. Objectives

The primary objective of this thesis is to explore the potential of amino acid-based ionic liquids (AAILs) for sustainable CO_2 capture and to integrate them with catalytic hydrogenation to formate and methanol. The overreaching goal is to develop energy-efficient strategies that help reducing greenhouse gas emissions and promoting sustainable carbon management. This work contributes to carbon neutrality and the circular economy by capturing CO_2 from low-concentration sources, such as ambient air, and directly converting it into valuable products, thereby minimizing reliance on fossil-based raw materials.

To achieve this, the research focuses on evaluating the performance of amino acid-based ILs in CO_2 absorption, particularly from dilute sources like air. ILs derived from basic amino acids, such as arginine and lysine, are of particular interest due to their high CO_2 absorption capacity. The presence of functional groups, such as the guanidino group in arginine, is expected to enhance CO_2 chemisorption by forming stable carbamates and bicarbonates.

Building on this, the study integrates CO_2 capture with catalytic hydrogenation using appropriate catalysts, facilitating the *in-situ* conversion of captured CO_2 into formate and methanol. This integrated approach seeks to lower energy and capital costs by eliminating the need for CO_2 desorption and compression, which are common in conventional processes. The role of amino acid-based ILs as CO_2 absorbents is investigated, with a focus on optimizing reaction conditions, e.g. temperature, pressure, solvent composition, and catalyst loading to maximize conversion efficiency and selectivity.A key aspect of this research is to demonstrate the feasibility of capturing CO_2 directly from air and converting it into value-added chemicals, contributing to sustainable hydrogen storage and alternative carbon feedstocks. Additionally, the stability and reusability of the catalysts are assessed to evaluate its potential for long-term industrial applications.By integrating CO_2 capture and hydrogenation, this research supports the transition toward a carbon-neutral and circular economy by recycling CO_2 into high-value products. The insights gained from this study provide a foundation for scalable, energy-efficient, and economically viable CO_2 utilization strategies, bridging the gap between laboratory research and real-world implementation.

3. Experimental part

The experimental procedures and analytical methods described in this chapter are adapted from the author's previously published works in ChemSusChem [133, 177].

3.1. Materials and methods

All catalytic hydrogenation reactions were performed under an argon atmosphere to prevent exposure to air or moisture. Organic solvents were purified using a solvent purification system and subsequently stored under argon over molecular sieves. Tetrahydrofuran (THF) was used in its unstabilized form for all hydrogenation experiments.

^{1}H NMR spectra were recorded on Bruker AV-300 (300 MHz) or Bruker AV-400 (400 MHz) spectrometers, while ^{13}C NMR spectra were measured at 75 MHz or 101 MHz. Chemical shifts (δ) are given in parts per million (ppm) relative to tetramethylsilane (TMS), referenced to the residual solvent proton and carbon signals. The following abbreviations are used to describe signal multiplicities: b = broad, s = singlet, d = doublet, t = triplet, q = quartet, m = multiplet. Mass spectrometric analyses were carried out on a Thermo Fisher MAT 95XP instrument equipped with an electrospray ionization (ESI) source.

Ru-MACHO·BH (**Ru-1**, 98%) and Ru-MACHO (**Ru-3**, 97%) were purchased from Strem Chemicals. Amino acids including L-lysine (98%), L-threonine (>99%), L-glutamic acid (>99%), L-serine (>99%), and L-glutamine (>99%) were supplied by TCI. L-arginine (>98%) was obtained from Fluorochem, while L-proline (>99%) was purchased from Acros Organics. L-valine (>98%) and L-alanine (>98%) were supplied by Sigma-Aldrich, and glycine (>99.7%) was purchased from Merck.

Tetrabutylammonium hydroxide (40% in water), (2-hydroxyethyl)trimethylammonium hydroxide (48% in water), and several imidazolium-based ionic liquids — 1-butyl-3-methylimidazolium bis(trifluoromethylsulfonyl)imide (>99%), 1-butyl-3-methylimidazolium hexafluorophosphate (>98%), 1-butyl-3-methylimidazolium hydroxide (>90%), 1-butyl-3-methylimidazolium tetrafluoroborate (>98%), 1-butyl-3-methylimidazolium triflate (>99%), and 1-butyl-3-methylimidazolium acetate (>98%) — were obtained from ABCR and TCI. Benzyltrimethylammonium hydroxide (40% in water) was purchased from Sigma-Aldrich. Additional salts, including

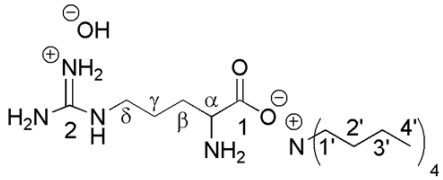
tetrabutylammonium acetate (>98%) and tetrabutylammonium chloride (>98%), were also purchased from Sigma-Aldrich. Deuterium oxide (99.9%) was supplied by Deutero.

TBA·Lys[178], TBA·Arg[179] , TMA·Arg[180], CHO·Arg[181], BMIM·Arg[182], TBP·Arg[183], Ru-MACHO$^{i\text{Pr}}$·BH **Ru-2** [184], Ru-MACHO$^{\text{NMe}}$ **Ru-4**[185], Mn[NH(C_2H_4P*i*$Pr_2)_2$])$(CO)_2$(Br) **Mn-1**[186], Fe-MACHO$^{i\text{Pr}}$-BH **Fe-1**[187], were synthesized according to published procedures.

3.2. Synthesis of Ionic Liquids

3.2.1. Tetrabutylammonium L-Arginine ([TBA][Arg])

The ionic liquid [TBA][Arg] (L-arginine·NBu_4) was prepared following a previously reported method.[179] Even after extended drying under high vacuum, the obtained material consistently retained small amounts of “confined” water.[188, 189] L-arginine possesses a highly basic guanidino side chain (pKa_2 = 9.0, pKa_3 = 13.8),[190] which tends to form a coordinated hydroxo complex rather than undergoing deprotonation under strongly basic conditions, irrespective of additional water content.[191] An aqueous 0.5 M solution of [TBA][Arg], corresponding to the standard hydrogenation reaction concentration, exhibited a pH of approximately 13.3. The structural identity of [TBA][Arg] was confirmed by ^{1}H and ^{13}C NMR spectroscopy, consistent with literature data. The corresponding NMR spectra are provided in Appendix (Figures A-1 and A-2) for reference and for comparison with the spectra of post-reaction solutions.

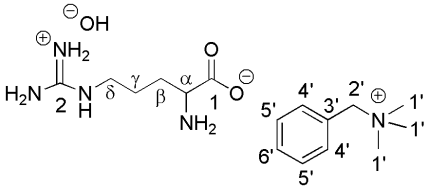


^{1}H NMR (400 MHz, D_2O) δ 3.28 – 3.05 (m, Hα/2Hδ+ 8H1‘), 1.67-1.56 (m, 2Hβ/2Hγ + 8H2‘), 1.34 (h, J = 7.4 Hz, 8H3‘), 0.93 (t, J = 7.4 Hz, 12H4‘).
^{13}C NMR (101 MHz, D_2O) δ 183.21 (C1), 157.21 (C2), 58.07 (C1’), 55.54 (Cα), 40.95 (Cβ), 31.63 (Cγ), 24.50 (Cδ), 23.08 (C2’), 19.10 (C3’), 12.77 (C4’).

3.2.2. Benzyltrimethylammonium L-arginine ([BTMA][Arg])

The ionic liquid [BTMA][Arg] (benzyltrimethylammonium L-argininate) was synthesized via a neutralization reaction between benzyltrimethylammonium hydroxide and L-arginine, following a modified literature procedure.[192] L-arginine (3.48 g, 20 mmol) was suspended

in an aqueous solution of benzyltrimethylammonium hydroxide (40% w/w in H_2O, 8 mL, 20 mmol) and stirred at room temperature for 24 h. The solvent was then removed under reduced pressure, and the resulting pale-yellow solid was dried at 50 °C under high vacuum for 72 h. The product was characterized by ^{1}H and ^{13}C NMR spectroscopy, confirming the formation of [BTMA][Arg]. The NMR spectra are presented in Appendix (Figures A-3 and A-4) for reference.



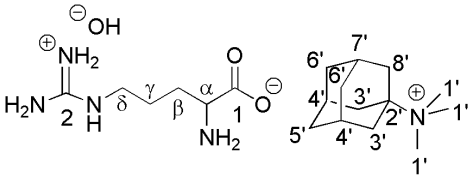
^{1}H NMR (300 MHz, D_2O) δ 7.64-7.38 (m, 2H4‘/2H5‘/H6‘), 4.42 (bs, 2H2‘), 3.22-2.97 (m, Hα/2Hδ+9H1‘) 1.74-1.41 (m, 2Hβ/2Hγ).

^{13}C NMR (75 MHz, D_2O) δ 183.21 (C1), 158.15 (C2), 132.72, 130.76, 129.11, 127.30, 69.47 (t, C2’), 55.58 (Cα), 52.26 (t, C1’), 41.03 (Cβ), 31.79 (Cγ), 24.70 (Cδ), 23.08 (C2’), 19.10 (C3’), 12.77 (C4’). Signals at 55.79, 40.52, 32.04, 28.17 are relative to excess free L-arginine.

3.2.3. *N,N,N*-trimethyl-1-adamantylammonium L-arginine ([TMAA][Arg])

The ionic liquid [TMAA][Arg] (N,N,N-trimethyl-1-adamantylammonium L-argininate) was synthesized via a neutralization reaction between N,N,N-trimethyl-1-adamantylammonium hydroxide and L-arginine, following a reported method.[192] L-arginine (3.48 g, 20 mmol) was suspended in an aqueous solution of N,N,N-trimethyl-1-adamantylammonium hydroxide (25% w/w in H_2O, 16 mL, 20 mmol) and stirred at room temperature for 24 h. The solvent was then removed under reduced pressure, and the obtained pale-yellow solid was dried at 50 °C under high vacuum for 72 h.

The product was characterized by ^{1}H and ^{13}C NMR spectroscopy. The NMR spectra are shown in Appendix (Figures A-5 and A-6).

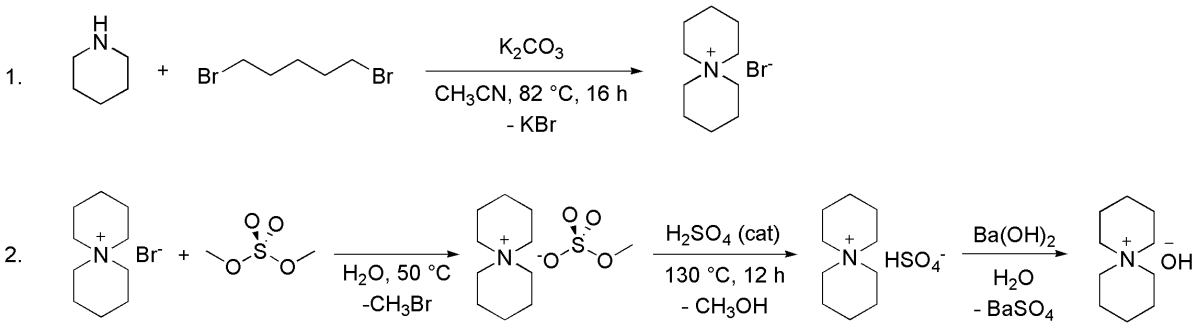


^{1}H NMR (300 MHz, D_2O) δ 3.24 – 3.16 (m, 1 Hα), 3.16 – 3.07 (m, 2Hδ), 2.95 (bs, 9H‘), 2.33 – 2.22 (bs, 2H4‘/H7‘), 2.03 (d, J = 3.1 Hz, 2H5‘/4H6‘), 1.81 – 1.35 (m, 4H3‘/2H8‘ + 2Hβ/2Hγ).

^{13}C NMR (75 MHz, D_2O) δ 183.15 (C1), 158.06 (C2), 72.55 (C2‘), 55.60 (Cα), 47.97 – 46.72 (m, C1‘), 41.05 (Cβ), 34.48 (C3‘/C8‘), 34.11 (C5‘/C6‘), 31.79 (Cγ), 29.94 (C4‘/C7) 24.71 (Cδ). Additional signals at 55.82, 40.55, 32.07, and 28.20 correspond to residual unreacted L-arginine.

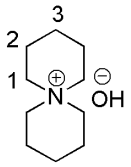
3.2.4. 6-Azonia-spiro[5.5]undecane Hydroxide ([ASU][OH])

An aqueous solution of 6-azonia-spiro[5.5]undecane hydroxide (38% w/w) was obtained from 6-azonia-spiro[5.5]undecane bromide through a three-step, one-pot synthesis following a reported procedure.[192] The detailed reaction scheme is shown in **Scheme 5.**



Scheme 5. Preparation of 6-azonia-spiro[5.5]undecane hydroxide. Reprint from ref.[177] with copyright permission.

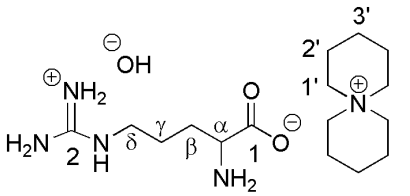
The composition of the resulting aqueous solution was determined by quantitative ^{1}H NMR spectroscopy using DMSO as the internal standard. A 0.2 mL aliquot of the hydroxide solution (0.21621 g) was diluted with 0.4 mL of D_2O (0.43835 g), followed by the addition of 30 µL (0.03298 g) of DMSO. The analysis was repeated twice, and the reported concentration corresponds to the average of both measurements. The ^{1}H NMR spectrum used for quantification is shown in Appendix (Figure A-7).



^{1}H NMR (400 MHz, D_2O) δ 3.32 – 3.19 (m, 8H1), 1.73 (p, J = 5.5 Hz, 8H2), 1.62 – 1.48 (m, 4H3).

3.2.5. 6-azonia-spiro[5.5]undecane L-Arginine ([ASU][Arg])

The ionic liquid [ASU][Arg] (6-azonia-spiro[5.5]undecane L-argininate) was prepared by neutralization of L-arginine with 6-azonia-spiro[5.5]undecane hydroxide. L-arginine (3.4371 g, 19.7 mmol) was suspended in 8.89 g (19.7 mmol) of an aqueous solution of 6-azonia-spiro[5.5]undecane hydroxide (38% w/w in H_2O) and stirred at 60 °C until a clear, colorless solution was obtained. The solvent was then removed under reduced pressure, and the resulting hygroscopic white solid was dried at 50 °C under high vacuum for 72 h. The product was characterized by ^1H and ^{13}C NMR spectroscopy. The corresponding NMR spectra are provided in Appendix (Figures A-8 and A-9).



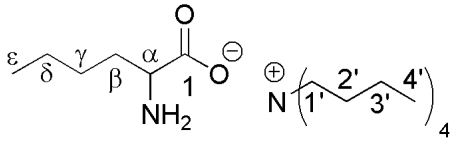
^1H NMR (400 MHz, D_2O) δ 3.39 – 3.32 (m, 8H, H1‘), 3.26 – 3.21 (m, Hα), 3.20 – 3.13 (m, 2Hδ), 1.90 – 1.76 (m, 8H2‘), 1.71 – 1.52 (m, 2Hβ + 2Hγ+ 4H3‘).

^{13}C NMR (101 MHz, D_2O) δ 183.20 (C1), 157.06 (C2), 59.44 (C1’), 55.54 (Cα), 40.95 (Cβ), 31.63 (Cγ), 24.48 (Cδ), 21.09 (C2’), 18.83 (C3’).

3.2.6. Tetrabutylammonium L-norleucine ([TBA][Nor])

The ionic liquid [TBA][Nor] (tetrabutylammonium L-norleucinate) was synthesized by neutralization of L-norleucine with tetrabutylammonium hydroxide. L-norleucine (1.802 g, 13.7 mmol) was suspended in 9 mL (13.7 mmol) of an aqueous solution of tetrabutylammonium hydroxide (40% w/w in H_2O) and stirred at 60 °C until a clear, colorless solution was obtained. The solvent was removed under reduced pressure, and the resulting viscous pale-yellow liquid was dried at 50 °C under high vacuum for 72 h.

The product was characterized by ^1H and ^{13}C NMR spectroscopy. The NMR spectra are shown in Appendix (Figures A-10 and A-11).

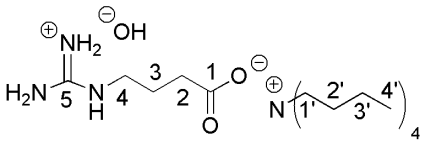


^{1}H NMR (400 MHz, D_2O) δ 3.30 – 3.08 (m, Hα + 8H1‘), 1.75 – 1.47 (m, 2Hβ + 8H2‘), 1.43 – 1.20 (m, 2Hδ+2Hγ + 8H3‘), 0.94 (t, J = 7.3 Hz, 12H4‘), 0.87 (t, J = 7.0 Hz, 3Hε).

^{13}C NMR (101 MHz, D_2O) δ 183.67 (C1), 58.08 (C1’), 55.93 (Cα), 34.20 (Cβ), 27.17 (Cγ), 23.10 (C2’), 21.98 (Cδ), 19.11 (C3’), 13.23 (C4’), 12.80 (Cε).

3.2.7. Tetrabutylammonium 4-guanidinobutirrate ([TBA][GB])

The ionic liquid [TBA][GB] (tetrabutylammonium 4-guanidinobutyrate) was prepared via neutralization of 4-guanidinobutyric acid with tetrabutylammonium hydroxide. 4-Guanidinobutyric acid (1.994 g, 13.7 mmol) was suspended in 9 mL (13.7 mmol) of an aqueous solution of tetrabutylammonium hydroxide (40% w/w in H_2O) and stirred at 60 °C until a clear, colorless solution was obtained. The solvent was removed under reduced pressure, and the resulting white solid was dried at 50 °C under high vacuum for 72 h. The corresponding NMR spectra are provided in Appendix A (Figures A-12 and A13).



^{1}H NMR (400 MHz, D_2O) δ 3.31 – 3.05 (m, 2H4 + 8H1‘), 2.21 (t, J = 7.3 Hz, 2H2), 1.79 (p, J = 7.2 Hz, 2H3), 1.72 – 1.53 (p, J = 7.8 Hz, 8H2‘), 1.34 (h, J = 7.4 Hz, 8H3‘), 0.92 (t, J = 7.4 Hz, 12H4‘).

^{13}C NMR (101 MHz, D_2O) δ 182.36 (C1), 157.46 (C5), 58.07 (C1‘) 40.84 (C4), 34.32 (C2), 25.02 (C3), 23.08 (C2‘), 19.10 (C3‘), 12.78 (C4‘).

3.3. CO_2 Capture experiments

3.3.1. CO_2 capture for formate production (aqueous system)

Capture with CO_2 (2 bar): CO_2 capture experiments were conducted in a 25 mL Schlenk tube equipped with a magnetic stirring bar. The absorbent (5.0 mmol) was combined with 5.0 mL of deionized water, and the system was subsequently charged with CO_2 gas (2 bar). The resulting mixture was stirred at room temperature for 0.5–18 h. The amount of absorbed CO_2 was determined gravimetrically using the following equation:

$Moles\ of\ captured\ \mathrm{CO2} = \Delta m / M\mathrm{CO2} \qquad \Delta m = weight\ of\ the\ solution\ after\ \mathrm{CO2}\ capture - weight\ of\ the\ solution\ before\ \mathrm{CO2}\ capture$

All experiments were performed at least in duplicate, and the average values are reported. The standard deviation of the measurements was below 10%. Evidence of CO_2 capture and the corresponding ^{13}C NMR spectra of the carbamate and bicarbonate species are provided in Appendix (Figure A-14).

Capture with CO_2 (20 bar): Absorbent (5.0 mmol) was added in a 100 mL autoclave equipped with a magnetic stir bar, followed with 5.0 mL of DI water, then 20 bar of CO_2 was charged into the 50 mL autoclave. Afterwards, the autoclave was closed and stirred at r.t. for 6 h. The captured CO_2 amounts were calculated by ^{13}C NMR-quant with 1,4-dioxane (50 µL, 0.58 mmol) as internal standard.[193-196] The corresponding ^{13}C NMR spectra are provided in Appendix (Figure A15).

Capture from ambient air: Direct air capture experiments were performed by dissolving [TBA][Arg] (5.0 mmol) in 20 mL of deionized water in a 25 mL vial. Ambient air containing approximately 400 ppm CO_2 was bubbled through the solution using a long needle at a flow rate of 1 L min^{-1} for five days. After completion of the bubbling process, 1,4-dioxane (50 µL, 0.58 mmol) was added as an internal standard, and the resulting solution was analyzed by quantitative ^{13}C NMR spectroscopy.

The corresponding ^{13}C NMR spectra confirming CO_2 capture from air are provided in Appendix (Figures A-16 and A-17).

3.3.2. CO_2 capture procedure for methanol production (organic media)

[TBA][Arg] (5.0 mmol) was suspended in 20 mL of 1,4-dioxane in a 25 mL vial, which was then sealed with a septum. Ambient air containing approximately 400 ppm CO_2 was bubbled through the suspension using a long needle at a flow rate of 450 mL min^{-1} while stirring at 500 rpm. The solvent level was continuously adjusted to compensate for evaporation and maintain a constant volume.

After 10 days, the air flow was stopped, and the solvent was allowed to evaporate to a final volume of 5 mL. Dimethylformamide (100 µL, 1.29 mmol) was then added as an internal standard, followed by 5 mL of deionized water to dissolve any remaining solids. The resulting 10 mL solution was analyzed by quantitative ^{13}C NMR spectroscopy to

identify bicarbonate and carbamate species.The corresponding ^{13}C NMR spectra is provided in Appendix (Figures A18).

3.4. Catalytic Hydrogenation of CO_2 to Formate

3.4.1. Procedure for the hydrogenation of gaseous CO_2

Ru-MACHO-BH, the absorbent (5.0 mmol), and solvent (10 mL) were introduced into a 100 mL stainless-steel autoclave equipped with a magnetic stirring bar. The reactor was sealed, pressurized with CO_2 and H_2 to the desired pressures, and then heated in a preheated oil bath under continuous stirring for 24 h.

After completion, the reactor was cooled to room temperature, and dimethylformamide (DMF, 250 µL, 3.24 mmol) was added as an internal standard. The post-reaction solution was analyzed by ^1H NMR spectroscopy after addition of a small amount of D_2O (approximately 2 mL) to stabilize the lock signals.[197]. Representative ^1H NMR spectra of the post-reaction solutions is provided in Appendix A (Figure A-19).

3.4.2. Procedure for the hydrogenation of captured CO_2

Prior to the hydrogenation experiments, CO_2 capture in aqueous ionic liquid solutions was carried out. The resulting solution was purged with argon for 30 minutes to remove dissolved gases. Subsequently, degassed THFand the Ru-MACHO-BH catalyst were added to a 100 mL stainless-steel autoclave equipped with a magnetic stirring bar. The autoclave was then sealed and pressurized with 60 bar of hydrogen.

The reaction mixture was heated to the desired temperature and maintained under continuous stirring for the duration of the experiment. After completion, the reactor was cooled to room temperature, and dimethylformamide (DMF, 250 µL, 3.24 mmol) was added as an internal standard. The post-reaction solution was analyzed by ^1H NMR spectroscopy after the addition of a few drops of D_2O to stabilize the lock signal. Representative ^1H NMR spectra of the post-reaction solution is shown in Appendix (Figure A-20).

3.5. Catalytic Hydrogenation of CO_2 to Methanol

3.5.1. Procedure for the hydrogenation of gaseous CO_2

In a typical experiment, the catalyst, absorbent, and solvent were sequentially introduced into a 100 mL stainless-steel autoclave equipped with a magnetic stirring bar. The reactor was then sealed and pressurized with CO_2 and H_2 to the desired total pressure. Subsequently, it was heated to the target temperature and maintained under continuous stirring for the specified reaction time. Upon completion, the autoclave was cooled using an ice–water bath, and the internal pressure was released gradually over five hours through a cooling trap containing 30 mL of THF maintained at either 5 °C or −78 °C.

3.5.2. Procedure for the hydrogenation of captured CO_2

After CO_2 capture, the reaction mixture was degassed to remove residual gases, and the resulting suspension was transferred to a 100 mL stainless-steel autoclave equipped with a magnetic stirring bar. Subsequently, 25 mL of 1,4-dioxane were added, followed by the catalyst. The autoclave was then sealed, pressurized with hydrogen to the desired pressure, and heated to the target temperature under continuous stirring for the duration of the experiment.

Upon completion, the reactor was cooled using an ice–water bath, and the pressure was released gradually over five hours through a cooling trap containing 30 mL of THF maintained at either 5 °C or –78 °C.

3.5.3. Post-Reaction Analysis

Post-reaction analysis of the gas phase: To quantify possible CH_3OH and $HCOOCH_3$ present in the gas phase, the released gas was bubbled through 30 mL of cooled THF containing dimethylformamide (DMF, 200 µL, 2.60 mmol) as an internal standard. A portion of the resulting solution was analyzed by gas chromatography (GC). In most cases, only trace amounts of methanol and methyl formate were detected by this method.

Additionally, a sample of the released gas was analyzed for CO content using permanent gas GC. A representative GC chromatogram of a gaseous sample used for gas-phase composition analysis is provided in Appendix A (Figure A21).

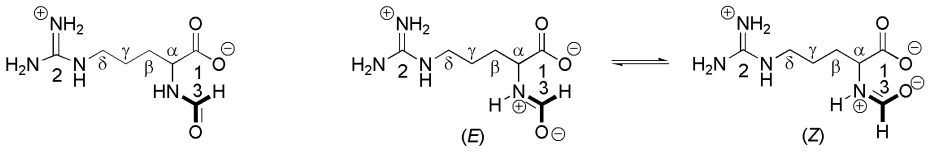
Post-reaction analysis of the condensed phase: Following the reaction, the mixture typically consisted of a heterogeneous system containing a solid residue and a supernatant organic phase. The organic layer was decanted, and the remaining solid was rinsed with fresh THF. The combined organic phases (total volume ≈ 40 mL) were treated with dimethylformamide (DMF, 200 µL, 2.6 mmol) as an internal standard and analyzed by GC to detect and quantify CH_3OH and $HCOOCH_3$. A representative GC chromatogram of the liquid organic phase obtained after CO_2 hydrogenation is shown in Appendix (Figure A22).

For NMR analysis, a sample of the organic phase was supplemented with a drop of THF-d_8 to stabilize the lock signal and analyzed by ^{1}H and ^{13}C NMR spectroscopy to identify and quantify (^{1}H NMR) other THF-soluble products.

The solid residue was dissolved in 30 mL of water, to which DMF (200 µL, 2.6 mmol) was added as an internal standard. This aqueous solution typically contained formate salts and amino acid–derived products. A sample of this solution, after addition of a drop of D_2O for lock purposes, was analyzed by ^{1}H and ^{13}C NMR spectroscopy to detect and quantify (^{1}H NMR) formate and amino acid–derived formamide species. Representative ^{1}H and ^{13}C NMR spectra of the post-reaction aqueous and organic phases are provided in Appendix (Figures A-23–A-26).

3.6. Synthesis of reaction intermediates:

N-α-formyl-L-Arginine: N-α-formyl-L-arginine was synthesized from L-arginine, formic acid, and formamide according to a reported procedure.[198] The product consisted of two isomeric forms, cis (Z) and trans (E). Since the specific configurations of these isomers have not been assigned, they are referred to as Major and Minor, corresponding to their relative amount. The characterization data, including the ^{1}H and ^{13}C NMR spectra, are provided in the Appendix (Figures A-27 and A-28).



^{1}H NMR (400 MHz, D_2O) δ 8.08 (d, J = 1.0 Hz, H3 Maj), 7.97 (s, H3, Min.), 4.27 (ddd, J = 7.8, 5.1, 1.0 Hz, Hα, Maj.), 4.02 (dd, J = 8.2, 5.0 Hz, Hα, Min.), 3.21 (t, J = 6.9 Hz, 2Hδ, Maj. + Min.), 1.94 – 1.80 (m, 1Hβ, Maj. + Min.), 1.79 – 1.69 (m, 1Hβ Maj. + Min.), 1.68 – 1.55 (m, 2Hγ Maj. + Min.).

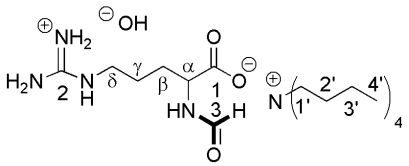
^{13}C NMR (101 MHz, D_2O) δ 178.10 (C1, Maj. and Min.), 166.96 (C3, Min.), 163.62 (C3, Maj.), 156.71(C2, Maj. and Min.) 57.27 (Cα, Min.), 53.29 (Cα, Maj.), 40.58 (Cδ, Maj. and Min.), 29.87 (Cβ, Min.), 28.78 (Cβ, Maj.), 24.35 (Cγ, Min.), 24.25(Cγ, Maj.).

ESI-HRMS (m/z, pos): Calculated for [C7H15N4O3] 203.1144; found: 203.1141 $[M+H]^+$.
ESI-HRMS (m/z, neg): Calculated for [C7H13N4O3] 201.0998; found: 201.0992 $[M-H]^-$.

N-α-formyl-L-Arginine·NBu$_4$: An aqueous solution of tetrabutylammonium hydroxide (NBu_4OH, 655 µL, 1 mmol, 40% w/w in H_2O) was added to a solution of N-α-formyl-L-arginine (202.2 mg, 1 mmol) in 16 mL of water. The mixture was stirred at room temperature until a clear, colorless solution was obtained. The solvent was then removed under reduced pressure while maintaining the temperature at 55 °C, yielding an off-white foam.

However, ^{1}H and ^{13}C NMR analyses indicated that partial hydrolysis of the N-formyl group occurred during concentration due to the high basicity of the medium, resulting in the release of formic acid. As a consequence, N-α-formyl-L-arginine·NBu_4 could not be isolated in pure form. The ^{1}H and ^{13}C NMR spectra of the isolated product are shown in Appendix (Figure A-29), and their comparison with the *in situ* (non-isolated) product is provided in Appendix (Figure A-30).

Comparison with the ^{1}H NMR spectrum of the concentrated product confirmed the incremental formation of HCOOH (δ = 8.42 ppm in D_2O) upon solvent removal. The ^{13}C NMR spectrum of N-α-formyl-L-arginine was further compared with that of a post-reaction water-soluble residue, which exhibited a resonance at 163.6 ppm corresponding to the Nα-formyl carbon, while the guanidinium carbon remained unshifted at 156.8 ppm, indicating no formylation at the guanidino nitrogens (Figure A-31).



^{1}H NMR (400 MHz, D_2O) 8.05 (d, J = 1.1 Hz, 1H, H3, Maj.), 7.94 (s, 1H, H3, Min.), δ 4.23 (ddd, J = 7.9, 5.0, 1.0 Hz, Hα, Maj.), 3.98 (dd, J = 8.4, 5.0 Hz, Hα, Min.), 3.24 –

3.04 (m, 8H1‘ + 2Hδ, Maj. + Min), 1.90 – 1.77 (m, 1Hβ, Maj. + Min.), 1.76 – 1.52 (m, 8H2‘ + 1Hβ, Maj. + Min., 2Hγ, Maj. + Min.), 1.33 (h, J = 7.4 Hz, 8H3‘), 0.92 (t, J = 7.4 Hz, 12H4‘).

4. Results and Discussion

This chapter presents the experimental results obtained in this work, organized into two main parts. The first part (Section 4.1) focuses on CO_2 capture using amino acid-based ionic liquids (AAILs) and their catalytic hydrogenation to formate, while the second part (Section 4.2) addresses the hydrogenation of CO_2 to methanol using AAIL-based systems under optimized conditions.

The results and discussions presented in this chapter are derived from the author's previously published articles. [133, 177]

4.1. CO_2 capture using amino acid based-Ionic liquids and subsequent catalytic hydrogenation to formate

4.1.1. Evaluation of ionic liquids for CO_2 capture

In this section of the thesis, we investigated the potential of various ionic liquids as green and efficient absorbents for CO_2 capture, with the aim of integrating them into CCU processes. For the development of a CCU concept, an absorbent must not only be environmentally friendly or compatible but also effectively absorb CO_2, as emphasized earlier in the introduction. ILs have emerged as promising candidates for CO_2 capture due to their unique properties, including low volatility, high thermal stability, and tunable physicochemical characteristics.[199, 200] Building upon previous research conducted in our group, where naturally occurring amino acids were successfully employed for CO_2 capture and subsequent hydrogenation to formate, [132] we extended this concept to amino acid-based ionic liquids (AAILs).

AAILs are expected to combine the CO_2-binding functionality of amino acids with the advantages of ILs, offering an efficient and environmentally friendly approach to CO_2 capture. Before focusing on AAILs, however, it was necessary to establish a reference by investigating the CO_2 absorption behavior of conventional ILs with different counterions. Therefore, we began our study by measuring the CO_2 capture capacity of several commercially available ILs containing a variety of counterions, including Br^-, OH^-, OAc^-, PF_6^-, BF_4^-, and $CF_3SO_3^-$.

In a standard experimental procedure, a glass pressure vessel was filled with carbon dioxide at 2 bar pressure and maintained at ambient temperature, with stirring

conducted for a period ranging from 0.5 to 18 hours. The amount of CO_2 absorbed was determined using gravimetric methods. However, the inherently high viscosity of ILs poses a challenge for CO_2 diffusion throughout the reaction medium. This elevated viscosity is associated with the distribution of partial charges on functional groups such as $-NH_2$, $-NH_3^+$, and $-NHCO_2^-$.[201] Additionally, as more CO_2 is absorbed, the viscosity increases further due to the formation of extensive hydrogen bonds. To address this limitation and enhance process efficiency, subsequent experiments employed aqueous solutions of ILs. An overview of the corresponding results is presented in Table 4.

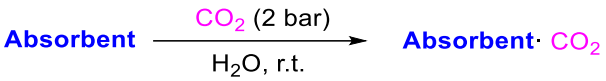
In the first phase of our experiments, we tested 1-butyl-3-methylimidazolium-based ILs with various counter anions (Table 4, entries 1-6), because Sans and others showed that this kind of ILs proved to be very efficient for transformation of CO_2.[202-204] Nevertheless, under the applied conditions, only limited quantities of CO_2 were captured, with the maximum uptake reaching just 0.21 mmol of CO_2 per mmol of absorbent when using the hydroxide anion. This reduced performance is most likely due to the higher basicity of hydroxide relative to other anions such as OAc^-, Br^-, and BF_4^- (Table 4, entries 1-6).

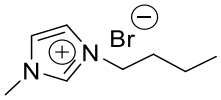
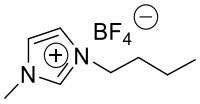
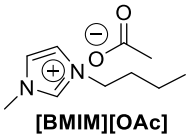
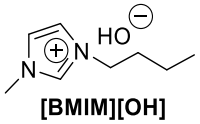
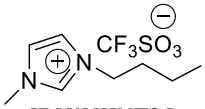
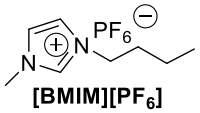
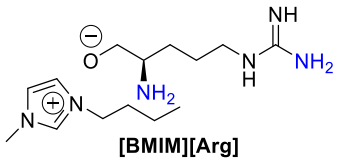
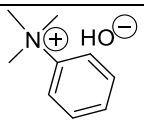
To enhance the CO_2 absorption capacity of the ionic liquid, various cations were evaluated in combination with the hydroxide anion. This modification led to improved uptake values, ranging from 1.06 mmol CO_2 per mmol absorbent for (2-hydroxyethyl) trimethylammonium ($[CHO]^+$) (Table 4, entry 9), to 1.00 for benzyltrimethylammonium ($[BTMA]^+$)(Table 4, entry 8), and up to 1.16 for tetrabutylammonium ($[TBA]^+$) (Table 4, entry 11).

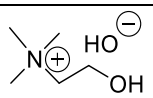
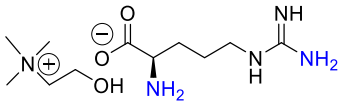
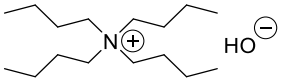
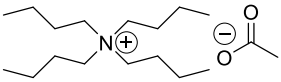
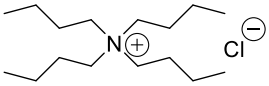
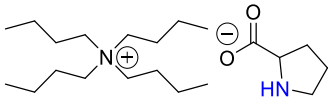
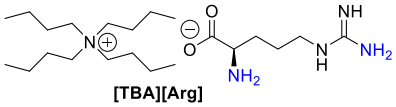
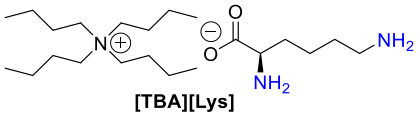
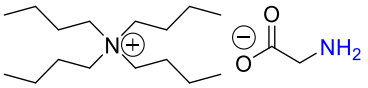
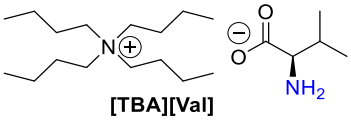
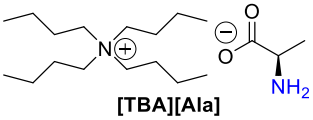
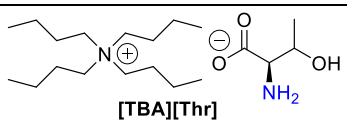
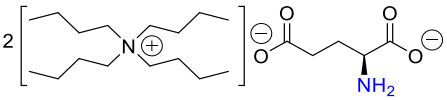
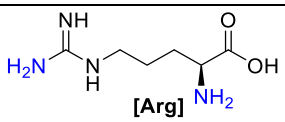
Given its superior performance, tetrabutylammonium was subsequently paired with different amino acid (AA) anions to investigate whether further enhancement in CO_2 capture could be achieved. Substitution of hydroxide with glycinate (Gly^-) (1.08 mmol, Table 4, entry 17), threoninate (Thr^-) (1.00 mmol, Table 4, entry 20), glutamate (Glu^-) (0.88 mmol, Table 4, entry 21), valinate (Val^-) (0.40 mmol, Table 4, entry 18), alaninate (Ala^-) (1.07 mmol, Table 4, entry 19), and prolinate (Pro^-) (0.85 mmol, Table 4, entry 14) did not result in any significant improvement. In contrast, the use of lysinate (Lys^-) (1.80 mmol, Table 4, entry 16) and argininate (Arg^-) (1.94 mmol, Table 4, entry 15) markedly increased the CO_2 capture capacity. This suggests that the presence of an additional basic site in the side chain of these amino acids plays a key role in enhancing

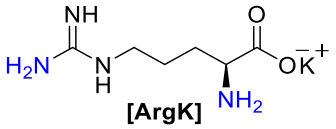
CO_2 uptake. Notably, [TBA][Arg] exhibited a higher CO_2 absorption than the corresponding ILs based on 1-butyl-3-methylimidazolium ($[BMIM]^+$) and $[CHO]^+$ cations (Table 4, entries 7 and 10). These results suggest that AAILs, particularly those with Lys^- and Arg^-, could also be promising candidates for DAC applications due to their strong binding affinities.

Table 4. CO_2 capture with absorbents under 2 bar of CO_2.



Entry	Absorbent	Captured CO_2 [mmol][a]	Captured CO_2/Absorbent[b]]
1	 **[BMIM][Br]**	0.62	0.12
2	 **[BMIM][BF_4]**	0.75	0.15
3	 **[BMIM][OAc]**	0.87	0.17
4	 **[BMIM][OH]**	1.05	0.21
5	 **[BMIM][NTf_2]**	0.78	0.15
6	 **[BMIM][PF_6]**	0.86	0.17
7	 **[BMIM][Arg]**	5.62	1.12
8	 **[BTMA][OH]**	5.01	1.00

9	 **[CHO][OH]**	5.34	1.06
10	 **[CHO][Arg]**	9.21	1.84
11	 **[TBA][OH]**	5.80	1.16
12	 **[TBA][OAc]**	0.76	0.15
13	 **[TBA][Cl]**	0.61	0.12
14	 **[TBA][Pro]**	4.30	0.85
15	 **[TBA][Arg]**	9.70	1.94
16	 **[TBA][Lys]**	9.02	1.80
17	 **[TBA][Gly]**	5.40	1.08
18	 **[TBA][Val]**	2.04	0.40
19	 **[TBA][Ala]**	5.38	1.07
20	 **[TBA][Thr]**	5.00	1.00
21	 **[TBA][Glu]**	4.40	0.88
22	 **[Arg]**	5.20	1.04

23	 **[ArgK]**	8.50	1.70
Reaction conditions: Absorbent (5.0 mmol), H_2O (5 mL), CO_2 (2 bar), stirred at r.t. (24 °C). [a] Determined via gravimetric analysis. [b] Calculated by (mmol captured CO_2)/ (mmol absorbent).			

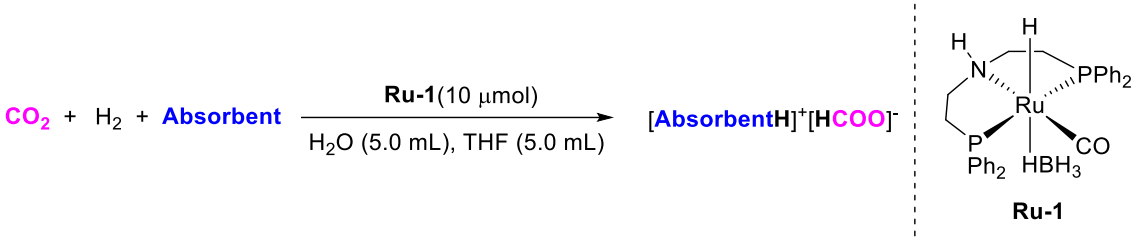
4.1.2. Hydrogenation of gaseous CO_2 to formate catalyzed by Ru-MACHO-BH

Following our evaluation of AAILs for CO_2 capture, we explored the direct hydrogenation of gaseous CO_2 to formate using Ru-MACHO-BH (**Ru-1**) as a catalyst in the presence of various ILs. This catalyst has previously been recognized as a highly effective catalyst for this transformation.[173, 205-208]

The reactions were carried out in a water/THF solvent mixture to improve catalyst solubility, under an initial total pressure of 80 bar (comprising 60 bar H_2 and 20 bar CO_2) at 80 °C for 24 hours. The corresponding outcomes are presented in Table 5. ILs containing Cl^-, Br^-, or OAc^- as anions, irrespective of the associated cation, exhibited either negligible or low activity, producing no more than 0.56 moles of formate per mole of IL (Table 5, entries 4, 5, 8, and 9). This limited performance is likely attributed to the weak basicity of these anions, which hampers their CO_2 binding capacity. On the other hand, ILs incorporating hydroxide anions demonstrated enhanced formate production, with notable variation depending on the cation. For example, benzyltrimethylammonium hydroxide ([BTMA][OH]) produced 0.76 mmol of formate per mmol of IL, while (2-hydroxyethyl)trimethylammonium hydroxide ([CHO][OH]) and tetrabutylammonium hydroxide ([TBA][OH]) achieved 0.91 and 1.22 mmol formate per mmol of IL, respectively (Table 5, entries 12, 6, and 3). The highest yield was obtained using [TBA][Arg], which delivered 1.91 mmol of formate per mmol of absorbent (Table 5, entry 1), underscoring the critical influence of both cation and anion selection in maximizing CO_2 hydrogenation efficiency.

For comparison, the reaction was also performed with arginine ([Arg]) or potassium argininate ([Arg][K]) instead of [TBA[Arg]. In both cases, the [TBA[Arg] gave clearly superior performance, in line with the trend observed in the CO_2-capture experiments (Table 5 entry 1 versus entries 13 and 14).

Table 5. CO_2 hydrogenation to formate in the presence of various absorbents.

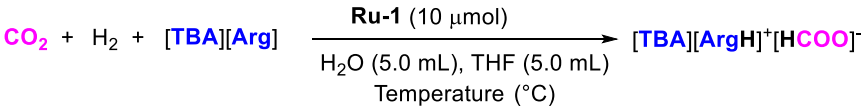


Entry	Absorbent	Formate [mmol][a]	Formate [TON][b]	Ratio Formate/Absorbent
1	[TBA[Arg]	9.59	959	1.91
2	[TBA][Lys]	8.84	884	1.76
3	[TBA][OH]	6.14	614	1.22
4	[TBA][Cl]	n.d.	-	-
5	[TBA][OAc]	2.04	204	0.40
6	[CHO][OH]	4.58	458	0.91
7	[CHO][Arg]	8.80	880	1.76
8	[BMIM][Br]	n.d.	-	-
9	[BMIM][OAc]	2.82	282	0.56
10	[BMIM[[OH]	1.10	110	0.22
11	[BMIM][Arg]	4.64	464	1.12
12	[BTMA][OH]	3.83	383	0.76
13	[Arg]	3.90	390	0.78
14	[Arg][K]	7.37	737	1.47

Reaction conditions: Absorbent (5.0 mmol), **Ru-1** (10 μmol), H_2O/THF (5/5 mL), CO_2/H_2 (20/60 bar), 80 °C, 24 h. [a] Determined by ^1H NMR with DMF (250 μL, 3.24 mmol) as internal standard. [b] Calculated by (mmol formate)/ (mmol catalyst). n.d.= not detectable.

Having identified [TBA][Arg] as the most effective ionic liquid among those tested, we next examined the influence of temperature and solvent composition. With all other reaction variables held constant, experiments were carried out at temperatures between 25 and 145 °C (Table 6). The highest formate yield (expressed as mmol of formate per mmol of absorbent) was achieved at 80 °C. At both lower and higher temperatures, the performance declined. Above 80 °C, measurable amounts of formamide began to appear and the selectivity toward formate dropped from 100 % at 80 °C to 64 % at 145 °C. Consequently, 80 °C was chosen for further optimization as it offered the most favorable combination of conversion and selectivity.

Table 6. Hydrogenation of CO_2 in the presence of [TBA][Arg]: Effect of temperature

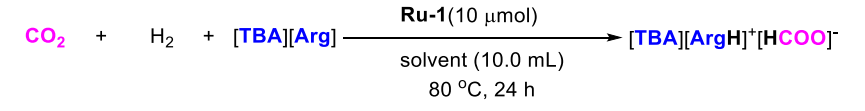


Entry	Temperature	Formate [mmol][a]	Formate [TON][b]	Formamide [mmol]	Ratio Formate/ Absorbent
1	145°C	5.85	585	3.25	1.82
2	115°C	8.51	851	0.80	1.86
3	90°C	9.00	900	0.34	1.87
4	80°C	9.59	959	n.d.	1.91
5	70°C	8.48	848	n.d.	1.69
6	50°C	4.42	442	n.d.	0.91
7	R.T.	0.33	33.0	n.d.	0.06

General conditions: [TBA][Arg] (5.0 mmol), Ru-1 (10 μmol), H_2O/THF (5/5 mL), CO_2/H_2 (20/60 bar), 24 h. [a] Determined by ^1H NMR with DMF (250 μL, 3.24 mmol) as internal standard. [b] Calculated by (mmol formate)/ (mmol catalyst). n.d.= not detectable.

To assess the influence of solvent composition on the reaction performance, a range of organic solvents other than THF was tested in combination with water. None of the co-solvents tested enhanced the performance of the system compared with THF. In fact, the TON achieved in pure THF (Table 7, entry 8; TON = 990) was essentially the same as that obtained with a THF/water mixture (Table 7, entry 1; TON = 959). The reaction could also be scaled up fivefold without any notable loss in formate production (Table 8, entry 6; TON = 938). Furthermore, to move towards a more sustainable process, the reaction was scaled up using only water as the solvent, which still afforded a high TON of 833 (Table 8, entry 5). Ru-MACHO-BH complex is badly soluble in sole water, however, in our work the CO_2 capture and hydrogenation in the presence of IL in water works well. This means that the IL additives help to dissolve the complex in water due to the good solubilities of ILs.

Table 7. Hydrogenation of CO_2 in the presence of [TBA][Arg]: Screening of solvents.



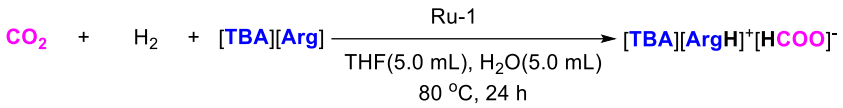
Entry	Solvent [mL]	Formate [mmol][a]	Formate [TON][b]	Formate/ Absorbent
1	THF [5] + H_2O [5]	9.59	959	1.91
2	Triglyme [5] + H_2O [5]	9.25	925	1.85
3	MeOH [5] + H_2O [5]	8.77	877	1.75
4	2-MTHF [5] + H_2O [5]	8.45	845	1.68

5	1,2-Dioxane [5] + H_2O [5]	8.15	815	1.63
6	Ethylene glycol [5] + H_2O [5]	8.10	810	1.62
7	H_2O [10]	3.01	301	0.60
8	THF [10]	9.90	990	1.98
General conditions: [TBA][Arg]: (5.0 mmol), **Ru-1** (10 μmol), CO_2/H_2 (20/60 bar), 80 °C, 24 h. [a] Determined by ^1H NMR with DMF (250 μL, 3.24 mmol) as internal standard. [b] Calculated by (mmol formate)/ (mmol catalyst).				

After optimizing the parameters for CO_2 conversion, efforts were directed toward increasing the TON of formate by reducing the catalyst loading. Lowering the catalyst amount from 10 μmol to 0.2 μmol led to a remarkable increase in TON, rising from 959 to 37,500 (Table 8, entries 1–4).

The reusability of the catalyst was also examined (Figure 6). Since the reaction mixture was homogeneous and no biphasic separation was observed after hydrogenation, as illustrated in Appendix Figure A-32 (showing the reaction mixture before and after hydrogenation), catalyst recycling was performed by releasing the gas at the end of each run and subsequently adding a fresh portion of [TBA][Arg] to the recovered reaction solution. The catalyst was successfully reused over five consecutive cycles. Although the formate yield per mmol of absorbent decreased slightly from 1.89 to 1.67, the cumulative turnover number (TON) exceeded 12,700. These results demonstrate both the stability and recyclability of the catalyst in the CO_2 hydrogenation process.

Table 8. Influence of catalyst loading and reaction scale-up on CO_2 hydrogenation in the presence of [TBA][Arg].



Entry	Solvent [mL]	Formate [mmol][a]	Formate [TON][b]	Formate/ Absorbent
1	10.00	9.59	959	1.91
2	3.50	9.46	2,702	1.89
3	2.00	8.80	4,400	1.76
4	0.20	7.50	37,500	1.50
5[c]	50.00	41.66	833	1.66

6[d]	50.00	46.93	938	1.88
General conditions: [TBA][Arg] (5.0 mmol), **Ru-1**, H_2O/THF (5/5 mL) CO_2/H_2 (20/60 bar), 80 °C, 24 h. [a] Determined by ^1H NMR with DMF (250 µL, 3.24 mmol) as internal standard. [b] Calculated by (mmol formate)/ (mmol catalyst). [c] 25 mmol [TBA][Arg], Ru-1 (50 µmol), H_2O (10 ml). [d] 25 mmol [TBA][Arg], **Ru-1** (50 µmol), H_2O/THF (25/25 mL).				

Gas chromatography confirmed minimal CO formation (<1 ppm), indicating high selectivity for formate (Figure A-33).

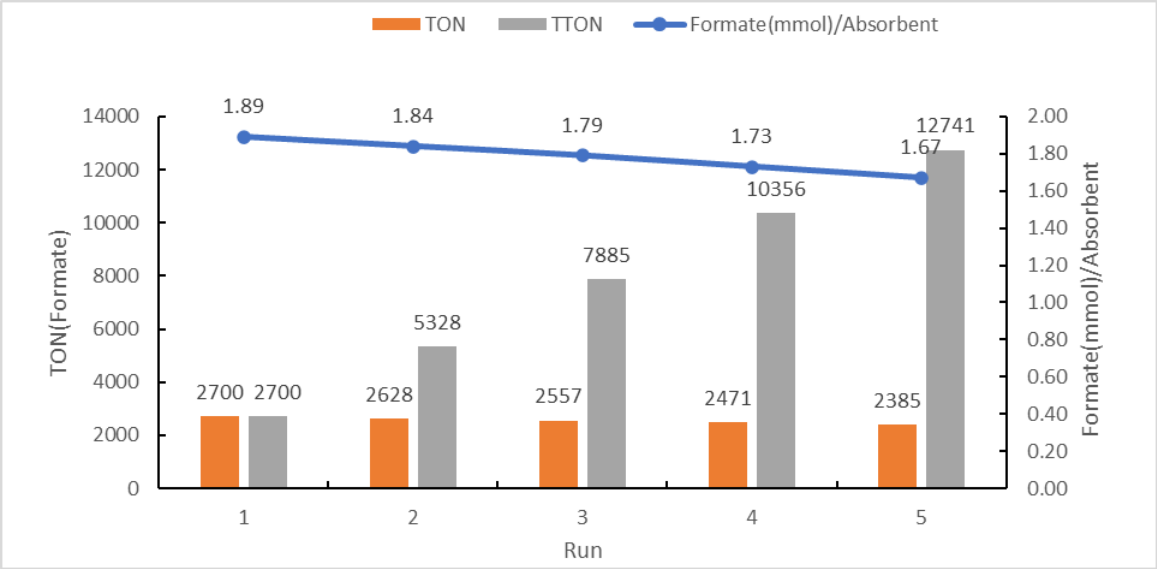


Figure 6. Catalyst reusability profile for hydrogenation of CO_2 to formate in the presence of [TBA][Arg]. Reaction conditions: [TBA][Arg] (5.0 mmol), **Ru-1**, H_2O/THF (5/5 mL) CO_2/H_2 (20/60 bar), 80 °C, 24 h. Reprint from ref.[133] with copyright permission.

To confirm that both the ionic liquid and the catalyst are essential for promoting CO_2 hydrogenation to formate, control experiments were carried out (Table 9). As expected, in the absence of the IL, the catalyst, or CO_2, no formate formation was observed.

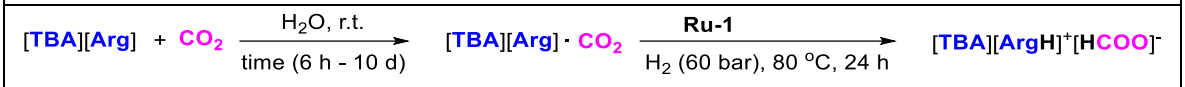
Table 9. Hydrogenation of CO_2 in the presence of [TBA][Arg] (blank experiments).

Entry	[TBA][Arg] [mmol]	Cat. [µmol]	Formate [mmol] [a]
1	5	None	n.d.
2	None	10	n.d.
3[b]	5	10	n.d.
Conditions: [TBA][Arg] (5.0 mmol), **Ru-1** (10 µmol), H_2O (5.0 mL), THF (5.0 mL), CO_2 (20 bar), H_2 (60 bar), 80 °C, 24 h. [a] Determined by ^1H NMR with DMF (250 µL, 3.24 mmol) as internal standard. [b] In the absence of CO_2. n.d.= not detectable.			

4.1.3. Integrated CO_2 capture and subsequent conversion to formate

Following separate investigations of (a) CO_2 absorption and (b) CO_2 reduction in the presence of [TBA][Arg], the overall carbon capture and utilization (CCU) process was demonstrated by integrating CO_2 capture with in situ hydrogenation to formate (Table 10). We attempted to directly convert the CO_2 captured by [TBA][Arg], as detailed in Table 4, into formate at 80 °C under 60 bar of hydrogen, without adding external CO_2. In the initial experiments, CO_2 absorption and subsequent hydrogenation were carried out at a CO_2 pressure of 20 bar. Under these conditions, 10.1 mmol of CO_2 was absorbed in the forms of carbamate and bicarbonate, as confirmed by ^{13}C-NMR (Figure A-15), resulting in 6.27 mmol of formate (Table 10, entry 1), corresponding to a turnover number (TON) of 627. When the CO_2 pressure was lowered to 2 bar, 9.70 mmol of CO_2 was captured (Carbamate and bicarbonate; Figure A-14) and then hydrogenated to produce 6.00 mmol of formate (Table10, entry 4), with a TON of 600.

Table 10. CO_2 capture and subsequent hydrogenation to formate in the presence of [TBA][Arg].



Entry	CO_2 source	Time [h]	Solvent	Captured CO_2 [mmol]	Formate [mmol][a]	Formate/Absorbent	TON[b]
1	CO_2 (20 bar)	6	H_2O/THF	10.1	1.25	1.25	627
2[c]	CO_2 (20 bar)	24	H_2O/THF	45.0	29.25	1.17	585
3[c]	CO_2 (20 bar)	24	H_2O	45.0	26.97	1.07	539
4	CO_2 (2 bar)	18	H_2O/THF	9.7	6.00	1.20	600
5[c]	CO_2 (2 bar)	96	H_2O/THF	44.1	28.79	1.15	575

6[c]	CO_2 (2 bar)	96	H_2O	44.1	26.00	1.04	520
7	Air	120	H_2O/THF	5.6	3.05	0.61	305
8[c]	Air	240	H_2O/THF	27.2	14.69	0.58	293
9[c]	Air	240	H_2O	27.2	12.90	0.51	258

Reaction conditions: CO_2 was first captured in an aqueous solution of [TBA][Arg] using the supplied CO_2 source for a period ranging from 6 to 240 hours, after which the resulting solution was subjected to hydrogenation. **Ru-1** (10 µmol), H_2O (5.0 mL), THF (5.0 mL), H_2 (60 bar), 80 °C, 24 h. [a] Determined by ^{1}H NMR with DMF (250 µL, 3.24 mmol) as internal standard. [b] Calculated by formate [mmol]/catalyst [mmol]. [c] 25 mmol [TBA][Arg], Ru-1 (50 µmol).

To assess the system's potential for DAC, ambient air was bubbled through an aqueous [TBA][Arg] solution (5 mmol) for five days, absorbing 5.61 mmol CO_2 as carbamate (Figure A-16). Subsequent hydrogenation produced 3.05 mmol formate (TON = 305; Table 10, entry 7). The procedure was scaled up fivefold and tested in both THF/water and pure water (Table 10, entries 2, 3, 5, 6, 8, and 9)

The catalyst's reusability was tested during scaled-up CO_2 capture (2 bar) and hydrogenation in sole water (Figure 7). Over three consecutive cycles ,using the same protocol, formate yield per mmol absorbent decreased slightly from 1.04 to 0.96, with a cumulative TON exceeding 7,200.

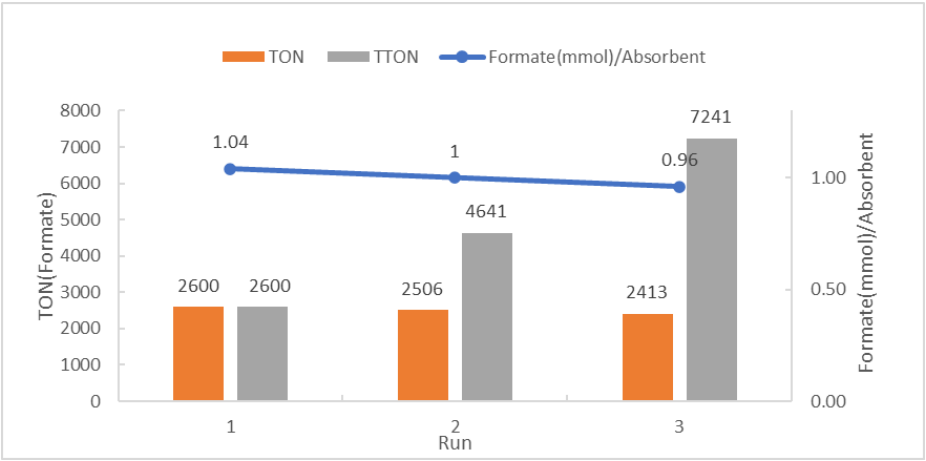


Figure 7. Catalyst reusability profile for the integrated CO_2 hydrogenation to formate. Reaction conditions adopted from Table 10, entry 6. Ru-1(10 µmol). Reprint from ref.[133] with copyright permission.

4.1.4. Summary

In summary, CO_2 capture followed by catalytic hydrogenation to formate was successfully achieved using AAILs as absorbents in aqueous THF solutions. Among the tested AAILs, [TBA][Arg] exhibited the highest CO_2 capture capacity. The captured CO_2 was efficiently hydrogenated to formate using the commercially available Ru-MACHO-BH (**Ru-1**) catalyst. The catalyst demonstrated excellent stability and reusability over five cycles, delivering an overall TON of 12,741 without significant loss of activity. Additionally, the CO_2 capture and hydrogenation process was successfully scaled up fivefold, achieving a total TON of 7,241 over three cycles even in the absence of organic co-solvent (THF). While 2 bar of pure CO_2 does not fully replicate real atmospheric conditions, the effective use of ambient air as a CO_2 source confirms the promising capability of amino acid-based ionic liquids for carbon capture and utilization.

4.2. CO_2 hydrogenation to methanol

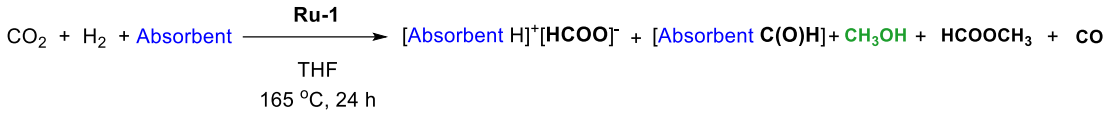
During the hydrogenation of CO_2 to formate in the presence of [TBA][Arg], the formation of formamide was observed as a result of the condensation of amino groups with formate. This transformation marks a key intermediate step in the sequential reduction of CO_2 toward methanol.[169] The formation of formamide became detectable at temperatures above 80 °C and significant at around 145 °C (Table 6). Consistent with literature reports, formamide hydrogenation represents the most challenging and kinetically demanding step in the overall CO_2-to-methanol pathway.[133] Building on these findings, we expanded our investigation to explore CO_2 hydrogenation to methanol using [TBA][Arg] and a series of other AAILs. The aim was to identify potential enhancements in the hydrogenation process for methanol production.

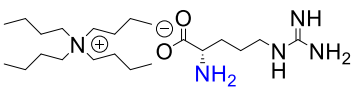
4.2.1. Screening of Amino Acid–Based Ionic Liquids

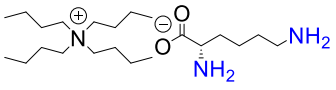
To identify suitable systems for the hydrogenation of CO_2 to methanol, a series of amino acid–based ionic liquids were screened under the specific reaction conditions required for methanol formation. This screening focused on evaluating how variations in the ionic liquid structure influence catalytic activity, selectivity, and stability under high-temperature hydrogenation conditions.

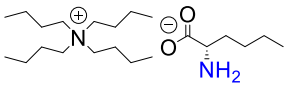
Experiments were conducted at 165 °C, the maximum temperature allowed by the autoclave and within the stable range of the **Ru-1** catalyst, due to its high chemical and thermal stability.[209] Reactions were carried out at 80 bar total pressure (H_2/CO_2 = 1:3) for 24 h in THF to aid catalyst dissolution. Unlike the hydrogenation experiments for CO_2 hydrogenation to formate, which were performed in mixed H_2O/THF media, water was deliberately excluded here because it promotes the hydrolysis of formamide back to formic acid. Therefore, only anhydrous THF was employed as solvent to suppress this side reaction and favor methanol formation. Formate and formamide were quantified by ^{1}H NMR, while methanol, methyl formate were analyzed by liquid chromatography. In addition, all the reactions were checked for CO formation using GC. Most experiments were performed in duplicate, and average values are reported in Table 11.

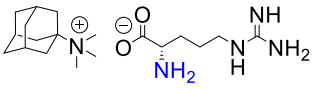
Table 11. Ru-1 aided CO_2 hydrogenation in the presence of various absorbents.

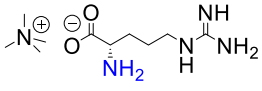


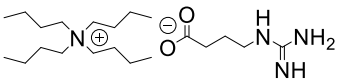

[TBA][Arg]

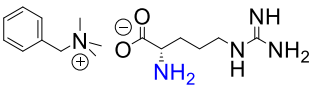

[TBA][Lys]

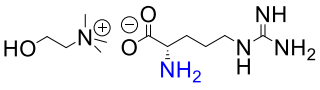

[TBA][Nor]

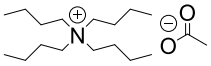

[TMAA][Arg]

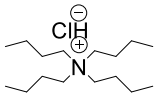

[TMA][Arg]

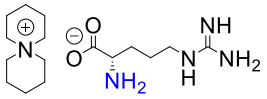

[TBA][GB]

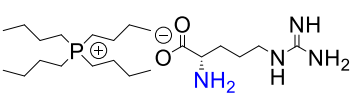

[BTMA][Arg]

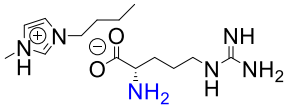

[CHO][Arg]


[TBA][OAc]


[TBA][Cl]


[ASU][Arg]


[TBP][Arg]


[BMIM][Arg]

entry	absorbent	formate[a] [mmol]	formamide[a] [mmol]	methanol[b] [mmol]	methyl formate[b] [mmol]	carbon monoxide[c] [mmol]
1	**[TBA][Arg]**	0.80	2.5	**2.5**	0.04	0.13
2	**[TBA[Lys]**	0.25	5.2	**0.14**	n.d.	0.13
3	**[TMAA][Arg]**	0.76	2.3	**1.4**	0.04	0.04
4	**[TMA][Arg]**	1.1	2.4	**1.3**	0.06	0.02
5	**[BTMA][Arg]**	0.98	2.1	**0.94**	0.01	0.02
6	**[CHO][Arg]**	1.4	1.8	**0.54**	0.01	0.15
7	**[ASU][Arg]**	3.5	3.8	**0.23**	0.004	0.07
8	**[TBP][Arg]**	4.1	2.6	**n.d.**	n.d.	0.17
9	**[BMIM][Arg]**	1.5	2.7	**0.13**	n.d.	0.12
10	**[TBA][OAc]**	n.d.	n.d.	**0.26**	0.02	0.08
11	**[TBA][Cl]**	n.d.	n.d.	**n.d.**	n.d.	n.d.
12	**[Arg]**	1.2	0.83	**0.11**	n.d.	0.06
13	**[Arg]+ K_3PO_4**	3.3	3.0	**0.12**	n.d.	0.06
14	**[Arg] + NBu_3**	1.4	1.6	**0.11**	n.d.	0.08
15	**[TBA][Nor]**	0.26	2.8	**n.d.**	n.d.	n.d.
16	**[TBA][GB]**	0.078	n.d.	**2.2**	0.15	0.17

Reaction conditions: Absorbent (5.0 mmol), **Ru-1**(10 µmol), THF (10 mL), CO_2/H_2 (20/60 bar), 165 °C, 24 h. [a] Determined by ^{1}H NMR with DMF (200 µL, 2.6 mmol) as internal standard. [b] Determined by LC with DMF (200 µL, 2.6 mmol) as internal standard. [c] Determined by gas GC. Experiments in entries 1-6, 9 and 14 were at least performed twice, and average values are shown. Standard deviations of main product amounts (formate, formamide, methanol) are 1-16 % of the average (except for formate in entry 4: 22% and methyl formate and carbon monoxide amounts < 0.15 mmol).

L-Argininate and L-lysinate tetrabutylammonium salts ([TBA][Arg] and [TBA][Lys]) were initially examined due to their superior performance, relative to other AAILs, in CO_2 capture and hydrogenation to formate using the **Ru-1** catalyst. Notably, the use of 5 mmol [TBA][Arg] led to the formation of 2.5 mmol methanol, along with 0.8 mmol formate and 2.5 mmol formamide (Table 11, entry 1). In contrast, [TBA][Lys] (Table 11, entry 2) produced 0.25 mmol formate and 5.2 mmol formamide, but yielded only 0.14 mmol methanol.

In reactions involving [TBA][Lys], high-resolution mass spectrometry (HRMS) of the post-reaction mixture revealed a lysine-derived fragment (Figure A-34), whose mass suggests that both the α- and ε-amino groups underwent formylation under the applied conditions. In contrast, when [TBA][Arg] was employed, only a mono-formylated group [210] was detected (Figure A-35). In this case, formylation at the α-amino group was confirmed through the independent synthesis of N-α-formyl-L-arginine and its corresponding TBA-based ionic liquid. The tetrabutylammonium salt (N-α-formyl-L-arginine·NBu_4) was prepared by neutralizing an aqueous solution of N-α-formyl-L-arginine with tetrabutylammonium hydroxide. However, since the synthesis involved a strongly basic aqueous medium, partial hydrolysis of the N-formyl group occurred during solvent removal under reduced pressure, releasing formic acid and preventing the isolation of a pure product (Figures A-29 and A-30).

A comparison between the ^{13}C NMR spectra of N-α-formyl-L-arginine and pure [TBA][Arg] with that of the post-reaction water-soluble residue obtained after CO_2 hydrogenation in the presence of [TBA][Arg] revealed a resonance at 163.6 ppm corresponding to the Nα-formyl carbon, while the guanidinium carbon remained unshifted at 156.8 ppm, confirming that no formylation occurred at the guanidino nitrogens (Figure A-31).

Hydrogenation of N-α-formyl-L-arginine under the same conditions outlined in Table 11, in the absence of CO_2, led to the formation of CH_3OH, supporting the role of the formamide intermediate as a viable precursor to methanol (Table 12, entry 1).

Table12. MeOH formation by Ru-1 catalyzed hydrogenation of *N*- α-formyl-L-Arginine.						
entry	**absorbent**	**formate**[a] [mmol]	**formamide**[a] [mmol]	**methanol**[b] [mmol]	**methyl formate**[b] [mmol]	**carbon monoxide**[c] [mmol]
1	Arg-N_α C(O)H + K_3PO_4	1.6	2.9	**0.42**	n.d.	0.03
2	TBA·Arg	1.1	3.6	**3.1**	0.005	1.5
General conditions: Absorbent (5.0 mmol), **Ru-1** (100 µmol), THF (10 mL), 150°C, 24 h); Entry 1: 5 mmol K_3PO_4, H_2 60 bars; Entry 2: CO_2/H_2 (20/60 bar), [a] Determined by ^{1}H NMR using DMF (200 µL, 2.6 mmol) as internal standard. [b] Determined by LC using DMF (200 µL, 2.6 mmol) as internal standard. [c] Determined by GC.						

Furthermore, when the TBA·Arg-assisted hydrogenation of CO_2 was carried out under otherwise identical conditions in the presence of varying amounts of CH_3OH to promote its condensation to methyl formate (Table 13, entries 2 and 3), no improvement in the overall methanol yield was observed, suggesting that ester hydrogenation is not the dominant pathway to CH_3OH.

Table 13. Influence of additives on CO_2 hydrogenation to methanol.

CO_2 + H_2 + TBA·Arg —(Ru-1; THF, 165 °C, 24 h; additive)→ TBA·[$ArgH^+$][$HCOO^-$] + TBA·[Arg**NC(O)H**] + CH_3OH + $HCOOCH_3$ + CO

entry	**additive**	**formate** [mmol] [a]	**formamide** [mmol] [a]	**methanol** [mmol] [b]	**methyl formate** [mmol] [b]	**carbon monoxide** [mmol] [c]
1	**-**	0.80	2.5	**2.5**	0.04	0.13
2	**methanol** [1.23 mmol]	0.63	2.4	**1.9**	0.06	0.12
3	**methanol** [50 µmol]	0.83	2.6	**2.4**	0.02	0.13
4	**K_3PO_4** [2 mmol]	1.4	2.0	**2.9**	0.04	0.14
5	**molecular sieves** [3 A°, 2 g]	0.57	2.3	**1.3**	0.04	0.11
General conditions: [TBA][Arg] (5.0 mmol), Ru-MACHO-BH (10 µmol), THF (10 mL), CO_2/H_2 (20/60 bar), 165 °C, 24 h. [a] Determined by ^{1}H NMR with DMF (200 µL, 2.6 mmol) as internal standard. [b] Determined by LC with DMF (200 µL, 2.6 mmol) as internal standard. [c] Determined by gas GC. Experiments in entries 1and 2 were at least performed twice, and average values are shown. Standard deviations of main product amounts (formate, formamide, methanol) are 1-12 % of the average (except for methanol in entry 2: 25% and methyl formate and carbon monoxide amounts < 0.10 mmol).						

Several other ammonium cations paired with L-arginine were evaluated, each featuring distinct nitrogen substituents. These included N,N,N-trimethyladamantan-1-ammonium ([TMAA][Arg], Table 11, entry 3, CH_3OH 1.4 mmol), tetramethylammonium ([TMA][Arg], Table 11, entry 4, CH_3OH 1.3 mmol), benzyltrimethylammonium ([BTMA][Arg], Table 11, entry 5, CH_3OH 0.94 mmol), choline ([CHO][Arg], Table 11, entry 6, CH_3OH 0.54 mmol) and 6-azonia-spiro[5.5]undecane ([ASU][Arg], Table 11, entry 7, CH_3OH 0.23 mmol), the latter being a more base-stable cation[211]: The amount of methanol produced in the presence of [TBA][Arg] exceeded that of all other ammonium-arginine combinations tested. Substituting the TBA cation with its phosphonium analogue ([TBP][Arg], Table 11, entry 8) resulted in a complete suppression of methanol formation, despite similar levels of formate (4.1 mmol) and formamide (2.6 mmol) being produced. When the 1-butyl-3-methylimidazolium cation was used instead, methanol production remained low, with only 0.13 mmol detected. ([BMIM][Arg], Table 11, entry 9). The critical contribution of the L-argininate anion was further highlighted by replacing it with other anions: only 0.26 mmol of CH_3OH was observed with acetate ([TBA][OAc], Table 11, entry 10), and virtually no methanol was detected with chloride ([TBA][Cl], Table 11, entry 11), likely due to catalytic inhibition by the chloride ion. Furthermore, using L-arginine alone (Table 11, entry 12), or in conjunction with external bases such as K_3PO_4 or NBu_3, resulted in only 0.11 mmol of methanol (Table 11, entry 13 and1 4). These findings underscore the synergistic interaction between the TBA cation and the L-argininate anion in enhancing CH_3OH production.

In order to investigate the effect of the amino acid side chain on CO_2 hydrogenation, [TBA][Nor] and [TBA][GB] were synthesized from L-norleucine and 4-guanidinobutyric acid, respectively. When [TBA][Nor] was employed, only about half the amounts of formate and formamide were produced compared to [TBA][Lys] (Table 11, entry 15; 0.26 mmol formate and 2.8 mmol formamide), indirectly suggesting that both amino groups in [TBA][Lys] participate in formylation. However, no methanol was detected with [TBA][Nor]. This absence of CH_3OH could be attributed to a lack of sufficient basicity in the medium once both amino groups are formylated, which may hinder further hydrogenation of the formamide.[212] In contrast, [TBA][GB] - lacking an amino group -yielded minimal formate (0.078 mmol) and no formamide (Table 11, entry 16), yet produced methanol levels similar to [TBA][Arg], underscoring the importance of the guanidino group in promoting CH_3OH formation.

Based on these findings, [TBA][Arg] emerged as the most effective ionic liquid among those tested and was selected for further studies aimed at probing the effects of key reaction variables, including solvent choice, temperature, CO_2/H_2 pressure ratio, and catalyst structure.

4.2.2. Effect of Reaction Parameters

Influence of solvent. Initial investigations explored alternative solvents to THF (**Figure 8**), given their potential influence on both thermodynamic and kinetic aspects of hydride transfer from the catalyst to CO_2 and formamide substrates.[213] Ethers generally showed the best performance, except cyclopentyl methyl ether, which produced no detectable methanol. In contrast, Alcohols negatively affected selectivity, producing minimal methanol and significant CO, likely due to aldehyde decarbonylation from **Ru-1**-catalyzed alcohol dehydrogenation.[212] Ethylene glycol exemplifies this effect, with CO levels reaching up to 5.7 mmol. Its tendency to undergo dehydrogenation to glycolate under high hydrogen pressure (70 bar) has previously been documented by Prakash in the **Ru-1**-mediated hydrogenation of air-captured CO_2 using hydroxide in ethylene glycol. [214] Since none of the tested solvents outperformed THF within error margins, THF was retained for further investigations.

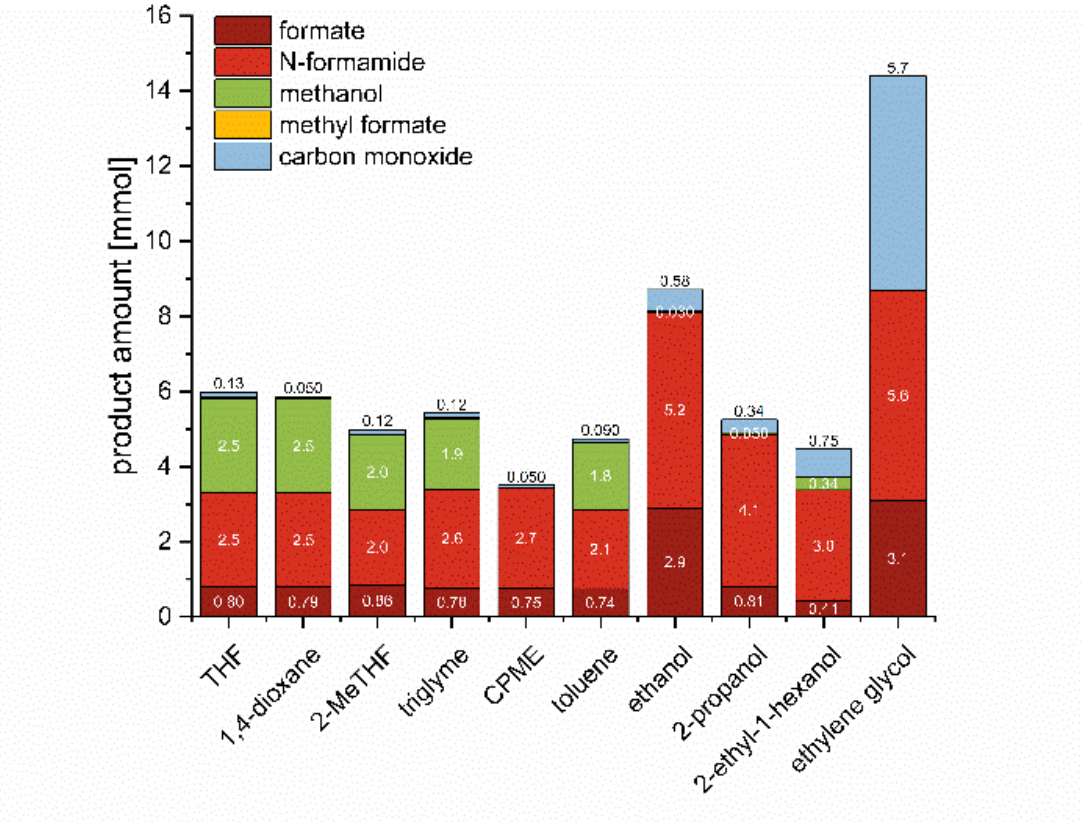
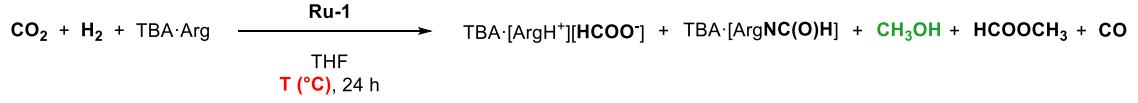


Figure 8. Effect of solvent on product distribution in the **Ru-1** catalyzed hydrogenation of CO_2. Reaction conditions: [TBA][Arg] (5.0 mmol), **Ru-1** (10 µmol), solvent (10 mL), CO_2/H_2 (20/60 bar), 165 °C, 24 h. CPME = cyclopentyl methyl ether. Numbers represent amounts (mmol) of formate, formamide, methanol, and carbon monoxide, respectively. Reprint from ref.[177] with copyright permission.

Influence of temperature. The effect of reaction temperature on product yields and distribution was examined between 110 and 165 °C (Table 14). Methanol formation was not observed below 110 °C, despite significant formate (11.2 mmol) and formamide (4.8 mmol) accumulation (Table 14, entry 1). Detectable amounts of methanol appeared at 120 °C, increased notably at 150 °C (Table 14, entry 5, 2.0 mmol), and peaked at 165 °C (Table 14, entry 8, 2.5 mmol). indicating that hydrogenation of formamide to methanol is more energy-demanding than CO_2-to-formate conversion.[212] Raising the temperature from 120 to 130 °C led to a marked decrease in formate concentration - from 8.8 mmol to 1.7 mmol - even though the formamide concentration rose only slightly (from 6.5 to 6.9 mmol), and methanol increased from 0.03 to 0.13 mmol (Table 14, entry 2 vs entry 3). This highlights the difficulty of aligning the temperature requirements for CO_2-to-formate conversion, which is favored at lower temperatures, with the subsequent steps formamide formation and its hydrogenation to methanol, which require more severe conditions.[215] At elevated temperatures, the reverse reaction, formate dehydrogenation, proceeds more readily, even under a total pressure of 80 bar.[216, 217] Concurrently, As formamide levels increase, water produced as a by-product may accumulate, potentially causing hydrolysis of formamide back to formate.[218] The use of molecular sieves to remove water - intended to suppress formamide hydrolysis and enhance its subsequent hydrogenation to methanol - proved ineffective (Table 13, entry 5). CO formation was detected above 110 °C and increased with temperature, reaching 0.13 mmol at 165 °C (Table 14, entry 8).

Table 14. Influence of temperature on CO_2 hydrogenation to methanol.



entry	T [°C]	formate[a] [mmol]	formamide[a] [mmol]	methanol[b] [mmol]	methyl formate[b] [mmol]	carbon monoxide[c] [mmol]
1	110	11.2	4.8	n.d.	n.d.	n.d.
2	120	8.8	6.5	0.03	n.d.	0.01
3	130	1.7	6.9	0.13	0.01	0.02

4	140	0.64	7.3	**0.41**	0.01	0.05
5	150	1.2	4.0	**2.0**	0.02	0.06
6	155	0.91	3.9	**2.2**	0.02	0.07
7	160	0.91	3.3	**2.4**	0.05	0.08
8	165	0.80	2.5	**2.5**	0.04	0.13

General conditions: [TBA][Arg] (5.0 mmol), Ru-MACHO-BH (10 µmol), THF (10 mL), CO_2/H_2 (20/60 bar), 165 °C, 24 h. [a] Determined by ^1H NMR with DMF (200 µL, 2.6 mmol) as internal standard. [b] Determined by LC with DMF (200 µL, 2.6 mmol) as internal standard. [c] Determined by gas GC. Experiments in entries 1 and 3-8 were at least performed twice, and average values are shown. Standard deviations of main product amounts (formate, formamide, methanol) are 2-12 % of the average (except for methyl formate and carbon monoxide amounts < 0.10 mmol).

Influence of CO_2/H_2 ratio. Literature reports indicate that decreasing the relative CO_2/H_2 pressure ratio can suppress CO formation during CO_2 hydrogenation to methanol[166, 219] — as CO acts as a catalyst poison— while simultaneously enhancing CH_3OH yield.[166, 220] To verify this in our system, we performed a series of experiments in which the CO_2 partial pressure was gradually reduced, while maintaining a constant total pressure of 80 bar. As shown in **Figure 9**, decreasing the CO_2 pressure from 30 to 5 bar led to an almost threefold reduction in CO formation (from 0.13 to 0.05 mmol), attributed to the lower CO_2 concentration in the reaction medium. Simultaneously, methanol production increased from 2.3 to 2.8 mmol, highlighting the positive influence of a higher H_2 partial pressure on the hydrogenation of formamide to methanol.

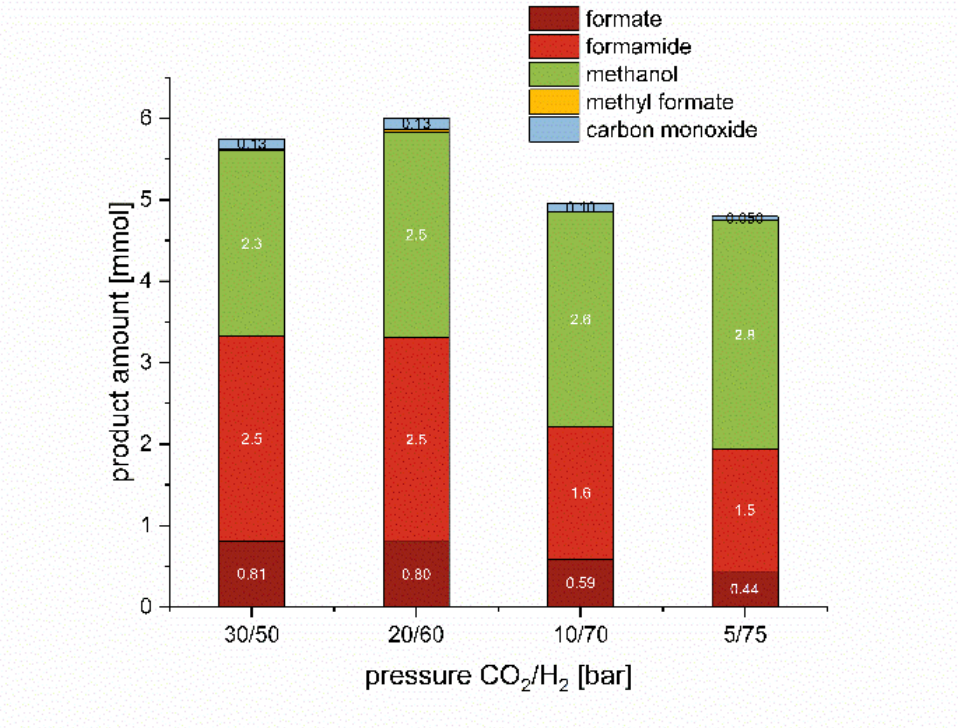
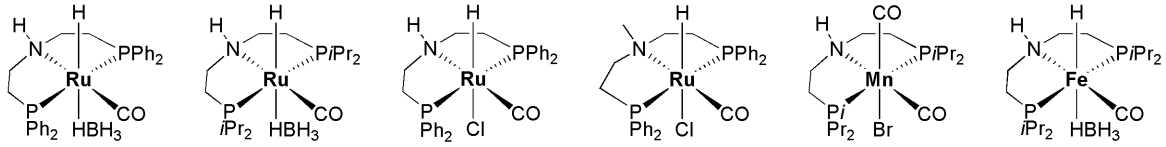


Figure 9. Product distribution as a function of relative CO_2/H_2 pressure ratio in the **Ru-1** promoted hydrogenation of CO_2. Reaction conditions: [TBA][Arg] (5.0 mmol), **Ru-1** (10 µmol), THF (10 mL), 165 °C, total pressure 80 bar, 24 h. Numbers represent amounts (mmol) of formate, formamide, methanol and carbon monoxide, respectively. Reprint from ref.[177] with copyright permission.

Influence of catalyst type. A series of alternative catalysts were examined to determine whether modifications in ligand structure and metal center could enhance CH_3OH production. The catalysts evaluated and their corresponding results are listed in Table 15. Substituting the phenyl groups with more electron-donating isopropyl substituents in **Ru-2** (Table 15, entry 2) led to a marginally increased formation of formate, though CH_3OH production declined. Further investigation showed that **Ru-3**, a chloride variant of **Ru-1**, also effectively catalyzes CO_2 hydrogenation to methanol (Table 15, entry 3). Additionally, **Ru-4** (Table 15, entry 4) was tested, where the ligand nitrogen's hydrogen was replaced by a methyl group.

Table 15. TBA·Arg- assisted hydrogenation of CO_2 in the presence of different catalyst precursors.





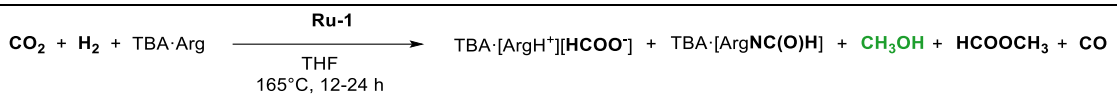
entry	catalyst	formate[a] [mmol]	formamide[a] [mmol]	methanol[b] [mmol]	methyl formate[b] [mmol]	carbon monoxide[c] [mmol]
1	**Ru-1**	1.2	4.0	**2.0**	0.02	0.06
2	**Ru-2**	1.3	5.4	**1.1**	0.02	0.007
3	**Ru-3**	0.81	3.0	**2.1**	0.01	0.07
4	**Ru-4**	0.73	4.2	**0.03**	n.d.	1.5
5	**Mn-1**	0.41	4.5	**0.02**	n.d.	n.d.
6	**Fe-1**	0.10	2.9	**n.d.**	n.d.	0.01

General conditions: [TBA][Arg] (5.0 mmol), catalyst (10 µmol), THF (10 mL), CO_2/H_2 (20/60 bar), 165 °C, 24 h. [a] Determined by ^{1}H NMR with DMF (200 µL, 2.6 mmol) as internal standard. [b] Determined by LC with DMF (200 µL, 2.6 mmol) as internal standard. [c] Determined by gas GC. Experiments in entries 1-3 were at least performed twice, and average values are shown. Standard deviations of main product amounts (formate, formamide, methanol) are 1-15 % of the average (except methyl formate and carbon monoxide amounts < 0.10 mmol).

Comparison of entries 3 and 4 in Table 15 shows that **Ru-4** efficiently hydrogenates CO_2 to formate but is much less effective in converting formamide to methanol via hydrogenolysis.[166] This pattern was also reported by Prakash et al. during Ru-4-catalyzed, amine-assisted CO_2 hydrogenation to CH_3OH. The data indicate that successful formamide hydrogenation to CH_3OH via formaldehyde requires ligand–metal cooperation, particularly involving an –NH group for hydrogen bonding and substrate activation.[221]. However, this interaction appears unnecessary for the initial conversion of CO_2 to formate.[222] When ruthenium was replaced by first-row transition metals - manganese in **Mn-1** (Table 15, entry 5) or iron in **Fe-1** (Table 15, entry 6) -

formate yields dropped significantly and methanol formation was almost entirely suppressed. These results align with previous studies, which showed that **Mn-1**[223] and **Fe-1**[170] catalysts cannot directly hydrogenate CO_2 to CH_3OH in the presence of amines.[224] Instead, a two-step, one-pot approach is needed: CO_2 is first hydrogenated to formate, and after releasing excess CO_2, the subsequent hydrogenation of the resulting formamide can proceed. This is because excess CO_2 inhibits the reduction of formamides.[211] This inhibitory effect, although less severe, was also noted for **Ru-1**, as illustrated earlier (Figure 9). Only a modest increase in CH_3OH productivity was obtained when, relative to the one-pot, one-step procedure at 165 °C (Table 16, entry 1; 2.3 mmol), the autoclave was vented to release excess CO_2 after the first step and then re-pressurized with H_2 alone to 60 bar (Table 16, entry 2; 2.6 mmol). By contrast, adding a second batch of **Ru-1** markedly improved the outcome (Table 16, entry 3; 3.0 mmol CH_3OH), indicating that thermal degradation of the catalyst during prolonged heating is the primary cause of unconverted formamide.

Table 16. Stepwise hydrogenation of CO_2 in the presence of [TBA][Arg].



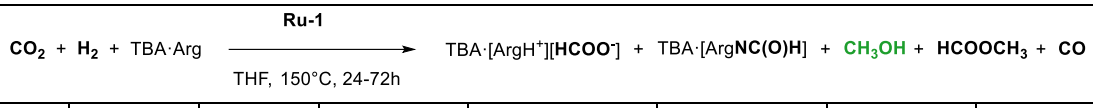
entry	step 1	step 2	formate [mmol] [a]	formamide [mmol] [a]	methanol [mmol] [b]	methyl formate [mmol] [b]	carbon monoxide [mmol] [c]
1	12 h CO_2/H_2 20/60 bars	-	1.3	2.1	**2.3**	0.02	0.09
2[d]	12 h CO_2/H_2 20/60 bars	12 h H_2 60 bars	0.47	1.8	**2.6**	0.01	0.10
3[e]	12 h CO_2/H_2 20/60 bars	12 h CO_2/H_2 20/60 bars	1.4	2.7	**3.0**	0.02	0.15

General conditions: [TBA][Arg] (5.0 mmol), Ru-MACHO-BH (10 µmol), THF (10 mL), 165 °C. [a] Determined by ^1H NMR with DMF (200 µL, 2.6 mmol) as internal standard. [b] Determined by LC with DMF (200 µL, 2.6 mmol) as internal standard. [c] Determined by permanent gas GC. [d] After the first step, pressure has been released and the autoclave

recharged with H_2 at the desired pressure. [e] After the first step, pressure has been released and the autoclave recharged with a new batch of catalyst and then pressurised with CO_2 and H_2 at the desired pressure.

Influence of catalyst amount. Regarding the effect of catalyst loading, increasing the catalyst concentration from 5 to 100 µmol led to nearly a twofold increase in methanol production (1.6 vs 3.0 mmol; Table 17, entries 2 to 5). Additionally, extending the reaction time to 48 hours resulted in a further 20% increase in methanol yield (Table 17, entry 6). Although the smallest amount of methanol (1.4 mmol) was produced when using just 2 µmol of catalyst, this condition delivered the highest turnover number (TON: 700, Table 17, entry 1). It is also worth noting that varying levels of carbon monoxide were detected across all experiments.

Table 17. Influence of catalyst loading on CO_2 hydrogenation to methanol.



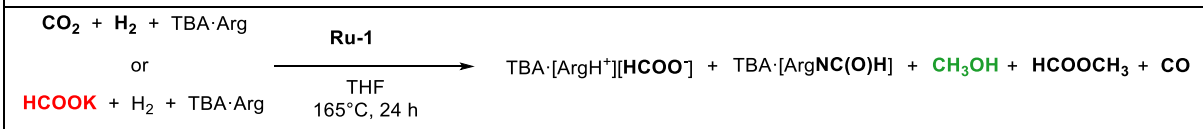
entry	Ru-1 [µmol]	time [h]	formate[a] [mmol]	formamide[a] [mmol]	methanol[b] [mmol]	methyl formate[b] [mmol]	carbon monoxide[c] [mmol]
1	2	24	0.71	3.4	**1.4**	0.02	0.01
2	5	24	0.68	3.7	**1.6**	0.02	0.02
3	10	24	1.2	4.0	**2.0**	0.02	0.06
4	50	24	0.74	4.8	**2.2**	0.001	0.76
5	100	24	1.2	3.5	**3.0**	0.005	1.6
6	100	48	0.99	4.2	**3.6**	0.008	2.7
7	100	72	0.84	4.2	**3.4**	0.005	3.0

General conditions: TBA·Arg (5.0 mmol), THF (10 mL), CO_2/H_2 (20/60 bar), 150 °C. [a] Determined by ^1H NMR with DMF (200 µL, 2.6 mmol) as internal standard. [b] Determined by LC with DMF (200 µL, 2.6 mmol) as internal standard. [c] Determined by permanent gas GC. Experiments in entries 1-5 and 7 were at least performed twice, and average values are shown. Standard deviations of main product amounts (formate, formamide, methanol) are 1-17 % of the average (except for formate and formamide in entry 7 (27% and 19%, respectively) and methyl formate and carbon monoxide amounts < 0.10 mmol).

In experiments where CO_2 hydrogenation was performed with [TBA][Arg] in THF using **Ru-1** under a CO_2/H_2 pressure of 20/60 bar, an increase in temperature (Table 14) and reaction time led to higher levels of CO formation. The CO concentration also appeared to correlate with the relative CO_2 pressure—greater CO_2/H_2 ratios resulted in higher formate ($HCOO^-$) yields and reduced methanol production, alongside an

increase in CO (Figure 9). Interestingly, no CO was detected when equimolar amounts of [TBA][Arg] and HCOOK were exposed to 60 bar H_2 at 165 °C in the presence of **Ru-1** (Table 18, entry 2), suggesting that formate is not the origin of CO in this system. A strong positive dependence on catalyst concentration was also observed (Table 17). For instance, when reactions were conducted in 10 mL of THF at 150 °C under 20/60 bar CO_2/H_2 for 24 hours, the CO amount rose from 0.01 mmol (Table 17, entry 1) to to 1.6 mmol (Table 17, entry 5) as the Ru-1 concentration increased from 2 µmol to 100 µmol. Extending the reaction duration to 48 hours caused the CO amount to nearly double, reaching 2.7 mmol (Table 17, entry 6).

Table 18. CO source



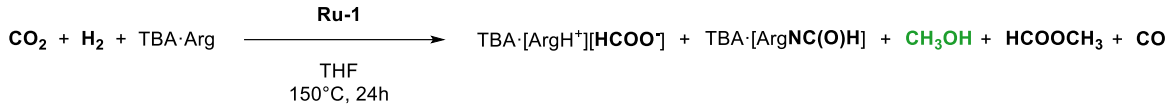
entry	CO_2 [bar]	H_2 [bar]	HCOOK addition [mmol]	formate[a] [mmol]	formamide[a] [mmol]	methanol[b] [mmol]	methyl formate[b] [mmol]	carbon monoxide[c] [mmol]
1	20	60	-	0.80	2.5	2.5	0.04	0.13
2	-	60	5	2.1	1.1	0.049	n.d.	n.d.

General conditions: TBA·Arg (5.0 mmol), **Ru-1** (10 µmol), THF (10 mL), 165 °C, 24 h. [a] Determined by ^{1}H NMR with DMF (200 µL, 2.6 mmol) as internal standard. [b] Determined by LC with DMF (200 µL, 2.6 mmol) as internal standard. [c] Determined by permanent gas GC.

Although the exact source of CO was not thoroughly investigated, the reaction conditions - temperatures between 120–165 °C and a total pressure of 80 bar - are consistent with the reverse water-gas shift (RWGS) reaction, which could be responsible for CO formation.[225] Additionally, CO may also originate from the decarbonylation of formaldehyde, an intermediate in the pathway from formamide to methanol. Notably, **Ru-4**, which features a methyl substituent on the ligand nitrogen, produced a significant amount of CO (1.5 mmol) but yielded almost no methanol, in contrast to Ru-1, which generated only 0.06 mmol CO alongside 2.0 mmol of CH_3OH (Table 15, entries 4 and 1, respectively). The elevated CO levels act as a catalyst poison by forming a ruthenium dicarbonyl species, a phenomenon previously detailed by Prakash in his investigation of ruthenium-pincer-catalyzed, amine-assisted CO_2 hydrogenation to methanol.[226] In support of this, when CO_2 hydrogenation was carried out using **Ru-1** in the presence of externally added CO from the start, the methanol yield was noticeably lower compared to the reaction performed without CO (Table 19,

entry 2 vs entry 1, 2.4 vs 3.0 mmol). However, the formation of formate and formamide remained largely unchanged, reinforcing Prakash's conclusion that the dicarbonyl complex can still catalyze CO_2 hydrogenation to formate salts, but is ineffective in facilitating the conversion of formamides into methanol and amines.[226]The dicarbonyl species can be converted back to the catalytically active dihydride species under high hydrogen pressure. The reduced efficiency of Ru-2 in producing methanol, compared to **Ru-1** (Table 15, entry 2 vs entry 1), is likely due to Ru-2's greater susceptibility to CO inhibition. In **Ru-2**, the stronger Ru–CO bond -resulting from increased electron density at the metal center - makes the displacement of CO by hydrogen more difficult, thereby hindering catalyst regeneration and activity.[226]

Table19. CO poisoning effect

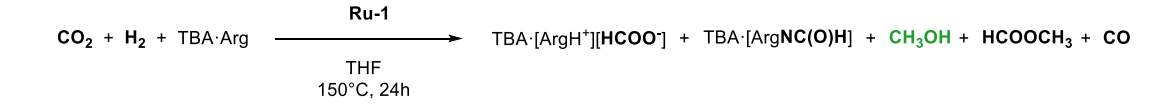


entry	addition of (exogenous) CO	formate[a] [mmol]	formamide[a] [mmol]	methanol[b] [mmol]	methyl formate[b] [mmol]	carbon monoxide[c] [mmol]
1	-	1.2	3.5	3.0	0.005	1.6
2[d]	+	1.0	3.2	2.4	0.01	7.8

General conditions: TBA·Arg (5.0 mmol), **Ru-1** (100 µmol), THF (10 mL), CO_2/H_2 20/60, 150 °C, 24 h. [a] Determined by ^1H NMR with DMF (200 µL, 2.6 mmol) as internal standard. [b] Determined by GC with DMF (200 µL, 2.6 mmol) as internal standard. [c] Determined by permanent gas GC. [d] The autoclave was purged with CO and subsequently pressurized with CO_2 and H_2 to the desired total pressure.

Impact of dilution: Increasing the volume of THF from 10 to 20 and then to 30 mL resulted in a modest rise in methanol yield, from 3.0 to 3.2 and then to 3.8 mmol (Table 20). However, the most notable effect was observed on CO formation, which was reduced by more than half upon dilution, decreasing from 1.6 (Table 20, entry 1) to 0.72 mmol at the highest solvent volume (Table 20, entry 3). This trend is consistent with the observations made at higher catalyst concentrations (Table 17).

Table 20. Influence of dilution on CO_2 hydrogenation to methanol.



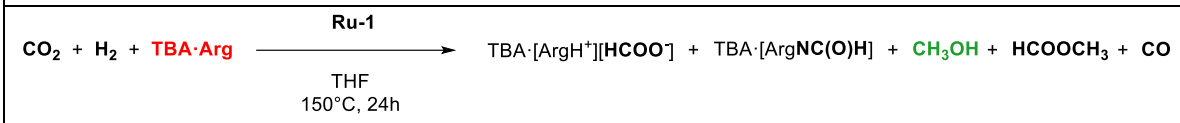
entry	THF [ml]	formate[a] [mmol]	formamide[a] [mmol]	methanol[b] [mmol]	methyl formate[b]	carbon monoxide[c]

					[mmol]	[mmol]
1	10	1.2	3.5	**3.0**	0.005	1.6
2	20	1.2	2.6	**3.2**	0.001	1.1
3	30	1.0	2.2	**3.8**	n.d.	0.72

General conditions: [TBA][Arg] (5.0 mmol), **Ru-1** (100 µmol), THF (10 mL), CO_2/H_2 20/60, 150 °C, 24 h. [a] Determined by ^{1}H NMR with DMF (200 µL, 2.6 mmol) as internal standard. [b] Determined by LC with DMF (200 µL, 2.6 mmol) as internal standard. [c] Determined by permanent gas GC. Experiments in entries 1 to 3 were at least performed twice, and average values are shown. Standard deviations of all product amounts are 1-13 % of the average.

Influence of [TBA][Arg] amount. doubling the quantity of [TBA][Arg] from 5 (Table 21, entry 1) to 10 mmol (Table 21, entry 2), in 10 mL of THF, while keeping other conditions constant, led to more than a twofold increase in both formate (from 1.2 to 2.1 mmol) and formamide (from 3.5 to 9.8 mmol). In contrast, the methanol amount increased only slightly, from 3.0 to 3.8 mmol. These findings suggest that [TBA][Arg] is an effective agent for CO_2 capture and activation, facilitating **Ru-1** catalyzed hydrogenation to formate and subsequent formamide formation. Nevertheless, the final step of reducing formamide to methanol remains challenging. Drawing on insights gained from screening various ionic liquids, catalyst precursors, and reaction conditions, an optimized experiment was conducted under the most favorable parameters, resulting in a nearly threefold increase in methanol yield, reaching 5.8 mmol (Figure 10).

Table 21. Influence of the amount of [TBA][Arg] on CO_2 hydrogenation to methanol.



entry	**TBA·Arg** [mmol]	**formate**[a] [mmol]	**formamide**[a] [mmol]	**methanol**[b] [mmol]	**methyl formate**[b] [mmol]	**carbon monoxide**[c] [mmol]
1	5	1.2	3.5	**3.0**	0.005	1.6
2	10	2.1	9.8	**3.8**	0.02	1.8

General conditions: **Ru-1** (100 µmol), THF (10 mL), 150 °C, 24 h. [a] Determined by ^{1}H NMR with DMF (200 µL, 2.6 mmol) as internal standard. [b] Determined by GC with DMF (200 µL, 2.6 mmol) as internal standard. [c] Determined by permanent gas GC. Experiments in entries 1 and 2 were at least performed twice, and average values are shown. Standard deviations of all product amounts are 0-11 % of the average.

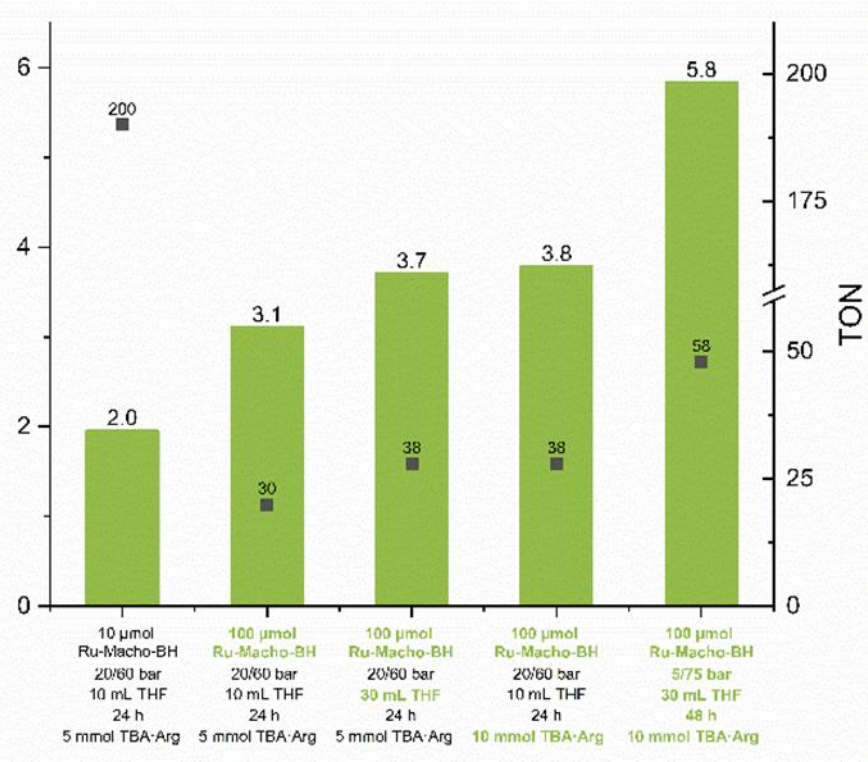
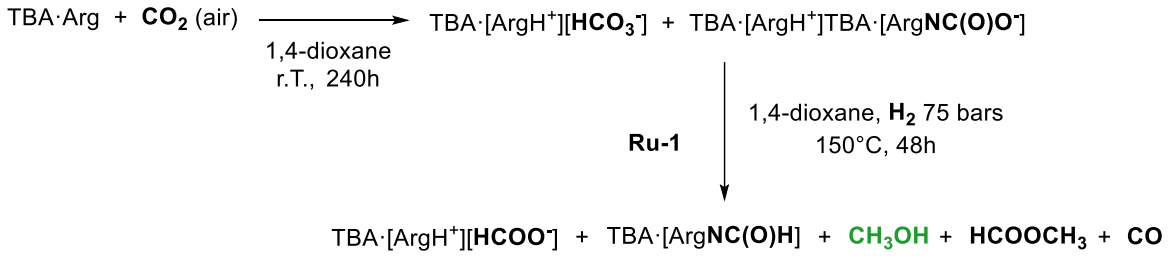


Figure 10. TBA·Arg-assisted hydrogenation of CO_2 catalysed by **Ru-1** under stepwise optimized conditions**.** General conditions: [TBA][Arg], solvent, catalyst, pressure CO_2/H_2 (bar/bar), 150°C. Reprint from ref.[177] with copyright permission.

4.2.3. CO_2 capture from air and subsequent hydrogenation to methanol

We also demonstrated the direct air capture of CO_2 using [TBA][Arg], (Table 22). Although the uptake was limited (CO_2/[TBA][Arg] ratio of 0.35) compared to 1.09 in aqueous solution, this difference is attributed to the low solubility of CO_2 in 1,4-dioxane at room temperature. The successful chemisorption of CO_2 was confirmed by ^{13}C NMR spectroscopy (Figure A-18). Despite the lower capture capacity, the absorbed CO_2 could be directly hydrogenated under optimized conditions, achieving 94% conversion and 80% selectivity toward methanol.

Table 22. CO_2 capture from air and subsequent hydrogenation to methanol.



captured CO_2[a] [mmol]	Formate[b] [mmol]	Formamide[b] [mmol]	Methanol[c] [mmol]	methyl formate[c] [mmol]	carbon monoxide[d] [mmol]
1.76	0.31	n.d.	**1.32**	n.d.	0.02

Reaction conditions: CO_2 capture: [TBA][Arg] (5 mmol), 1,4-dioxane (20 mL); hydrogenation of captured CO_2: **Ru-1** (100 µmol), 1,4-dioxane (30 mL), H_2 (75 bar), 150°C, 48 h. [a] Determined by quantitative ^{13}C NMR with DMF (100 µL, 1.3 mmol) as internal standard (exp. 1). [b] ^{1}H NMR with DMF (200 µL, 2.6 mmol) as internal standard. [c] Determined by LC with DMF (200 µL, 2.6 mmol) as internal standard. [d] Determined by permanent gas GC.

4.2.4. Structural and Functional Characteristics of [TBA][Arg] in CO_2 Hydrogenation to Methanol

Among the ILs tested, the combination of the tetrabutylammonium (TBA) cation with the L-arginine anion proved to be the most effective reaction system. Although both basic amino acids, e.g. L-arginine and L-lysine, can form ILs with the TBA cation and exhibit similar performance in CO_2 capture and its Ru-1-catalyzed hydrogenation to formate (Table 11, entries 1 and 2), the L-arginine-based system showed significantly greater efficiency in promoting the further reduction to methanol. This enhanced performance is likely due to the presence of the guanidino group in L-arginine, which distinguishes it structurally and functionally from L-lysine.

[TBA][Arg] is synthesized by reacting an aqueous solution of NBu_4·OH with L-arginine in its zwitterionic form. [179] Despite extended drying under high vacuum, the resulting ionic liquid consistently retains trace amounts of “confined” water.[188] Due to the high basicity of the guanidino side chain (pKa_3 = 13.8),[190] it remains protonated and tends to form a coordinated hydroxo complex, even in the presence of excess hydroxide ions

and regardless of additional water content.[191] This behavior also explains why the guanidino group - unlike the α-amino group of the arginine anion - does not undergo formylation. Nevertheless, the methanol yield achieved with [TBA][GB] is similar to that obtained using [TBA][Arg] (Table 11, entry 1 vs entry 16). [TBA][GB] lacks an amino group and in fact no formamide was detected (Table 11, Entry 16, Figures A-36 and A-37). This observation suggests that, in this case, methanol is likely produced via Ru-1-catalyzed ester hydrogenation. Supporting this, both n-butanol (from base-induced degradation of the TBA cation) and n-butyl formate (n-BuOOCH) were detected in the THF post-reaction solution obtained after Ru-1-catalyzed CO_2 hydrogenation in the presence of [TBA][GB] (Figures A-38 and A-39).

Notably, TBA cation degradation also occurs with [TBA][Lys], yet the methanol yield remains lower than that observed with [TBA][GB] under comparable conditions. These findings highlight the importance of the guanidino group in promoting methanol formation.

It is well established that guanidinium cations whether unsubstituted or mono-substituted act as strong hydrogen bond donors, and through such interactions with suitable substrates, they can enhance and direct organic transformations.[227] In the current study, hydrogen bonding between the arginine-derived moiety and intermediates such as formamides or formate esters may increase their electrophilicity, thereby facilitating their reduction and contributing to the higher activity observed with [TBA][Arg]. Moreover, this interaction may also aid in the initial activation of CO_2, as L-arginine frequently appears in the CO_2-binding sites of enzymes. [227, 228] Structural data from CO_2-binding proteins reveal a recurring feature in which the protonated side chain of basic amino acid residues, notably arginine or lysine, forms hydrogen bonds with one of CO_2's oxygen atoms.[228] This interaction enhances the polarization of the CO_2 molecule, making the central carbon more susceptible to nucleophilic attack. However, attempts to improve CH_3OH productivity through recycling experiments were unsuccessful. Under the reaction conditions, the TBA cation degraded into tributylamine, butene, and butanol (Figures A-34, A-40 and A-41).

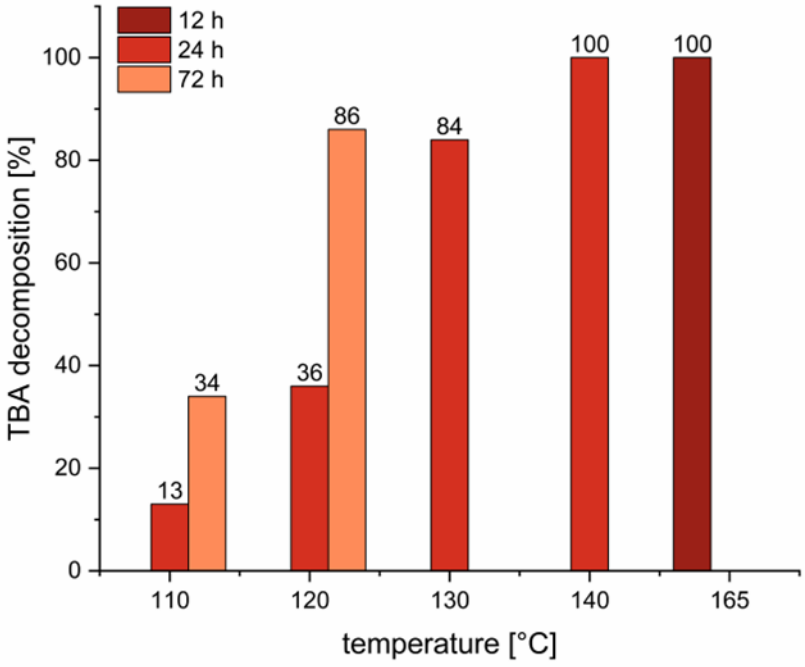
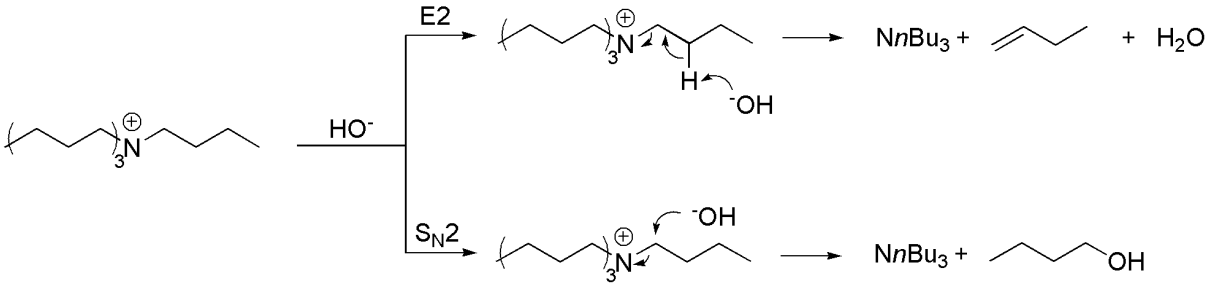


Figure 11. Decomposition of TBA·Arg *f* (T, t). Reprint from ref.[177] with copyright permission.

Decomposition occurs via two parallel mechanisms (Scheme 6): (i) an E2-type Hofmann elimination and (ii) an S_n2 substitution pathway, both promoted by the highly basic (E2) and nucleophilic (S_n2) unsolvated OH^- present in the water-lean reaction media. The extent of degradation was assessed by ^1H NMR, quantifying NBu_3 against DMF as an internal standard. The degree of TBA^+ decomposition increased with temperature and reaction time (Figure 11) and was less pronounced in alcoholic solvents, where hydroxide ions are better solvated. However, reactions conducted in alcohols afforded very poor methanol yields, indicating a trade-off between ionic liquid stability and catalytic activity. Control experiments indicated that the **Ru-1** hydride species may also play a role by degrading the TBA cation, as degradation was less pronounced when hydrogen was excluded (Table 23, entry 3 vs entry 4).



Scheme 6. Decomposition mechanisms of the TBA cation (E2 Hofmann elimination and SN2 substitution). Reprint from ref.[177] with copyright permission.

Table 23 Hydrogenation of CO_2 in the presence of [TBA][Arg] (blank reactions)

CO_2 + H_2 + TBA·Arg —(Ru-1, THF, 165 °C, 24 h)→ TBA·[ArgH⁺][HCOO⁻] + TBA·[ArgNC(O)H] + CH_3OH + $HCOOCH_3$ + CO

entry	[TBA][Arg]	Cat.	H_2	CO_2	formate[a] [mmol]	form-amide[a] [mmol]	methanol[b] [mmol]	methyl formate[b] [mmol]	carbon monoxide[c] [mmol]	TBA·Arg[d] Degradation (%)
1	+	-	+	+	n.d.	n.d.	n.d.	n.d.	n.d.	24
2	-	+	+	+	n.d.	n.d.	n.d.	n.d.	n.d.	-
3	+	+	-	+	-	-	-	-		57
4	+	+	+	-	-	-	-	-	-	> 95

General conditions: [TBA][Arg] (5.0 mmol), **Ru-1** (10 µmol), THF (10 mL), CO_2 20 bars, H_2 60 bars, 165 °C, 24 h. [a] Determined by ^{1}H NMR with DMF (200 µL, 2.6 mmol) as internal standard. [b] Determined by LC with DMF (200 µL, 2.6 mmol) as internal standard. [c] Determined by gas GC. [d] Determined by ^{1}H NMR quantification of by-product NBu_3 with DMF (200 µL, 2.6 mmol) as internal standard.

4.2.5. Summary

In summary, our findings confirm that [TBA][Arg] can chemisorb CO_2 and catalyze its hydrogenation to formate and methanol without additional bases or additives. Combining [TBA][Arg] with the ruthenium complex Ru-MACHO-BH enabled significant methanol yields under optimized conditions, achieving a turnover number (TON) of up to 700. This efficiency stems from its multifunctional design: an amino group for CO_2 fixation, a built-in strong base promoting catalyst turnover, and a hydrogen bond donor activating the substrate. Moreover, direct air capture of CO_2 using [TBA][Arg] was

demonstrated, with a CO_2/[TBA][Arg] ratio of 0.35 (compared to 1.09 in water) due to its limited solubility in 1,4-dioxane at room temperature. The captured CO_2 was subsequently hydrogenated under optimized conditions. Future work should focus on exploring milder conditions and new pathways for CO_2 conversion using [TBA][Arg], aiming to preserve cation stability.

5. Outlook and final remarks

The research presented in this work has demonstrated the potential of amino acid-based ionic liquids (AAILs) as efficient CO_2 capture agents, offering a viable alternative to conventional amines. By effectively integrating CO_2 absorption with catalytic transformation, this approach enhances sustainable carbon utilization and supports the advancement of carbon-neutral technologies. The promising results obtained with AAILs, particularly in the hydrogenation of CO_2 to formate and methanol using Ru-MACHO-BH catalyst, underscore key opportunities for further innovation in tackling climate change and fostering a circular carbon economy.

A major research direction moving forward is the optimization of catalytic performance. While ruthenium-based systems have shown high activity and selectivity, future work should explore earth-abundant alternatives, such as manganese- or iron-based catalysts, to enhance cost-effectiveness and sustainability. Additionally, modifications to ligand structures could improve catalyst stability, recyclability, and resistance to degradation under industrial conditions, further supporting carbon neutrality efforts.

Process scalability remains another critical factor for industrial applicability. Although the current studies have demonstrated successful CO_2 conversion under controlled laboratory conditions, translating these findings into large-scale operations will require the development of continuous-flow systems. The integration of CO_2 capture and conversion within a single, energy-efficient process will be essential to minimize operational costs and maximize yield.

Furthermore, the direct air capture (DAC) of CO_2, in combination with AAILs, represents a highly promising approach for reducing atmospheric CO_2 levels and closing the carbon cycle.

The long-term stability and reusability of AAILs must be systematically investigated. While AAILs exhibit favorable absorption capacities, their performance under prolonged reaction cycles and varying operational conditions needs thorough assessment. Strategies such as molecular tailoring of IL structures and solvent engineering could enhance their durability and efficiency, making them more viable for industrial applications.

Another promising avenue is the functionalization of ILs to optimize CO_2 absorption and activation properties. Fine-tuning interactions between CO_2 and the ionic liquid framework, particularly through the introduction of specific functional groups, could improve reaction kinetics and selectivity. The rational design of next-generation ILs may enable more efficient CO_2 capture and its direct hydrogenation to high-value products such as methanol and formate under milder conditions, further contributing to sustainable chemical production and carbon neutrality.

Overall, this thesis provides a strong foundation for the continued development of integrated CO_2 capture and conversion systems. The synergistic combination of AA-ILs with tailored catalytic approaches represents a viable pathway toward more sustainable chemical processes. Future research should focus on enhancing catalyst robustness, optimizing reaction conditions, and advancing scalable process designs to bridge the gap between laboratory feasibility and industrial implementation. By addressing these challenges, the AAIL-assisted CO_2 hydrogenation strategy could play a pivotal role in achieving a circular carbon economy, enabling direct air capture, and mitigating global CO_2 emissions to combat climate change effectively.

6. References

(1) Gür, T. M. Carbon Dioxide Emissions, Capture, Storage and Utilization: Review of Materials, Processes and Technologies. *Prog. Energy Combust. Sci.* **2022**, *89*, 100965.
(2) Ritchie, H.; Roser, M. Sector by Sector: Where Do Global Greenhouse Gas Emissions Come From? *Our World in Data* **2024**. https://ourworldindata.org/greenhouse-gas-emissions-by-sector (accessed 2024).
(3) Tans, P.; Keeling, R. *Global Monitoring Laboratory – CO_2 Trends*. NOAA Global Monitoring Laboratory. https://gml.noaa.gov/ccgg/trends/ (accessed November, 2024).
(4) NOAA. *Trends in Atmospheric Carbon Dioxide (CO_2)*. https://www.climate.gov/news-features/understanding-climate/climate-change-atmospheric-carbon-dioxide (accessed November 2024).
(5) International Energy Agency (IEA). *World Energy Outlook 2023*. https://www.iea.org/reports/world-energy-outlook-2023 (accessed October 24, 2023).
(6) Al Mubarak, F.; Rezaee, R.; Wood, D. A. Economic, Societal, and Environmental Impacts of Available Energy Sources: A Review. *Eng.* **2024**, *5* (3), 1232–1265.
(7) Lindsey, R. *Climate Change: Atmospheric Carbon Dioxide.* NOAA Climate.gov,. https://www.climate.gov/news-features/understanding-climate/climate-change-atmospheric-carbon-dioxide (accessed May 21, 2025).
(8) Smith, P.; House, J. I.; Bustamante, M.; Sobocká, J.; Harper, R.; Pan, G.; West, P. C.; Clark, J. M.; Adhya, T.; Rumpel, C. Global Change Pressures on Soils from Land Use and Management. *Glob. Change Biol.* **2016**, *22* (3), 1008–1028.
(9) Smith, P.; Calvin, K.; Nkem, J.; Campbell, D.; Cherubini, F.; Grassi, G.; Korotkov, V.; Le Hoang, A.; Lwasa, S.; McElwee, P. Which Practices Co-Deliver Food Security, Climate Change Mitigation and Adaptation, and Combat Land Degradation and Desertification? *Glob. Change Biol.* **2020**, *26* (3), 1532–1575.
(10) Simoni, M.; Wilkes, M. D.; Brown, S.; Provis, J. L.; Kinoshita, H.; Hanein, T. Decarbonising the Lime Industry: State-of-the-Art. *Renew. Sustain. Energy Rev.* **2022**, *168*, 112765.
(11) Sivaramanan, S. Global Warming and Climate Change, Causes, Impacts and Mitigation. *Cent. Environ. Auth.* **2015**, *2* (4).
(12) Kumar, S.; Chatterjee, U.; David Raj, A.; Sooryamol, K**.** Global Warming and Climate Crisis/Extreme Events. In *Climate Crisis: Adaptive Approaches and Sustainability*; Springer: Cham, **2024**; pp 3–18.
(13) Duchenne-Moutien, R. A.; Neetoo, H. Climate Change and Emerging Food Safety Issues: A Review. *J. Food Prot.* **2021**, *84* (11), 1884–1897.
(14) Feely, R. A.; Doney, S. C.; Cooley, S. R. Ocean Acidification: Present Conditions and Future Changes in a High-CO_2 World. *Oceanography.* **2009**, *22* (4), 36–47.
(15) *The Paris Agreement. What is the Paris Agreement?* United Nations, https://unfccc.int/process-and-meetings/the-paris-agreement (accessed Mai, 2024).
(16) Kumar, A.; Gao, C. Homogeneous (De)hydrogenative Catalysis for Circular Chemistry–Using Waste as a Resource. *ChemCatChem* .**2021**, *13* (4), 1105–1134.
(17) Lau, H. C.; Ramakrishna, S.; Zhang, K.; Radhamani, A. V. The role of carbon capture and storage in the energy transition. *Energy & Fuels.* **2021**, *35* (9), 7364–7386.
(18) Pan, Y.; Birdsey, R. A.; Phillips, O. L.; Houghton, R. A.; Fang, J.; Kauppi, P. E.; Keith, H.; Kurz, W. A.; Ito, A.; Lewis, S. L. The Enduring World Forest Carbon Sink. *Nature.* **2024**, *631* (8021), 563–569.

(19) Yang, M.; Chen, L.; Wang, J.; Msigwa, G.; Osman, A. I.; Fawzy, S.; Rooney, D. W.; Yap, P.-S. Circular Economy Strategies for Combating Climate Change and Other Environmental Issues. *Environ. Chem. Lett.* **2023**, *21* (1), 55–80.
(20) Gallego-Schmid, A.; Chen, H.-M.; Sharmina, M.; Mendoza, J. M. F. Links between Circular Economy and Climate Change Mitigation in the Built Environment. *J. Clean. Prod.* **2020**, *260*, 121115.
(21) Mohamed, A.-M. O.; El-Gamal, M.; Hameedi, S. *Sustainable utilization of carbon dioxide in waste management: Moving toward reducing environmental impact*; Elsevier, **2022**.
(22) Lehtonen, J.; Järnefelt, V.; Alakurtti, S.; Arasto, A.; Hannula, I.; Harlin, A.; Koljonen, T.; Lantto, R.; Lienemann, M.; Onarheim, K. *The Carbon Reuse Economy: Transforming CO_2 from a Pollutant into a Resource*; VTT Technical Research Centre of Finland: Espoo, **2019**.
(23) Shah, Y. T. *CO_2 Capture, Utilization, and Sequestration Strategies*; CRC Press: Boca Raton, **2021**.
(24) Dibenedetto, A.; Angelini, A.; Stufano, P. Use of Carbon Dioxide as Feedstock for Chemicals and Fuels: Homogeneous and Heterogeneous Catalysis. *J. Chem. Technol. Biotechnol.* **2014**, *89* (3), 334–353.
(25) Fotias, S. P.; Gaganis, V.; Bellas, S. Integrated Raw Material Approach to Sustainable Geothermal Energy Production: Harnessing CO_2 for Enhanced Resource Utilization. *Tech. Ann.* **2024**, *1* (5).
(26) Sibhat, M.; Yao, G.; Zhu, N.; Tsegay, G.; Fang, K.; Zhu, Q.; Zhou, Y.; Zhao, J. Advancement in Sodium Carbonation Pathways for Sustainable Carbon Capture and Utilization: A Review. *Results Eng.* **2024**, 102536.
(27) Aresta, M. *Carbon Dioxide as Chemical Feedstock*; John Wiley & Sons: Weinheim, 2010.
(28) Keijer, T.; Bakker, V.; Slootweg, J. C. Circular Chemistry to Enable a Circular Economy. *Nat. Chem.* **2019**, *11* (3), 190–195.
(29) Domenech, T.; Stegemann, J. A. *The Circular Economy: Concept, Tools and Implementation*; CRC Press: Boca Raton, **2021**.
(30) McLaughlin, H.; Littlefield, A. A.; Menefee, M.; Kinzer, A.; Hull, T.; Sovacool, B. K.; Bazilian, M. D.; Kim, J.; Griffiths, S. Carbon Capture Utilization and Storage in Review: Sociotechnical Implications for a Carbon Reliant World. *Renew. Sustain. Energy Rev.* **2023**, *177*, 113215.
(31) Nwabueze, Q. A.; Leggett, S. Advancements in the Application of CO_2 Capture and Utilization Technologies—A Comprehensive Review. *Fuels.* **2024**, *5* (3), 508–532.
(32) Gupta, A.; Paul, A. R.; Saha, S. C. Decarbonizing the Atmosphere Using Carbon Capture, Utilization, and Sequestration: Challenges, Opportunities, and Policy Implications in India. *Atmosphere* **2023**, *14* (10), 1546.
(33) Feron, P. *Absorption-Based Post-Combustion Capture of Carbon Dioxide*; Woodhead Publishing: Cambridge, **2016**.
(34) Rubin, E. S. Understanding the Pitfalls of CCS Cost Estimates. *Int. J. Greenh. Gas Control* **2012**, *10*, 181–190.
(35) Olah, G. A.; Mathew, T.; Goeppert, A.; Surya Prakash, G. Difference and Significance of Regenerative versus Renewable Carbon Fuels and Products. *Top. Catal.* **2018**, *61*, 522–529.
(36) Mondal, M. K.; Balsora, H. K.; Varshney, P. Progress and Trends in CO_2 Capture/Separation Technologies: A Review. *Energy.* **2012**, *46* (1), 431–441.
(37) Song, C.; Liu, Q.; Deng, S.; Li, H.; Kitamura, Y. Cryogenic-Based CO_2 Capture Technologies: State-of-the-Art Developments and Current Challenges. *Renew. Sustain. Energy Rev.* **2019**, *101*, 265–278.
(38) Islam, M.; Yusoff, R.; Ali, B. Degradation Studies of Amines and Alkanolamines during CO_2 Absorption and Stripping System. *Eng. e-Trans.* **2010**, *5* (2), 97–109.

(39) Li, W.; Zhang, X.; Lu, B.; Sun, C.; Li, S.; Zhang, S. Performance of a Hybrid Solvent of Amino Acid and Ionic Liquid for CO_2 Capture. *Int. J. Greenh. Gas Control* **2015**, *42*, 400–404.
(40) Zheng, Q.; Martin, G. J.; Kentish, S. E. Energy Efficient Transfer of Carbon Dioxide from Flue Gases to Microalgal Systems. *Energy Environ. Sci.* **2016**, *9* (3), 1074–1082.
(41) Ozden, A. CO_2 Capture via Electrochemical pH-Mediated Systems. *ACS Energy Lett.* **2025**, *10*, 1550–1576.
(42) Almajed, H. M.; Kas, R.; Brimley, P.; Crow, A. M.; Somoza-Tornos, A.; Hodge, B.-M.; Burdyny, T. E.; Smith, W. A. Closing the Loop: Unexamined Performance Trade-Offs of Integrating Direct Air Capture with (Bi)carbonate Electrolysis. *ACS Energy Lett.* **2024**, *9* (5), 2472–2483.
(43) Aghaie, M.; Rezaei, N.; Zendehboudi, S. A Systematic Review on CO_2 Capture with Ionic Liquids: Current Status and Future Prospects. *Renew. Sustain. Energy Rev.* **2018**, *96*, 502–525.
(44) Karadas, F.; Atilhan, M.; Aparicio, S. Review on the Use of Ionic Liquids (ILs) as Alternative Fluids for CO_2 Capture and Natural Gas Sweetening. *Energy Fuels.* **2010**, *24* (11), 5817–5828.
(45) Wasserscheid, P.; Welton, T. *Ionic Liquids in Synthesis*; Wiley-VCH: Weinheim, **2007**.
(46) Almantariotis, D.; Gefflaut, T.; Pádua, A. A. H.; Coxam, J.-Y.; Costa Gomes, M. F. Effect of Fluorination and Size of the Alkyl Side-Chain on the Solubility of Carbon Dioxide in 1-Alkyl-3-Methylimidazolium Bis(trifluoromethylsulfonyl)amide Ionic Liquids. *J. Phys. Chem. B.* **2010**, *114* (10), 3608–3617.
(47) Baltus, R. E.; Culbertson, B. H.; Dai, S.; Luo, H.; DePaoli, D. W. Low-Pressure Solubility of Carbon Dioxide in Room-Temperature Ionic Liquids Measured with a Quartz Crystal Microbalance. *J. Phys. Chem. B.* **2004**, *108* (2), 721–727.
(48) Anderson, J. L.; Dixon, J. K.; Brennecke, J. F. Solubility of CO_2, CH_4, C_2H_6, C_2H_4, O_2, and N_2 in 1-Hexyl-3-Methylpyridinium Bis(trifluoromethylsulfonyl)imide: Comparison to Other Ionic Liquids. *Acc. Chem. Res.* **2007**, *40* (11), 1208–1216.
(49) Zhang, J.; Sun, J.; Zhang, X.; Zhao, Y.; Zhang, S. The Recent Development of CO_2 Fixation and Conversion by Ionic Liquid. *Greenh. Gases Sci. Technol.* **2011**, *1* (2), 142–159.
(50) Ramdin, M.; de Loos, T. W.; Vlugt, T. J. H. State-of-the-Art of CO_2 Capture with Ionic Liquids. *Ind. Eng. Chem. Res.* **2012**, *51* (24), 8149–8177.
(51) Mattedi, S.; Carvalho, P. J.; Coutinho, J. A. P.; Alvarez, V. H.; Iglesias, M. High-Pressure CO_2 Solubility in *N*-Methyl-2-hydroxyethylammonium Protic Ionic Liquids. *J. Supercrit. Fluids* **2011**, *56* (3), 224–230.
(52) Revelli, A.-L.; Mutelet, F.; Jaubert, J.-N. High Carbon Dioxide Solubilities in Imidazolium-Based Ionic Liquids and in Poly(ethylene glycol) Dimethyl Ether. *J. Phys. Chem. B.* **2010**, *114* (40), 12908–12913.
(53) Carvalho, P. J.; Alvarez, V. H.; Marrucho, I. M.; Aznar, M.; Coutinho, J. A. P. High Carbon Dioxide Solubilities in Trihexyltetradecylphosphonium-Based Ionic Liquids. *J. Supercrit. Fluids.* **2010**, *52* (3), 258–265.
(54) Aki, S. N. V. K.; Mellein, B. R.; Saurer, E. M.; Brennecke, J. F. High-Pressure Phase Behavior of Carbon Dioxide with Imidazolium-Based Ionic Liquids. *J. Phys. Chem. B.* **2004**, *108* (52), 20355–20365.
(55) Cadena, C.; Anthony, J. L.; Shah, J. K.; Morrow, T. I.; Brennecke, J. F.; Maginn, E. J. Why Is CO_2 so Soluble in Imidazolium-Based Ionic Liquids? *J. Am. Chem. Soc.* **2004**, *126* (16), 5300–5308.
(56) Sánchez, L. G.; Meindersma, G. W.; de Haan, A. B. Solvent Properties of Functionalized Ionic Liquids for CO_2 Absorption. *Chem. Eng. Res. Des.* **2007**, *85* (1), 31–39.
(57) Kim, Y.; Choi, W.; Jang, J.; Yoo, K.-P.; Lee, C. Solubility Measurement and Prediction of Carbon Dioxide in Ionic Liquids. *Fluid Phase Equilib.* **2005**, *228*, 439–445.

(58) Bates, E. D.; Mayton, R. D.; Ntai, I.; Davis, J. H. CO_2 Capture by a Task-Specific Ionic Liquid. *J. Am. Chem. Soc.* **2002**, *124* (6), 926–927.
(59) Goodrich, B. F.; De La Fuente, J. C.; Gurkan, B. E.; Zadigian, D. J.; Price, E. A.; Huang, Y.; Brennecke, J. F. Experimental Measurements of Amine-Functionalized Anion-Tethered Ionic Liquids with Carbon Dioxide. *Ind. Eng. Chem. Res.* **2011**, *50* (1), 111–118.
(60) van Holst, J.; Versteeg, G. F.; Brilman, D. W. F.; Hogendoorn, J. A. Kinetic Study of CO_2 with Various Amino Acid Salts in Aqueous Solution. *Chem. Eng. Sci.* **2009**, *64* (1), 59–68.
(61) Al-Mamoori, A.; Krishnamurthy, A.; Rownaghi, A. A.; Rezaei, F. Carbon Capture and Utilization Update. *Energy Technol.* **2017**, *5* (6), 834–849.
(62) Lv, B.; Xia, Y.; Shi, Y.; Liu, N.; Li, W.; Li, S. A Novel Hydrophilic Amino Acid Ionic Liquid [C_2OHmim][Gly] as Aqueous Sorbent for CO_2 Capture. *Int. J. Greenh. Gas Control* **2016**, *46*, 1–6.
(63) Liu, Q.; Wu, L.; Jackstell, R.; Beller, M. Using Carbon Dioxide as a Building Block in Organic Synthesis. *Nat. Commun.* **2015**, *6* (1), 1–15.
(64) Sarp, S.; Hernandez, S. G.; Chen, C.; Sheehan, S. W. Alcohol production from carbon dioxide: methanol as a fuel and chemical feedstock. *Joule.* **2021**, *5* (1), 59–76.
(65) Yarulina, I.; Chowdhury, A. D.; Meirer, F.; Weckhuysen, B. M.; Gascon, J. Recent Trends and Fundamental Insights in the Methanol-to-Hydrocarbons Process. *Nat. Catal.* **2018**, *1* (6), 398–411.
(66) Mishra, A.; Kim, D.; Altahtamouni, T.; Kasak, P.; Popelka, A.; Park, H.; Han, D. S. A Comparative Study on Carbon Neutral Hydrogen Carrier Production: Formic Acid from CO_2 vs Ammonia. *J. CO_2 Util.* **2024**, *82*, 102756.
(67) Sordakis, K.; Tang, C.; Vogt, L. K.; Junge, H.; Dyson, P. J.; Beller, M.; Laurenczy, G. Homogeneous Catalysis for Sustainable Hydrogen Storage in Formic Acid and Alcohols. *Chem. Rev.* **2018**, *118* (2), 372–433.
(68) Gibson, H. W. Chemistry of Formic Acid and Its Simple Derivatives. *Chem. Rev.* **1969**, *69* (5), 673–692.
(69) Aresta, M.; Dibenedetto, A.; Angelini, A. Catalysis for the Valorization of Exhaust Carbon: From CO_2 to Chemicals, Materials, and Fuels. Technological Use of CO_2. *Chem. Rev.* **2014**, *114* (3), 1709–1742.
(70) Li, Y.; Wang, Z.; Liu, Q. Progress in Homogeneous Catalytic Hydrogenation of CO_2. *Chin. J. Org. Chem.* **2017**, *37* (8), 1978.
(71) Jiang, K.; Zhang, H.-X.; Zou, S.; Cai, W.-B. Electrocatalysis of Formic Acid on Palladium and Platinum Surfaces: From Fundamental Mechanisms to Fuel Cell Applications. *Phys. Chem. Chem. Phys.* **2014**, *16* (38), 20360–20376.
(72) Klankermayer, J.; Wesselbaum, S.; Beydoun, K.; Leitner, W. Selective Catalytic Synthesis Using the Combination of Carbon Dioxide and Hydrogen: Catalytic Chess at the Interface of Energy and Chemistry. *Angew. Chem., Int. Ed.* **2016**, *55* (26), 7296–7343.
(73) Chen, Y. Recent Advances in Methylation: A Guide for Selecting Methylation Reagents. *Chem. Eur. J.* **2019**, *25* (14), 3405–3439.
(74) Wölfel, R.; Taccardi, N.; Bösmann, A.; Wasserscheid, P. Selective catalytic conversion of biobased carbohydrates to formic acid using molecular oxygen. *Green Chem*.**2011**, *13* (10), 2759–2763.
(75) Li, J.; Ding, D. J.; Deng, L.; Guo, Q. X.; Fu, Y. Catalytic Air Oxidation of Biomass-Derived Carbohydrates to Formic Acid. *ChemSusChem* **2012**, *5* (7), 1313–1318.
(76) Albert, J.; Wölfel, R.; Bösmann, A.; Wasserscheid, P. Selective Oxidation of Complex, Water-Insoluble Biomass to Formic Acid Using Additives as Reaction Accelerators. *Energy Environ. Sci.* **2012**, *5* (7), 7956–7962.

(77) Zassinovich, G.; Mestroni, G.; Gladiali, S. Asymmetric Hydrogen Transfer Reactions Promoted by Homogeneous Transition Metal Catalysts. *Chem. Rev.* **1992**, *92* (5), 1051–1069.
(78) Yu, X.; Pickup, P. G. Recent Advances in Direct Formic Acid Fuel Cells (DFAFC). *J. Power Sources* **2008**, *182* (1), 124–132.
(79) Williams, R.; Crandall, R. S.; Bloom, A. Use of Carbon Dioxide in Energy Storage. *Appl. Phys. Lett.* **1978**, *33* (5), 381–381.
(80) Loges, B.; Boddien, A.; Junge, H.; Beller, M. Kontrollierte Wasserstofferzeugung aus Ameisensäure-Amin-Addukten bei Raumtemperatur und Direkte Nutzung in H_2/O_2-Brennstoffzellen. *Angew. Chem.* **2008**, *120* (21), 4026–4029.
(81) Enthaler, S. Carbon Dioxide—The Hydrogen-Storage Material of the Future? *ChemSusChem*.**2008**, *1* (10), 801–804.
(82) Supronowicz, W.; Ignatyev, I.; Lolli, G.; Wolf, A.; Zhao, L.; Mleczko, L. Formic Acid: A Future Bridge between the Power and Chemical Industries. *Green Chem.* **2015**, *17* (5), 2904–2911.
(83) Dutta, I.; Chatterjee, S.; Cheng, H.; Parsapur, R. K.; Liu, Z.; Li, Z.; Ye, E.; Kawanami, H.; Low, J. S. C.; Lai, Z. Formic Acid to Power towards Low-Carbon Economy. *Adv. Energy Mater.* **2022**, *12* (15), 2103799..
(84) Chen, Y.; Yang, Y.; Liu, X.; Shi, X.; Wang, C.; Zhong, H.; Jin, F. Sustainable Production of Formic Acid and Acetic Acid from Biomass. *Mol. Catal.* **2023**, *545*, 113199.
(85) Peng, Y.; Alberico, E.; Junge, H.; Beller, M. Homogeneous Catalytic Hydrogenation of CO_2–Amino Acid-Based Capture and Utilization. *Chem. Soc. Rev.* **2025**.
(86) on der Assen, N.; Voll, P.; Peters, M.; Bardow, A. Life Cycle Assessment of CO_2 Capture and Utilization: A Tutorial Review. *Chem. Soc. Rev.* **2014**, *43* (23), 7982–7994.
(87) Schaub, T.; Paciello, R. A. Ein Verfahren zur Herstellung von Ameisensäure durch CO_2-Hydrierung: Thermodynamik und die Rolle von CO. *Angew. Chem.* **2011**, *123* (32), 7416–7420.
(88) Leitner, W.; Dinjus, E.; Gassner, F.; Cornils, B.; Herrmann, W. Aqueous-Phase Organometallic Catalysis; Wiley-VCH: Weinheim, **1998**; p 486.
(89) Leitner, W.; Dinjus, E.; Gaßner, F. Activation of Carbon Dioxide. IV. Rhodium-Catalysed Hydrogenation of Carbon Dioxide to Formic Acid. *J. Organomet. Chem.* **1994**, *475* (1–2), 257–266.
(90) Schwarz, H. Metal-Mediated Activation of Carbon Dioxide in the Gas Phase: Mechanistic Insight Derived from a Combined Experimental/Computational Approach. *Coord. Chem. Rev.* **2017**, *334*, 112–123.
(91) Sakaki, S.; Ohkubo, K. *Ab Initio* MO Study of Carbon Dioxide Insertion into a Copper(I)–Hydrogen Bond: Semiquantitative Understanding of Changes in Geometry, Bonding, and Electron Distribution during the Reaction. *Inorg. Chem.* **1989**, *28* (13), 2583–2590.
(92) Tanaka, R.; Yamashita, M.; Nozaki, K. Catalytic Hydrogenation of Carbon Dioxide Using Ir(III)–Pincer Complexes. *J. Am. Chem. Soc.* **2009**, *131* (40), 14168–14169.
(93) Tanaka, R.; Yamashita, M.; Chung, L. W.; Morokuma, K.; Nozaki, K. Mechanistic Studies on the Reversible Hydrogenation of Carbon Dioxide Catalyzed by an Ir–PNP Complex. *Organometallics* **2011**, *30* (24), 6742–6750.
(94) Behr, A.; Nowakowski, K. Catalytic Hydrogenation of Carbon Dioxide to Formic Acid. In *Advances in Inorganic Chemistry*; Vol. 66; Elsevier: Amsterdam, **2014**; pp 223–258.
(95) Inoue, Y.; Izumida, H.; Sasaki, Y.; Hashimoto, H. Catalytic Fixation of Carbon Dioxide to Formic Acid by Transition-Metal Complexes under Mild Conditions. *Chem. Lett.* **1976**, *5* (8), 863–864.
(96) Inoue, Y.; Sasaki, Y.; Hashimoto, H. Synthesis of Formates from Alcohols, Carbon Dioxide, and Hydrogen Catalysed by a Combination of Group VIII Transition-Metal Complexes and Tertiary Amines. *J. Chem. Soc., Chem. Commun.* **1975**, (17), 718–719.

(97) Langer, R.; Diskin-Posner, Y.; Leitus, G.; Shimon, L. J. W.; Ben-David, Y.; Milstein, D. Low-Pressure Hydrogenation of Carbon Dioxide Catalyzed by an Iron Pincer Complex Exhibiting Noble Metal Activity. *Angew. Chem.* **2011**, *123* (42), 10122–10126.
(98) Zhu, F.; Zhu-Ge, L.; Yang, G.; Zhou, S. Iron-Catalyzed Hydrogenation of Bicarbonates and Carbon Dioxide to Formates. *ChemSusChem.* **2015**, *8* (4), 609–612.
(99) Badiei, Y. M.; Wang, W.-H.; Hull, J. F.; Szalda, D. J.; Muckerman, J. T.; Himeda, Y.; Fujita, E. Cp*Co(III) Catalysts with Proton-Responsive Ligands for Carbon Dioxide Hydrogenation in Aqueous Media. *Inorg. Chem.* **2013**, *52* (21), 12576–12586.
(100) Federsel, C.; Ziebart, C.; Jackstell, R.; Baumann, W.; Beller, M. Catalytic Hydrogenation of Carbon Dioxide and Bicarbonates with a Well-Defined Cobalt Dihydrogen Complex. *Chem. Eur. J.* **2012**, *18* (1), 72–75.
(101) Jeletic, M. S.; Mock, M. T.; Appel, A. M.; Linehan, J. C. A Cobalt-Based Catalyst for the Hydrogenation of CO_2 under Ambient Conditions. *J. Am. Chem. Soc.* **2013**, *135* (31), 11533–11536.
(102) Kothandaraman, J.; Czaun, M.; Goeppert, A.; Haiges, R.; Jones, J. P.; May, R. B.; Prakash, G. K. S.; Olah, G. A. Amine-Free Reversible Hydrogen Storage in Formate Salts Catalyzed by a Ruthenium Pincer Complex without pH Control or Solvent Change. *ChemSusChem* **2015**, *8* (8), 1442–1451.
(103) Filonenko, G. A.; van Putten, R.; Schulpen, E. N.; Hensen, E. J. M.; Pidko, E. A. Highly Efficient Reversible Hydrogenation of Carbon Dioxide to Formates Using a Ruthenium PNP-Pincer Catalyst. *ChemCatChem*. **2014**, *6* (6), 1526–1530.
(104) Federsel, C.; Jackstell, R.; Boddien, A.; Laurenczy, G.; Beller, M. Ruthenium-Catalyzed Hydrogenation of Bicarbonate in Water. *ChemSusChem.* **2010**, *3* (9), 1048–1050.
(105) Schmeier, T. J.; Dobereiner, G. E.; Crabtree, R. H.; Hazari, N. Secondary Coordination Sphere Interactions Facilitate the Insertion Step in an Iridium(III) CO_2 Reduction Catalyst. *J. Am. Chem. Soc.* **2011**, *133* (24), 9274–9277.
(106) Xu, S.; Onishi, N.; Tsurusaki, A.; Manaka, Y.; Wang, W.-H.; Muckerman, J. T.; Fujita, E.; Himeda, Y. Efficient Cp*Ir Catalysts with Imidazoline Ligands for CO_2 Hydrogenation. *Eur. J. Inorg. Chem.* **2015**, *2015* (34), 5591–5594.
(107) Rohmann, K.; Kothe, J.; Haenel, M. W.; Englert, U.; Hölscher, M.; Leitner, W. Hydrogenation of CO_2 to Formic Acid with a Highly Active Ruthenium Acriphos Complex in DMSO and DMSO/Water. *Angew. Chem., Int. Ed.* **2016**, *55* (31), 8966–8969.
(108) Li, Y.-N.; He, L.-N.; Liu, A.-H.; Lang, X.-D.; Yang, Z.-Z.; Yu, B.; Luan, C.-R. *In Situ* Hydrogenation of Captured CO_2 to Formate with Polyethyleneimine and a Rh/Monophosphine System. *Green Chem.* **2013**, *15* (10), 2825–2829.
(109) Azua, A.; Sanz, S.; Peris, E. Water-Soluble Ir(III) N-Heterocyclic Carbene-Based Catalysts for the Reduction of CO_2 to Formate by Transfer Hydrogenation and the Deuteration of Aryl Amines in Water. *Chem. Eur. J.* **2011**, *17* (14), 3963–3967.
(110) Hull, J. F.; Himeda, Y.; Wang, W.-H.; Hashiguchi, B.; Periana, R.; Szalda, D. J.; Muckerman, J. T.; Fujita, E. Reversible Hydrogen Storage Using CO_2 and a Proton-Switchable Iridium Catalyst in Aqueous Media under Mild Temperatures and Pressures. *Nat. Chem.* **2012**, *4* (5), 383–388.
(111) Enthaler, S.; Brück, A.; Kammer, A.; Junge, H.; Irran, E.; Gülak, S. Exploring the Reactivity of Nickel Pincer Complexes in the Decomposition of Formic Acid to CO_2/H_2 and the Hydrogenation of $NaHCO_3$ to HCOONa. *ChemCatChem* **2015**, *7* (1), 65–69.
(112) Bertini, F.; Glatz, M.; Gorgas, N.; Stöger, B.; Peruzzini, M.; Veiros, L. F.; Kirchner, K.; Gonsalvi, L. Carbon Dioxide Hydrogenation Catalysed by Well-Defined Mn(I) PNP Pincer Hydride Complexes. *Chem. Sci.* **2017**, *8* (7), 5024–5029.

(113) Zhang, Y.; MacIntosh, A. D.; Wong, J. L.; Bielinski, E. A.; Williard, P. G.; Mercado, B. Q.; Hazari, N.; Bernskoetter, W. H. Iron-Catalyzed CO_2 Hydrogenation to Formate Enhanced by Lewis Acid Co-Catalysts. *Chem. Sci.* **2015**, *6* (7), 4291–4299.
(114) Cammarota, R. C.; Vollmer, M. V.; Xie, J.; Ye, J.; Linehan, J. C.; Burgess, S. A.; Appel, A. M.; Gagliardi, L.; Lu, C. C. A Bimetallic Nickel–Gallium Complex Catalyzes CO_2 Hydrogenation via the Intermediacy of an Anionic d^{10} Nickel Hydride. *J. Am. Chem. Soc.* **2017**, *139* (40), 14244–14250.
(115) Chaudhary, K.; Trivedi, M.; Masram, D.; Kumar, A.; Kumar, G.; Husain, A.; Rath, N. P. A Highly Active Copper Catalyst for the Hydrogenation of Carbon Dioxide to Formate under Ambient Conditions. *Dalton Trans.* **2020**, *49* (9), 2994–3000.
(116) Weilhard, A.; Argent, S. P.; Sans, V. Efficient Carbon Dioxide Hydrogenation to Formic Acid with Buffering Ionic Liquids. *Nat. Commun.* **2021**, *12* (1), 231.
(117) Wei, D.; Sang, R.; Sponholz, P.; Junge, H.; Beller, M. Reversible Hydrogenation of Carbon Dioxide to Formic Acid Using a Mn-Pincer Complex in the Presence of Lysine. *Nat. Energy* **2022**, *7* (5), 438–447.
(118) Kostera, S.; Gobbo, A.; Guelfi, M.; Zacchini, S.; Manca, G.; Marchetti, F.; Gonsalvi, L. Carbon Dioxide Hydrogenation to Formate Catalyzed by Highly Active Ru–Tris(pyrazolyl)methane Complexes. *J. Catal.* **2025**, *116231*.
(119) Su, J.; Lu, M.; Lin, H. High-Yield Production of Formate by Hydrogenating CO_2-Derived Ammonium Carbamate/Carbonate at Room Temperature. *Green Chem.* **2015**, *17* (5), 2769–2773.
(120) Moret, S.; Dyson, P. J.; Laurenczy, G. Direct Synthesis of Formic Acid from Carbon Dioxide by Hydrogenation in Acidic Media. *Nat. Commun.* **2014**, *5* (1), 4017.
(121) Schuchmann, K.; Müller, V. Direct and Reversible Hydrogenation of CO_2 to Formate by a Bacterial Carbon Dioxide Reductase. *Science*.**2013**, *342* (6164), 1382–1385.
(122) Wang, W.-H.; Himeda, Y.; Muckerman, J. T.; Manbeck, G. F.; Fujita, E. CO_2 Hydrogenation to Formate and Methanol as an Alternative to Photo- and Electrochemical CO_2 Reduction. *Chem. Rev.* **2015**, *115* (23), 12936–12973.
(123) Li, Y.-N.; He, L.-N.; Lang, X.-D.; Liu, X.-F.; Zhang, S. An Integrated Process of CO_2 Capture and *In Situ* Hydrogenation to Formate Using a Tunable Ethoxyl-Functionalized Amidine and a Rh/Bisphosphine System. *RSC Adv.* **2014**, *4* (91), 49995–50002.
(124) Zhang, S.; Li, Y.-N.; Zhang, Y.-W.; He, L.-N.; Yu, B.; Song, Q.-W.; Lang, X.-D. Equimolar Carbon Absorption by Potassium Phthalimide and *In Situ* Catalytic Conversion under Mild Conditions. *ChemSusChem* **2014**, *7* (5), 1484–1489.
(125) Yadav, M.; Linehan, J. C.; Karkamkar, A. J.; van der Eide, E.; Heldebrant, D. J. Homogeneous Hydrogenation of CO_2 to Methyl Formate Utilizing Switchable Ionic Liquids. *Inorg. Chem.* **2014**, *53* (18), 9849–9854.
(126) McNamara, N. D.; Hicks, J. C. CO_2 Capture and Conversion with a Multifunctional Polyethyleneimine-Tethered Iminophosphine Iridium Catalyst/Adsorbent. *ChemSusChem* **2014**, *7* (4), 1114–1124.
(127) Kothandaraman, J.; Goeppert, A.; Czaun, M.; Olah, G. A.; Prakash, G. K. S. CO_2 Capture by Amines in Aqueous Media and Its Subsequent Conversion to Formate with Reusable Ruthenium and Iron Catalysts. *Green Chem.* **2016**, *18* (21), 5831–5838.
(128) Scott, M.; Blas Molinos, B.; Westhues, C.; Franciò, G.; Leitner, W. Aqueous Biphasic Systems for the Synthesis of Formates by Catalytic CO_2 Hydrogenation: Integrated Reaction and Catalyst Separation for CO_2-Scrubbing Solutions. *ChemSusChem.* **2017**, *10* (6), 1085–1093.

(129) Guan, C.; Pan, Y.; Ang, E. P. L.; Hu, J.; Yao, C.; Huang, M.-H.; Li, H.; Lai, Z.; Huang, K.-W. Conversion of CO_2 from Air into Formate Using Amines and Phosphorus–Nitrogen PN_3P–Ru(II) Pincer Complexes. *Green Chem.* **2018**, *20* (18), 4201–4205.
(130) Kar, S.; Goeppert, A.; Galvan, V.; Chowdhury, R.; Olah, J.; Prakash, G. K. S. A Carbon-Neutral CO_2 Capture, Conversion, and Utilization Cycle with Low-Temperature Regeneration of Sodium Hydroxide. *J. Am. Chem. Soc.* **2018**, *140* (49), 16873–16876.
(131) Bhardwaj, R.; Kumar, A.; Choudhury, J. An All-Aqueous and Phosphine-Free Integrated Amine-Assisted CO_2 Capture and Catalytic Conversion to Formic Acid. *Chem. Commun.* **2022**, *58* (82), 11531–11534.
(132) Wei, D.; Junge, H.; Beller, M. An Amino Acid-Based System for CO_2 Capture and Catalytic Utilization to Produce Formates. *Chem. Sci.* **2021**, *12* (17), 6020–6024.
(133) Moazezbarabadi, A.; Wei, D.; Junge, H.; Beller, M. Improved CO_2 Capture and Catalytic Hydrogenation Using Amino Acid-Based Ionic Liquids. *ChemSusChem* **2022**, *15* (23), e202201502..
(134) Bertau, M.; Kraft, M.; Plass, L.; Wernicke, H.-J. Methanol. In *Handbook of Fuels: Energy Sources for Transportation*; **2021**; pp 245–306.
(135) Verhelst, S.; Turner, J. W.; Sileghem, L.; Vancoillie, J. Methanol as a Fuel for Internal Combustion Engines. *Prog. Energy Combust. Sci.* **2019**, *70*, 43–88.
(136) Dorokhov, Y. L.; Shindyapina, A. V.; Sheshukova, E. V.; Komarova, T. V. Metabolic Methanol: Molecular Pathways and Physiological Roles. *Physiol. Rev.* **2015**, *95* (2), 603–644.
(137) Amin, M. The Catalytic CO_2 Reforming of Methane for the Low-Temperature Production of Methanol. *(unpublished or incomplete reference; publication details needed for ACS formatting).*
(138) Olah, G. A.; Goeppert, A.; Prakash, G. K. S. *Beyond Oil and Gas: The Methanol Economy*; John Wiley & Sons: Weinheim, **2018**.
(139) Stöcker, M. Methanol to Olefins (MTO) and Methanol to Gasoline (MTG). In *Zeolites and Catalysis: Synthesis, Reactions and Applications*; **2010**; pp 687–711.
(140) Alberico, E.; Nielsen, M. Towards a Methanol Economy Based on Homogeneous Catalysis: Methanol to H_2 and CO_2 to Methanol. *Chem. Commun.* **2015**, *51* (31), 6714–6725.
141) Bertau, M.; Offermanns, H.; Plass, L.; Schmidt, F.; Wernicke, H.-J. *Methanol: The Basic Chemical and Energy Feedstock of the Future*; Springer: Berlin, **2014**.
(142) Owusu, P. A.; Asumadu-Sarkodie, S. A Review of Renewable Energy Sources, Sustainability Issues, and Climate Change Mitigation. *Cogent Eng.* **2016**, *3* (1), 1167990.
(143) Sen, R.; Goeppert, A.; Prakash, G. K. S. Carbon Dioxide Capture and Recycling to Methanol: Building a Carbon-Neutral Methanol Economy. *Aldrichim. Acta* **2020**, *53*, 39–56.
(144) Zhen, X.; Wang, Y. An Overview of Methanol as an Internal Combustion Engine Fuel. *Renewable Sustainable Energy Rev.* **2015**, *52*, 477–493.
(145) Kamarudin, S. K.; Achmad, F.; Daud, W. R. W. Overview on the Application of Direct Methanol Fuel Cells (DMFCs) for Portable Electronic Devices. *Int. J. Hydrogen Energy* **2009**, *34* (16), 6902–6916.
(146) Li, X.; Faghri, A. Review and Advances of Direct Methanol Fuel Cells (DMFCs). Part I: Design, Fabrication, and Testing with High-Concentration Methanol Solutions. *J. Power Sources* **2013**, *226*, 223–240.
(147) Demirbas, A.; Balubaid, M.; Basahel, A.; Ahmad, W.; Sheikh, M. Octane Rating of Gasoline and Octane Booster Additives. *Pet. Sci. Technol.* **2015**, *33* (11), 1190–1197.
(148) Lee, H.; Jung, I.; Roh, G.; Na, Y.; Kang, H. Comparative Analysis of On-Board Methane and Methanol Reforming Systems Combined with HT-PEM Fuel Cell and CO_2 Capture/Liquefaction System for Hydrogen-Fueled Ship Application. *Energies* **2020**, *13* (1), 224.

(149) Sun, Z.; Sun, Z.-Q. Hydrogen Generation from Methanol Reforming for Fuel Cell Applications: A Review. *J. Cent. South Univ.* **2020**, *27* (4), 1074–1103.
(150) Avgouropoulos, G.; Paxinou, A.; Neophytides, S. *In Situ* Hydrogen Utilization in an Internal Reforming Methanol Fuel Cell. *Int. J. Hydrogen Energy* **2014**, *39* (31), 18103–18108.
(151) Kothandaraman, J.; Kar, S.; Goeppert, A.; Sen, R.; Prakash, G. K. S. Advances in Homogeneous Catalysis for Low-Temperature Methanol Reforming in the Context of the Methanol Economy. *Top. Catal.* **2018**, *61*, 542–559.
(152) Tabibian, S. S.; Sharifzadeh, M. Statistical and Analytical Investigation of Methanol Applications, Production Technologies, Value-Chain, and Economy with a Special Focus on Renewable Methanol. *Renewable Sustainable Energy Rev.* **2023**, *179*, 113281.
(153) Ott, J.; Gronemann, V.; Pontzen, F.; Fiedler, E.; Grossmann, G.; Kersebohm, D. B.; Weiss, G.; Witte, C. Methanol. In *Ullmann's Encyclopedia of Industrial Chemistry*; Wiley-VCH: Weinheim, **2012**; Vol. 10, a16_465.
(154) Methanol Institute. Methanol Applications. https://www.methanol.org/applications/.
155) Sen, R.; Goeppert, A.; Prakash, G. K. S. Homogeneous Hydrogenation of CO_2 and CO to Methanol: The Renaissance of Low-Temperature Catalysis in the Context of the Methanol Economy. *Angew. Chem., Int. Ed.* **2022**, *61* (42), e202207278.
(156) Onishi, N.; Himeda, Y. CO_2 Hydrogenation to Methanol by Organometallic Catalysts. *Chem Catal.* **2022**, *2* (2), 242–252.
(157) Dub, P. A.; Ikariya, T. Catalytic Reductive Transformations of Carboxylic and Carbonic Acid Derivatives Using Molecular Hydrogen. *ACS Catal.* **2012**, *2* (8), 1718–1741.
(158) Werkmeister, S.; Junge, K.; Beller, M. Catalytic Hydrogenation of Carboxylic Acid Esters, Amides, and Nitriles with Homogeneous Catalysts. *Org. Process Res. Dev.* **2014**, *18* (2), 289–302.
(159) Huff, C. A.; Sanford, M. S. Cascade Catalysis for the Homogeneous Hydrogenation of CO_2 to Methanol. *J. Am. Chem. Soc.* **2011**, *133* (45), 18122–18125.
(160) Chu, W.-Y.; Culakova, Z.; Wang, B. T.; Goldberg, K. I. Acid-Assisted Hydrogenation of CO_2 to Methanol in a Homogeneous Catalytic Cascade System. *ACS Catal.* **2019**, *9* (10), 9317–9326.
(161) Scharnagl, F. K.; Hertrich, M. F.; Neitzel, G.; Jackstell, R.; Beller, M. Homogeneous Catalytic Hydrogenation of CO_2 to Methanol—Improvements with Tailored Ligands. *Adv. Synth. Catal.* **2019**, *361* (2), 374–379.
(162) Wesselbaum, S.; Moha, V.; Meuresch, M.; Brosinski, S.; Thenert, K. M.; Kothe, J.; vom Stein, T.; Englert, U.; Hölscher, M.; Klankermayer, J. Hydrogenation of Carbon Dioxide to Methanol Using a Homogeneous Ruthenium–Triphos Catalyst: From Mechanistic Investigations to Multiphase Catalysis. *Chem. Sci.* **2015**, *6* (1), 693–704.
(163) Rayder, T. M.; Adillon, E. H.; Byers, J. A.; Tsung, C.-K. A Bioinspired Multicomponent Catalytic System for Converting Carbon Dioxide into Methanol Autocatalytically. *Chem*. **2020**, *6* (7), 1742–1754.
(164) Rezayee, N. M.; Huff, C. A.; Sanford, M. S. Tandem Amine and Ruthenium-Catalyzed Hydrogenation of CO_2 to Methanol. *J. Am. Chem. Soc.* **2015**, *137* (3), 1028–1031.
(165) Zhang, L.; Han, Z.; Zhao, X.; Wang, Z.; Ding, K. Highly Efficient Ruthenium-Catalyzed N-Formylation of Amines with H_2 and CO_2. *Angew. Chem., Int. Ed.* **2015**, *54* (21), 6186–6189.
(166) Kothandaraman, J.; Goeppert, A.; Czaun, M.; Olah, G. A.; Prakash, G. K. S. Conversion of CO_2 from Air into Methanol Using a Polyamine and a Homogeneous Ruthenium Catalyst. *J. Am. Chem. Soc.* **2016**, *138* (3), 778–781.
(167) Everett, M.; Wass, D. Highly Productive CO_2 Hydrogenation to Methanol—A Tandem Catalytic Approach via Amide Intermediates. *Chem. Commun.* **2017**, *53* (68), 9502–9504.

(168) Yoshimura, A.; Watari, R.; Kuwata, S.; Kayaki, Y. Poly(ethyleneimine)-Mediated Consecutive Hydrogenation of Carbon Dioxide to Methanol with Ru Catalysts. *Eur. J. Inorg. Chem.* **2019**, *2019* (18), 2375–2380.
(169) Kar, S.; Goeppert, A.; Kothandaraman, J.; Prakash, G. K. S. Manganese-Catalyzed Sequential Hydrogenation of CO_2 to Methanol via Formamide. *ACS Catal.* **2017**, *7* (9), 6347–6351.
(170) Lane, E. M.; Zhang, Y.; Hazari, N.; Bernskoetter, W. H. Sequential Hydrogenation of CO_2 to Methanol Using a Pincer Iron Catalyst. *Organometallics.* **2019**, *38* (15), 3084–3091.
(171) Koch, C. J.; Goeppert, A.; Surya Prakash, G. Addition of Imidazolium-Based Ionic Liquid to Improve Methanol Production in Polyamine-Assisted CO2 Capture and Conversion Systems Using Pincer Catalysts. *ChemSusChem.* **2024**, *17* (18), e202301789.
(172) Khusnutdinova, J. R.; Garg, J. A.; Milstein, D. Combining low-pressure CO2 capture and hydrogenation to form methanol. *Acs Catalysis* **2015**, *5* (4), 2416–2422.
(173) Rezayee, N. M.; Huff, C. A.; Sanford, M. S. Tandem amine and ruthenium-catalyzed hydrogenation of CO2 to methanol. *J. Am. Chem. Soc.* **2015**, *137* (3), 1028–1031.
(174) Sen, R.; Goeppert, A.; Kar, S.; Prakash, G. S. Hydroxide based integrated CO2 capture from air and conversion to methanol. *J. Am. Chem. Soc.* **2020**, *142* (10), 4544–4549.
(175) Kothandaraman, J.; Heldebrant, D. J. Catalytic Coproduction of Methanol and Glycol in One Pot from Epoxide, CO_2, and H_2. *RSC Adv.* **2020**, *10* (69), 42557–42563.
(176) Kar, S.; Sen, R.; Goeppert, A.; Prakash, G. K. S. Integrative CO_2 Capture and Hydrogenation to Methanol with Reusable Catalyst and Amine: Toward a Carbon-Neutral Methanol Economy. *J. Am. Chem. Soc.* **2018**, *140* (5), 1580–1583.
(177) Moazezbarabadi, A.; Kammer, A.; Alberico, E.; Junge, H.; Beller, M. Amino Acid-Based Ionic Liquids-Aided CO_2 Hydrogenation to Methanol. *ChemSusChem.* **2025**, *18* (7), e202401813.
(178) Song, Z.; Liang, Y.; Fan, M.; Zhou, F.; Liu, W. Ionic Liquids from Amino Acids: Fully Green Fluid Lubricants for Various Surface Contacts. *RSC Adv.* **2014**, *4* (37), 19396–19402.
(179) Carreira, A. R.; Rocha, S. N.; e Silva, F. A.; Sintra, T. E.; Passos, H.; Ventura, S. P. M.; Coutinho, J. A. P. Amino Acid-Based Chiral Ionic Liquids: Characterization and Application in Aqueous Biphasic Systems. *Fluid Phase Equilib.* **2021**, *542*, 113091.
(180) Fang, W.; Zhang, Y.; Yang, Z.; Zhang, Z.; Xu, F.; Wang, W.; He, H.; Diao, Y.; Zhang, Y.; Luo, Y. Efficient Activation of Dimethyl Carbonate to Synthesize Bio-Based Polycarbonate by Eco-Friendly Amino Acid Ionic Liquid Catalyst. *Appl. Catal., A*. **2021**, *617*, 118111
(181) Guncheva, M.; Ossowicz, P.; Janus, E.; Todinova, S.; Yancheva, D. Elucidation of the Effect of Some Cholinium Amino Acid Ionic Liquids on the Thermal and Conformational Stability of Insulin. *J. Mol. Liq.* **2019**, *283*, 257–262.
(182) Sistla, Y. S.; Khanna, A. CO_2 Absorption Studies in Amino Acid-Anion-Based Ionic Liquids. *Chem. Eng. J.* **2015**, *273*, 268–276.
(183) Lang, X.-D.; Zhang, S.; Song, Q.-W.; He, L.-N. Tetrabutylphosphonium Arginine-Based Ionic Liquid-Promoted Cyclization of 2-Aminobenzonitrile with Carbon Dioxide. *RSC Adv.* **2015**, *5* (20), 15668–15673.
(184) Zhang, L.; Raffa, G.; Nguyen, D. H.; Swesi, Y.; Corbel-Demailly, L.; Capet, F.; Trivelli, X.; Desset, S.; Paul, S.; Paul, J.-F. Acceptorless Dehydrogenative Coupling of Alcohols Catalyzed by Ruthenium PNP Complexes: Influence of Catalyst Structure and Hydrogen Mass Transfer. *J. Catal.* **2016**, *340*, 331–343.
(185) Chen, J.; Wang, J.; Tu, T. Ruthenium-Pincer-Catalyzed Hydrogenation of Lactams to Amino Alcohols. *Chem. Asian J.* **2018**, *13* (17), 2559–2565.

(186) Elangovan, S.; Topf, C.; Fischer, S.; Jiao, H.; Spannenberg, A.; Baumann, W.; Ludwig, R.; Junge, K.; Beller, M. Selective Catalytic Hydrogenations of Nitriles, Ketones, and Aldehydes by Well-Defined Manganese Pincer Complexes. *J. Am. Chem. Soc.* **2016**, *138* (28), 8809–8814.
(187) Alberico, E.; Sponholz, P.; Cordes, C.; Nielsen, M.; Drexler, H. J.; Baumann, W.; Junge, H.; Beller, M. Selective Hydrogen Production from Methanol with a Defined Iron Pincer Catalyst under Mild Conditions. *Angew. Chem.* **2013**, *125* (52), 14412–14416.
(188) Zanatta, M.; Girard, A.-L.; Marin, G.; Ebeling, G.; Dos Santos, F. P.; Valsecchi, C.; Stassen, H.; Livotto, P. R.; Lewis, W.; Dupont, J. Confined Water in Imidazolium-Based Ionic Liquids: A Supramolecular Guest@Host Complex Case. *Phys. Chem. Chem. Phys.* **2016**, *18* (27), 18297–18304.
(189) Zanatta, M.; Simon, N. M.; Dupont, J. The Nature of Carbon Dioxide in Bare Ionic Liquids. *ChemSusChem* **2020**, *13* (12), 3101–3109.
(190) Fitch, C. A.; Platzer, G.; Okon, M.; Garcia-Moreno, E. B.; McIntosh, L. P. Arginine: Its pK_a Value Revisited. *Protein Sci.* **2015**, *24* (5), 752–761.
(191) Banyikwa, A. T.; Miller, S. E.; Krebs, R. A.; Xiao, Y.; Carney, J. M.; Braiman, M. S. Anhydrous Monoalkylguanidines in Aprotic and Nonpolar Solvents: Models for Deprotonated Arginine Side Chains in Membrane Environments. *ACS Omega* **2017**, *2* (10), 7239–7252.
(192) Fukumoto, K.; Yoshizawa, M.; Ohno, H. Room-Temperature Ionic Liquids from 20 Natural Amino Acids. *J. Am. Chem. Soc.* **2005**, *127* (8), 2398–2399.
(193) Barzagli, F.; Mani, F.; Peruzzini, M. A ^{13}C NMR Study of the Carbon Dioxide Absorption and Desorption Equilibria by Aqueous 2-Aminoethanol and N-Methyl-Substituted 2-Aminoethanol. *Energy Environ. Sci.* **2009**, *2* (3), 322–330. DOI: 10.1039/B814670E.
(194) Barbarossa, V.; Barzagli, F.; Mani, F.; Lai, S.; Stoppioni, P.; Vanga, G. Efficient CO_2 Capture by Non-Aqueous 2-Amino-2-Methyl-1-Propanol (AMP) and Low-Temperature Solvent Regeneration. *RSC Adv.* **2013**, *3* (30), 12349–12355. DOI: 10.1039/C3RA40933C.
(195) Perinu, C.; Arstad, B.; Jens, K.-J. ^{13}C NMR Experiments and Methods Used to Investigate Amine–CO_2–H_2O Systems. *Energy Procedia* **2013**, *37*, 7310–7317.
(196) Kothandaraman, J.; Goeppert, A.; Czaun, M.; Olah, G. A.; Prakash, G. K. S. Conversion of CO_2 from Air into Methanol Using a Polyamine and a Homogeneous Ruthenium Catalyst. *J. Am. Chem. Soc.* **2016**, *138* (3), 778–781. DOI: 10.1021/jacs.5b12354.
(197) Dubey, A.; Nencini, L.; Fayzullin, R. R.; Nervi, C.; Khusnutdinova, J. R. Bio-Inspired Mn(I) Complexes for the Hydrogenation of CO_2 to Formate and Formamide. *ACS Catal.* **2017**, *7* (6), 3864–3868.
(198) Micheel, F.; Krzeminski, Z.; Himmelmann, W.; Kühlkamp, A. Die Kondensation von Thiosäureamiden mit Aminen, Aminosäuren und Proteinen. *Justus Liebigs Ann. Chem.* **1952**, *575* (1), 90–105.
(199) Zeng, S.; Zhang, X.; Bai, L.; Zhang, X.; Wang, H.; Wang, J.; Bao, D.; Li, M.; Liu, X.; Zhang, S. Ionic-Liquid-Based CO_2 Capture Systems: Structure, Interaction, and Process. *Chem. Rev.* **2017**, *117* (14), 9625–9673.
(200) Ali, S. A.; Mulk, W. U.; Ullah, Z.; Khan, H.; Zahid, A.; Shah, M. U. H.; Shah, S. N. Recent Advances in the Synthesis, Application, and Economic Feasibility of Ionic Liquids and Deep Eutectic Solvents for CO_2 Capture: A Review. *Energies* **2022**, *15* (23), 9098.
(201) Gutowski, K. E.; Maginn, E. J. Amine-Functionalized Task-Specific Ionic Liquids: A Mechanistic Explanation for the Dramatic Increase in Viscosity upon Complexation with CO_2 from Molecular Simulation. *J. Am. Chem. Soc.* **2008**, *130* (44), 14690–14704.
(202) Wu, Y.; Zhao, Y.; Wang, H.; Yu, B.; Yu, X.; Zhang, H.; Liu, Z. 110th Anniversary: Ionic Liquid Promoted CO_2 Hydrogenation to Free Formic Acid over Pd/C. *Ind. Eng. Chem. Res.* **2019**, *58* (16), 6333–6339.

(203) Simkovičová, K.; Qadir, M. I.; Žilková, N.; Olszówka, J. E.; Sialini, P.; Kvítek, L.; Vajda, Š. Hydrogenation of CO_2 on Nanostructured Cu/FeO_x Catalysts: The Effect of Morphology and Cu Load on Selectivity. *Catalysts* **2022**, *12* (5), 516.
(204) Weilhard, A.; Argent, S. P.; Sans, V. Efficient Carbon Dioxide Hydrogenation to Formic Acid with Buffering Ionic Liquids. *Nat. Commun.* **2021**, *12* (1), 1–7.
(205) Kar, S.; Kothandaraman, J.; Goeppert, A.; Prakash, G. K. S. Advances in Catalytic Homogeneous Hydrogenation of Carbon Dioxide to Methanol. *J. CO_2 Util.* **2018**, *23*, 212–218.

(206) Piccirilli, L.; Lobo Justo Pinheiro, D.; Nielsen, M. Recent Progress with Pincer Transition Metal Catalysts for Sustainability. *Catalysts.* **2020**, *10* (7), 773.
(207) Gunanathan, C.; Milstein, D. Bond Activation and Catalysis by Ruthenium Pincer Complexes. *Chem. Rev.* **2014**, *114* (24), 12024–12087.
(208) Wei, D.; Junge, H.; Beller, M. An Amino Acid-Based System for CO_2 Capture and Catalytic Utilization to Produce Formates. *Chem. Sci.* **2021**, *12* (17), 6020–6024.
(209) Ogata, O.; Kuriyama, W. Development of Homogeneous PNP-Ruthenium Complexes (Ru-MACHO Family) for Hydrogenation of Esters and Beyond. *J. Synth. Org. Chem., Jpn.* **2023**, *81* (11), 1040–1049.
(210) Wang, Y.; Zhang, J.; Liu, J.; Zhang, C.; Zhang, Z.; Xu, J.; Xu, S.; Wang, F.; Wang, F. C–N and N–H Bond Metathesis Reactions Mediated by Carbon Dioxide. *ChemSusChem* **2015**, *8* (12), 2066–2072.
(211) Singh, A.; Kemper, G.; Weyhermüller, T.; Kaeffer, N.; Leitner, W. Activated Mn-MACHO Complexes Form Stable CO_2 Adducts. *Chem.–Eur. J.* **2024**, *30* (9), e202303438.
(212) Kothandaraman, J.; Heldebrant, D. J.; Lopez, J. S.; Dagle, R. A. Mechanistic Insights to Drive Catalytic Hydrogenation of Formamide Intermediates to Methanol via Deaminative Hydrogenation. *Front. Energy Res.* **2023**, *11*, 1158499.
(213) Wiedner, E. S.; Linehan, J. C. Making a Splash in Homogeneous CO_2 Hydrogenation: Elucidating the Impact of Solvent on Catalytic Mechanisms. *Chem.–Eur. J.* **2018**, *24* (64), 16964–16971.
(214) Sen, R.; Goeppert, A.; Kar, S.; Prakash, G. K. S. Hydroxide-Based Integrated CO_2 Capture from Air and Conversion to Methanol. *J. Am. Chem. Soc.* **2020**, *142* (10), 4544–4549.
(215) Kuhlmann, R.; Nowotny, M.; Künnemann, K. U.; Behr, A.; Vorholt, A. J. Identification of Key Mechanics in the Ruthenium-Catalyzed Synthesis of N,N-Dimethylformamide from Carbon Dioxide in Biphasic Solvent Systems. *J. Catal.* **2018**, *361*, 45–50.
(216) Piccirilli, L.; Rabell, B.; Padilla, R.; Riisager, A.; Das, S.; Nielsen, M. Versatile CO_2 Hydrogenation–Dehydrogenation Catalysis with a Ru–PNP/Ionic Liquid System. *J. Am. Chem. Soc.* **2023**, *145* (10), 5655–5663.
(217) Patra, S.; Maji, B.; Kawanami, H.; Himeda, Y. High-Pressure Hydrogen Generation from Dehydrogenation of Formic Acid. *RSC Sustain.* **2023**, *1* (7), 1655–1671.
(218) Ślebocka-Tilk, H.; Neverov, A. A.; Brown, R. Proton Inventory Study of the Base-Catalyzed Hydrolysis of Formamide: Consideration of the Nucleophilic and General Base Mechanisms. *J. Am. Chem. Soc.* **2003**, *125* (7), 1851–1858.
(219) Bansode, A.; Urakawa, A. Towards Full One-Pass Conversion of Carbon Dioxide to Methanol and Methanol-Derived Products. *J. Catal.* **2014**, *309*, 66–70.
(220) Zhang, F. H.; Liu, C.; Li, W.; Tian, G. L.; Xie, J. H.; Zhou, Q. L. An Efficient Ruthenium Catalyst Bearing a Tetradentate Ligand for Hydrogenations of Carbon Dioxide. *Chin. J. Chem.* **2018**, *36* (11), 1000–1002.
(221) Dub, P. A.; Gordon, J. C. The Role of the Metal-Bound N–H Functionality in Noyori-Type Molecular Catalysts. *Nat. Rev. Chem.* **2018**, *2* (12), 396–408.

(222) Dub, P. A.; Scott, B. L.; Gordon, J. C. Why Does Alkylation of the N–H Functionality within M/NH Bifunctional Noyori-Type Catalysts Lead to Turnover? *J. Am. Chem. Soc.* **2017**, *139* (3), 1245–1260.
(223) Kar, S.; Goeppert, A.; Sen, R.; Kothandaraman, J.; Prakash, G. K. S. Regioselective Deuteration of Alcohols in D_2O Catalyzed by Homogeneous Manganese and Iron Pincer Complexes. *Green Chem.* **2018**, *20* (12), 2706–2710.
(224) Kar, S.; Sen, R.; Goeppert, A.; Prakash, G. K. S. Integrative CO_2 Capture and Hydrogenation to Methanol with Reusable Catalyst and Amine: Toward a Carbon-Neutral Methanol Economy. *J. Am. Chem. Soc.* **2018**, *140* (5), 1580–1583.
(225) Khan, M. T.; Halligudi, S.; Shukla, S. Reduction of CO_2 by Molecular Hydrogen to Formic Acid and Formaldehyde and Their Decomposition to CO and H_2O. *J. Mol. Catal.* **1989**, *57* (1), 47–60.
(226) Kar, S.; Sen, R.; Kothandaraman, J.; Goeppert, A.; Chowdhury, R.; Munoz, S. B.; Haiges, R.; Prakash, G. S. Mechanistic insights into ruthenium-pincer-catalyzed amine-assisted homogeneous hydrogenation of CO2 to methanol. *J. Am. Chem. Soc.* ***2019***, *141* (7), 3160–3170.
(227) Kobayashi, Y.; Takemoto, Y. Bifunctional Guanidines as Hydrogen-Bond-Donating Catalysts. *Guanidines as Reagents and Catalysts.***2017**, 71–94.
(228) Cundari, T. R.; Wilson, A. K.; Drummond, M. L.; Gonzalez, H. E.; Jorgensen, K. R.; Payne, S.; Braunfeld, J.; De Jesus, M.; Johnson, V. M. CO_2-Formatics: How Do Proteins Bind Carbon Dioxide? *J. Chem. Inf. Model.* **2009**, *49* (9), 2111–2115.

7. Appendix

All NMR and GC spectra presented in this Appendix are reproduced from the author's publications in ChemSusChem (Wiley-VCH).[133, 177] *Permission for reuse has been granted by Wiley-VCH.*

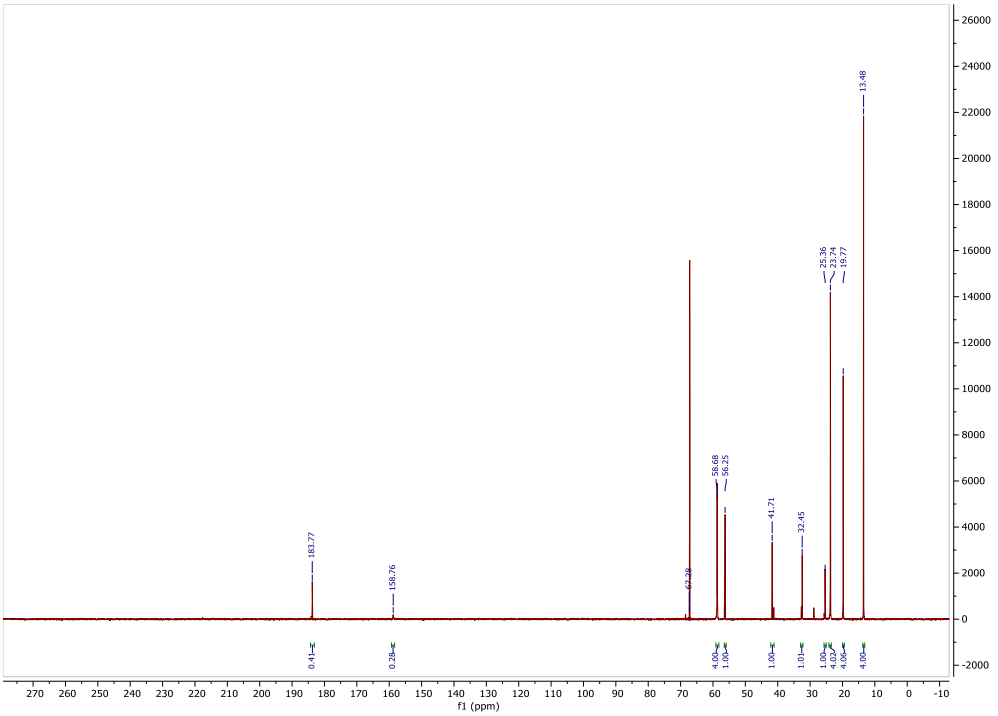


Figure A-1. ^{13}C NMR of [TBA][Arg] in D_2O.Reproduced from ref.[177]

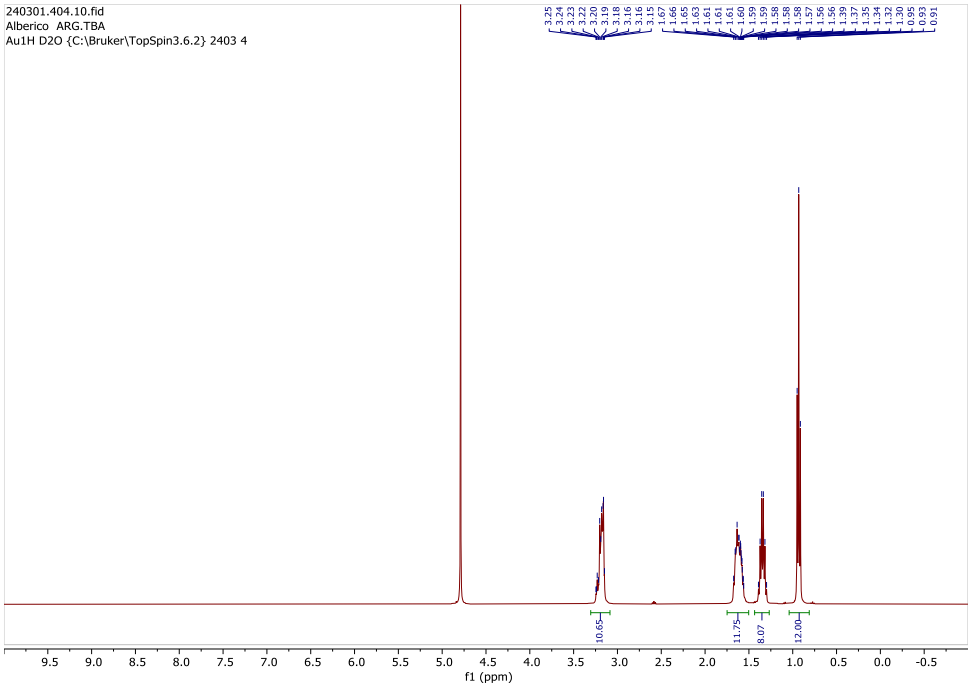


Figure A-2. ^{1}H NMR of [TBA][Arg] in D_2O. Reproduced from ref.[177]

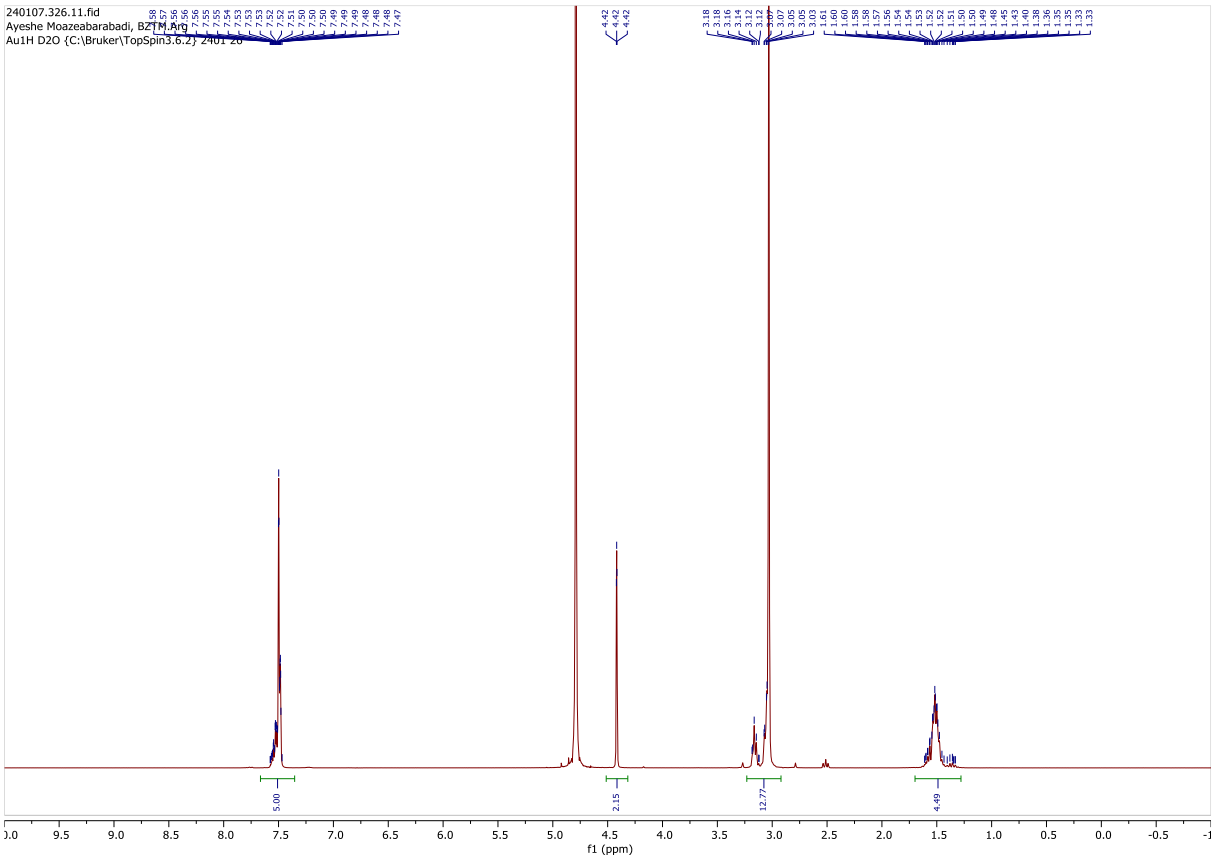


Figure A-3. ^{1}H NMR of [BTMA][Arg] in D_2O. Reproduced from ref.[177]

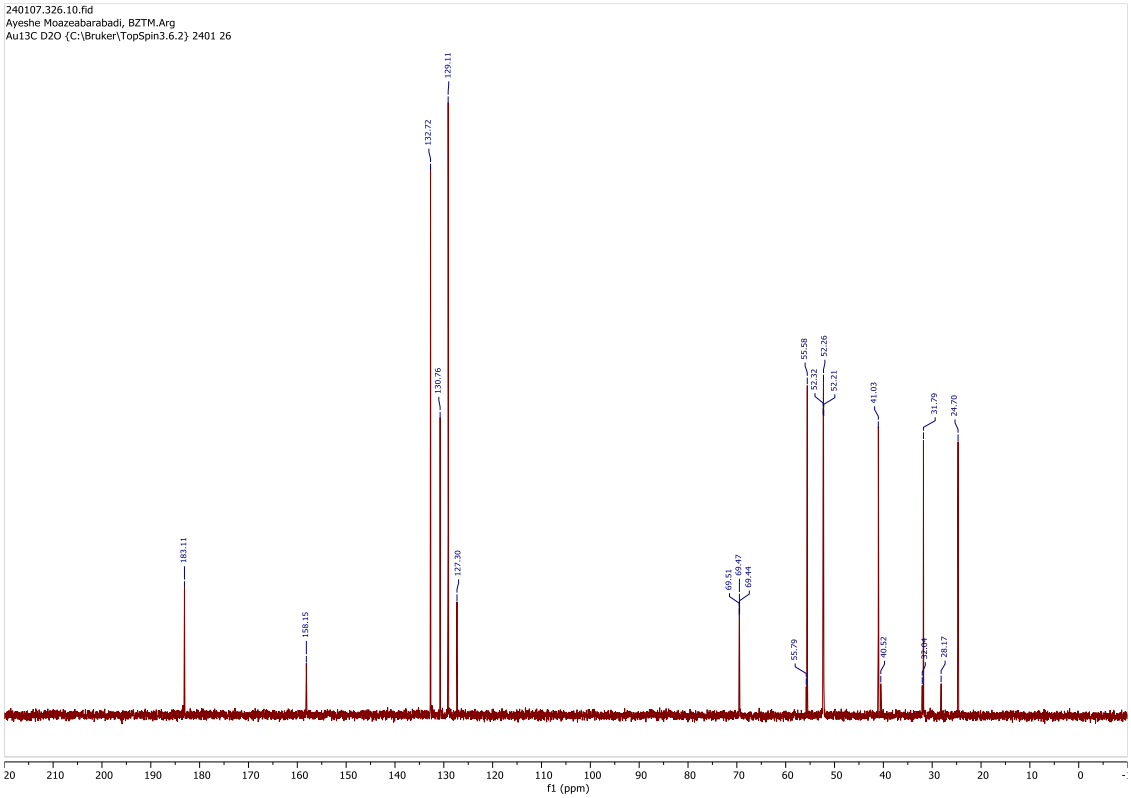


Figure A-4. ^{13}C NMR of [BTMA][Arg] in D_2O.

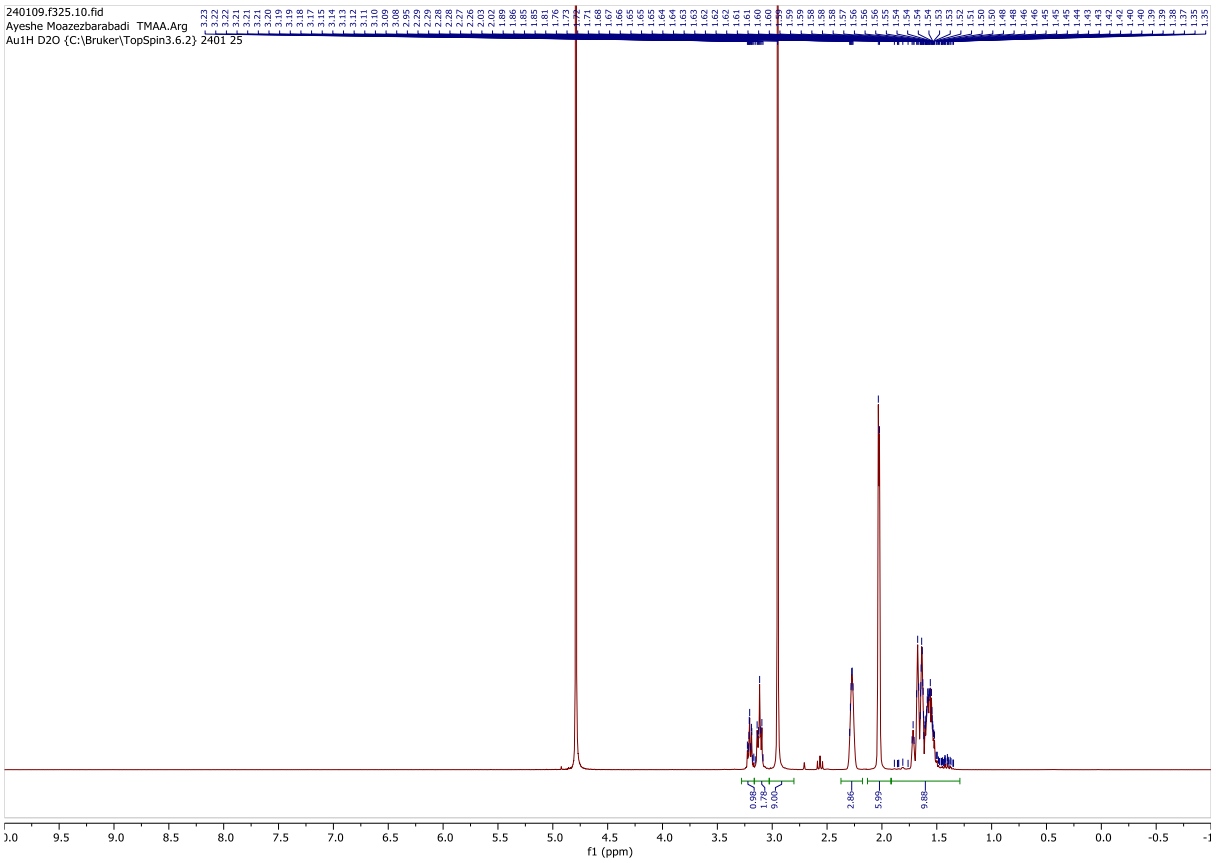


Figure A-5. ^{1}H NMR of [TMAA][Arg] in D_2O. Reproduced from ref.[177]

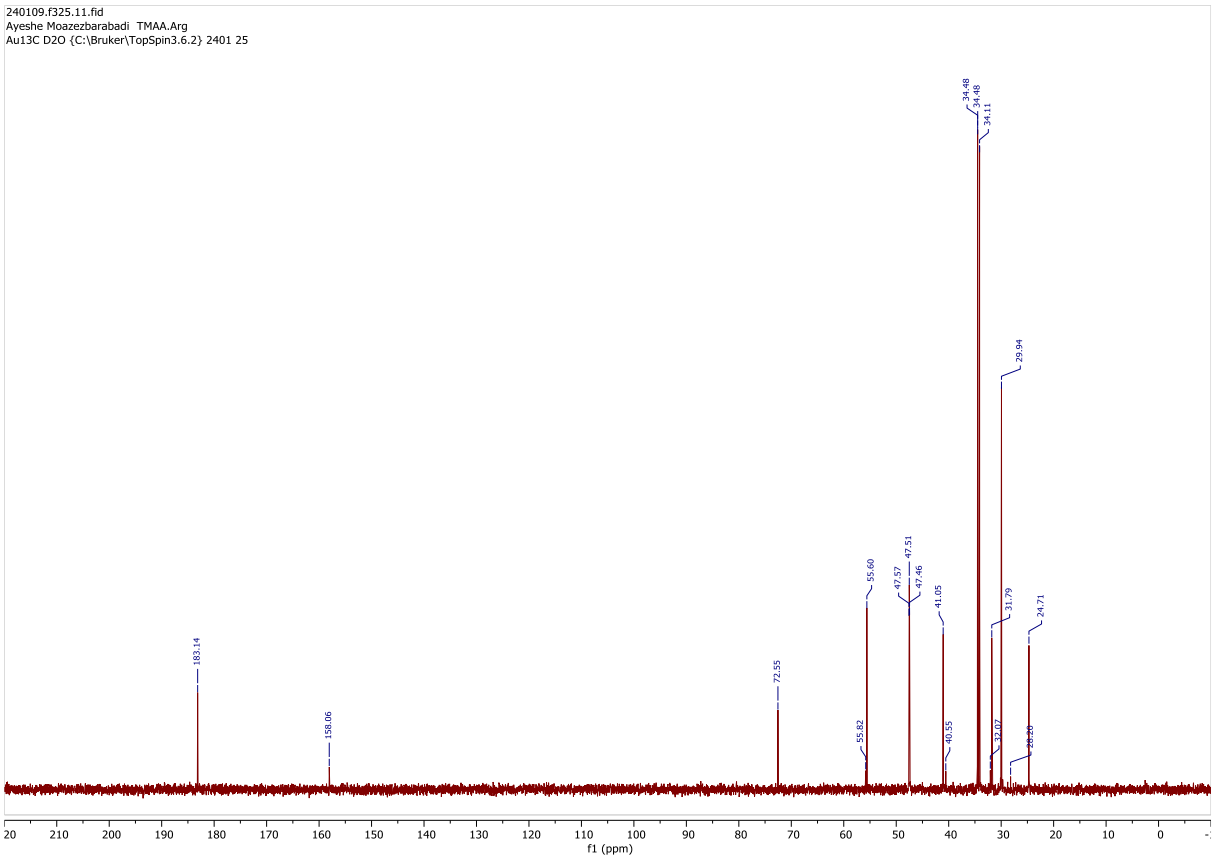


Figure A-6. ^{13}C NMR of [TMAA][Arg] in D_2O. Reproduced from ref.[177]

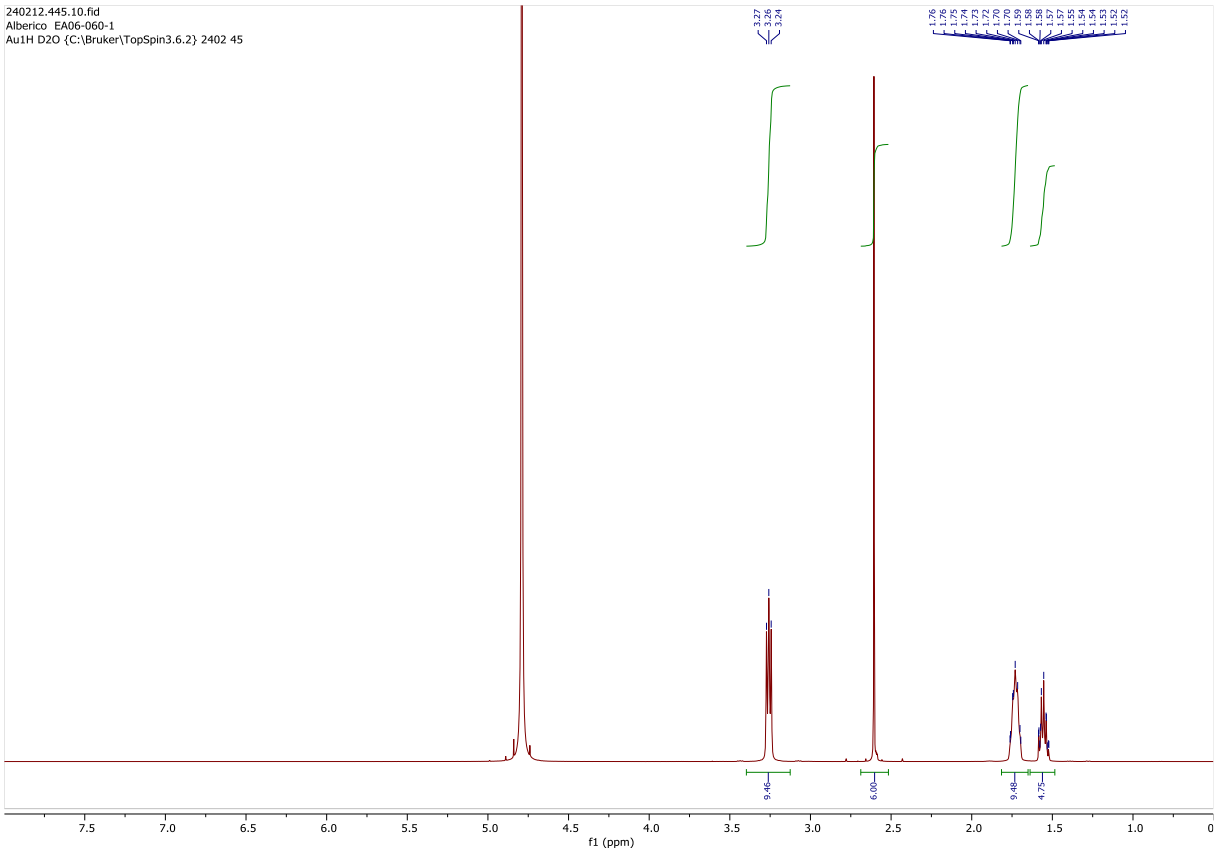


Figure A-7. ^{1}H NMR of [ASU][OH] in D_2O. Reproduced from ref.[177]

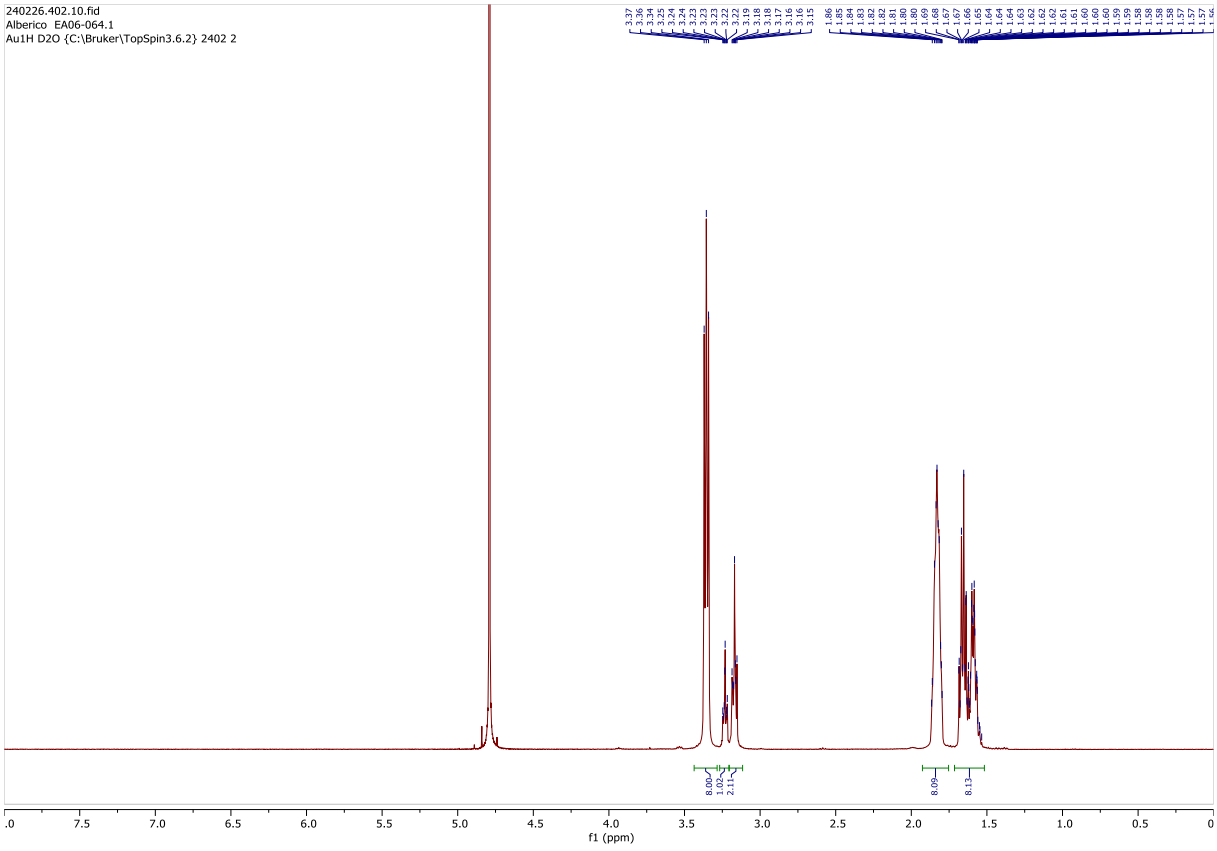


Figure A-8. ^{1}H NMR of [ASU][Arg] in D_2O. Reproduced from ref.[177]

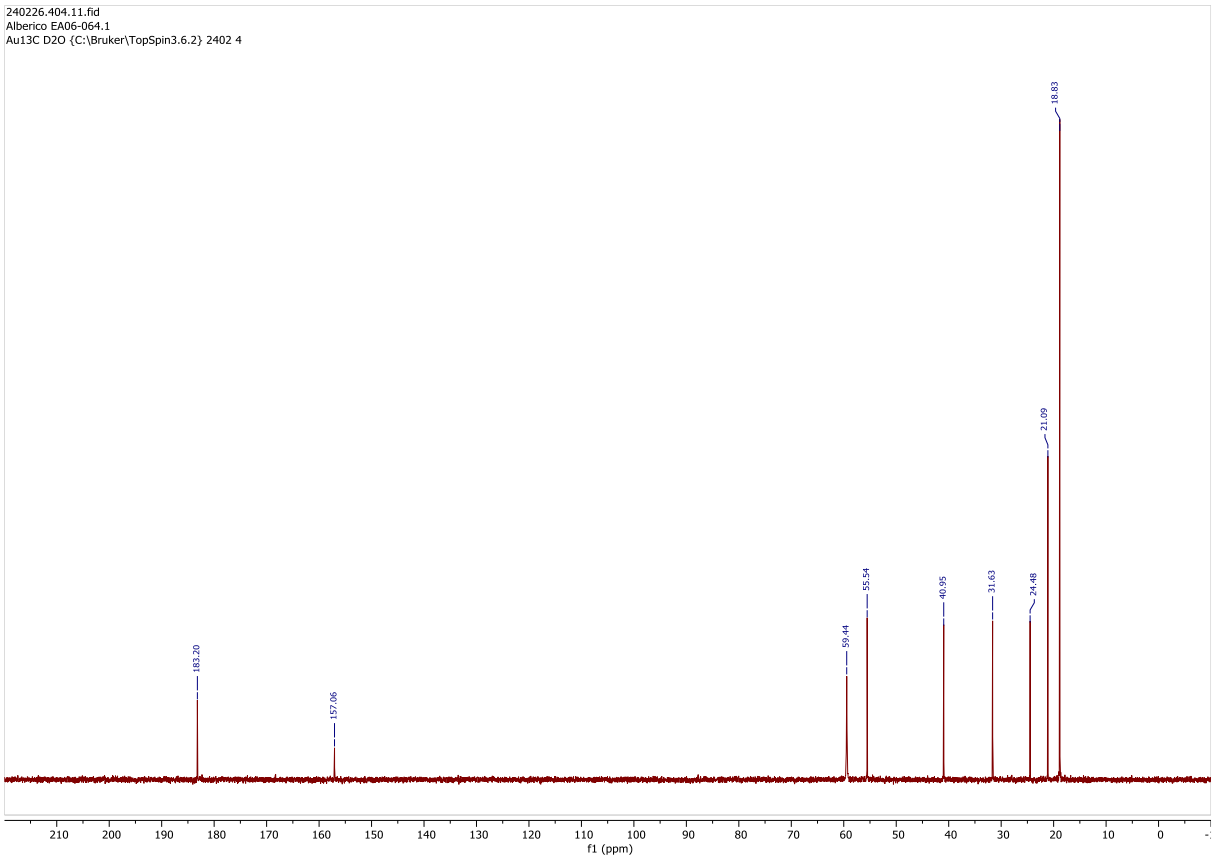


Figure A-9. ^{13}C NMR of [ASU][Arg] in D_2O. Reproduced from ref.[177]

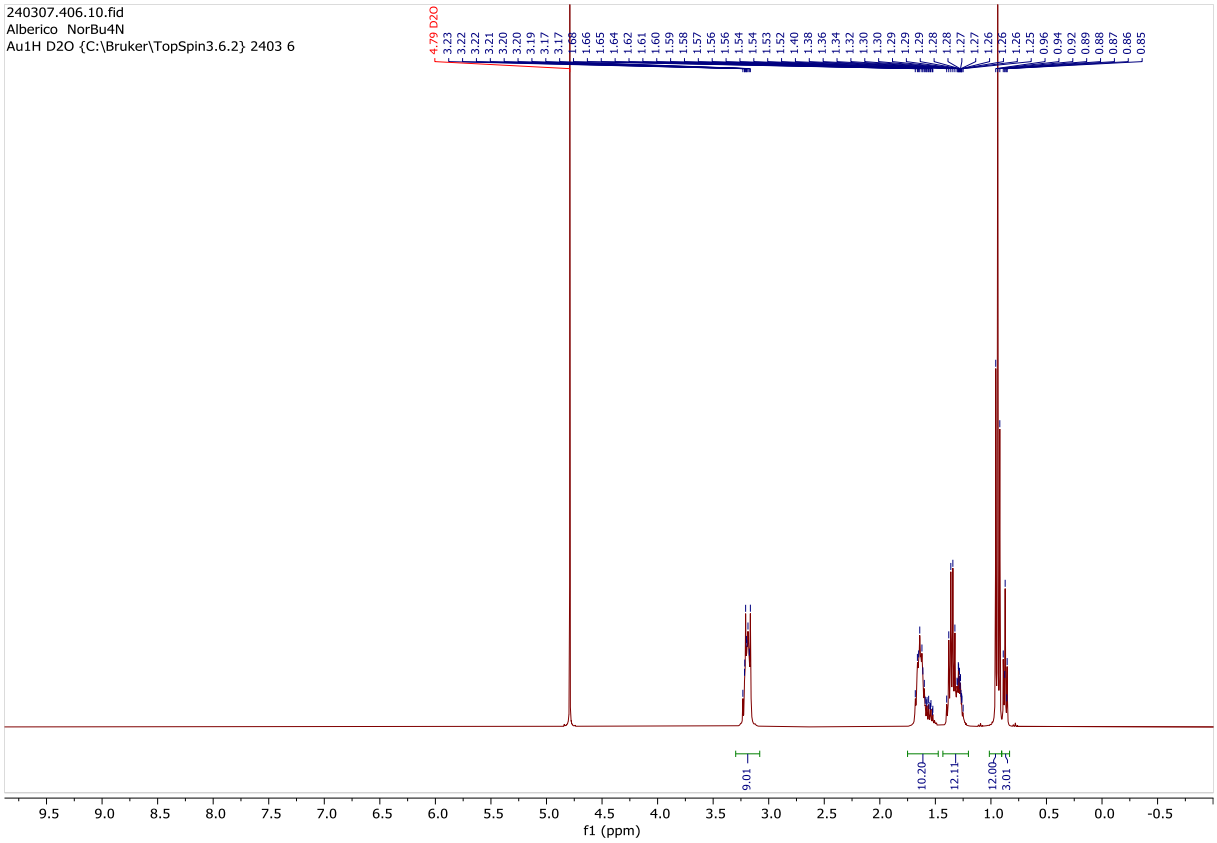


Figure A-10. ^{1}H NMR of [TBA][Nor] in D_2O. Reproduced from ref.[177]

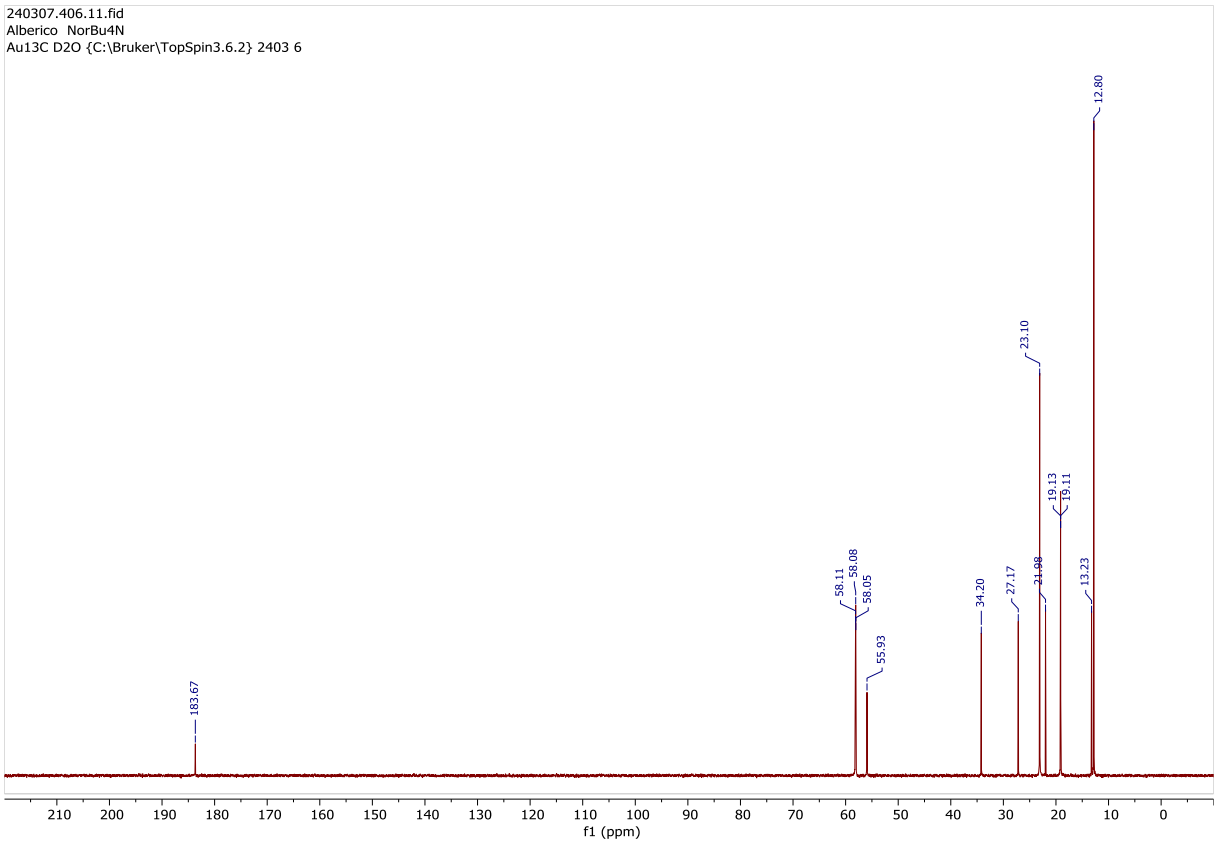


Figure A-11. ^{13}C NMR of [TBA][Nor] in D_2O. Reproduced from ref.[177]

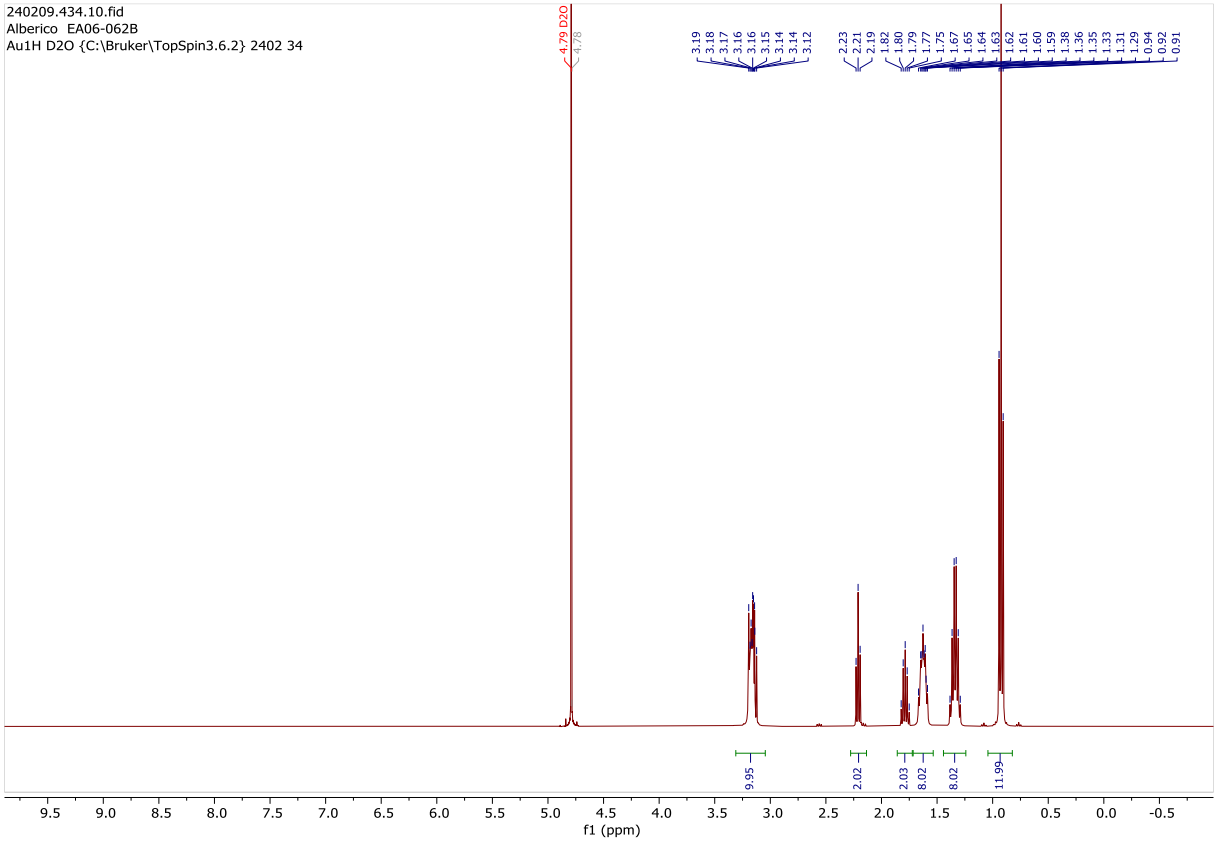


Figure A-12. ^{1}H NMR of [TBA][GB] in D_2O. Reproduced from ref.[177]

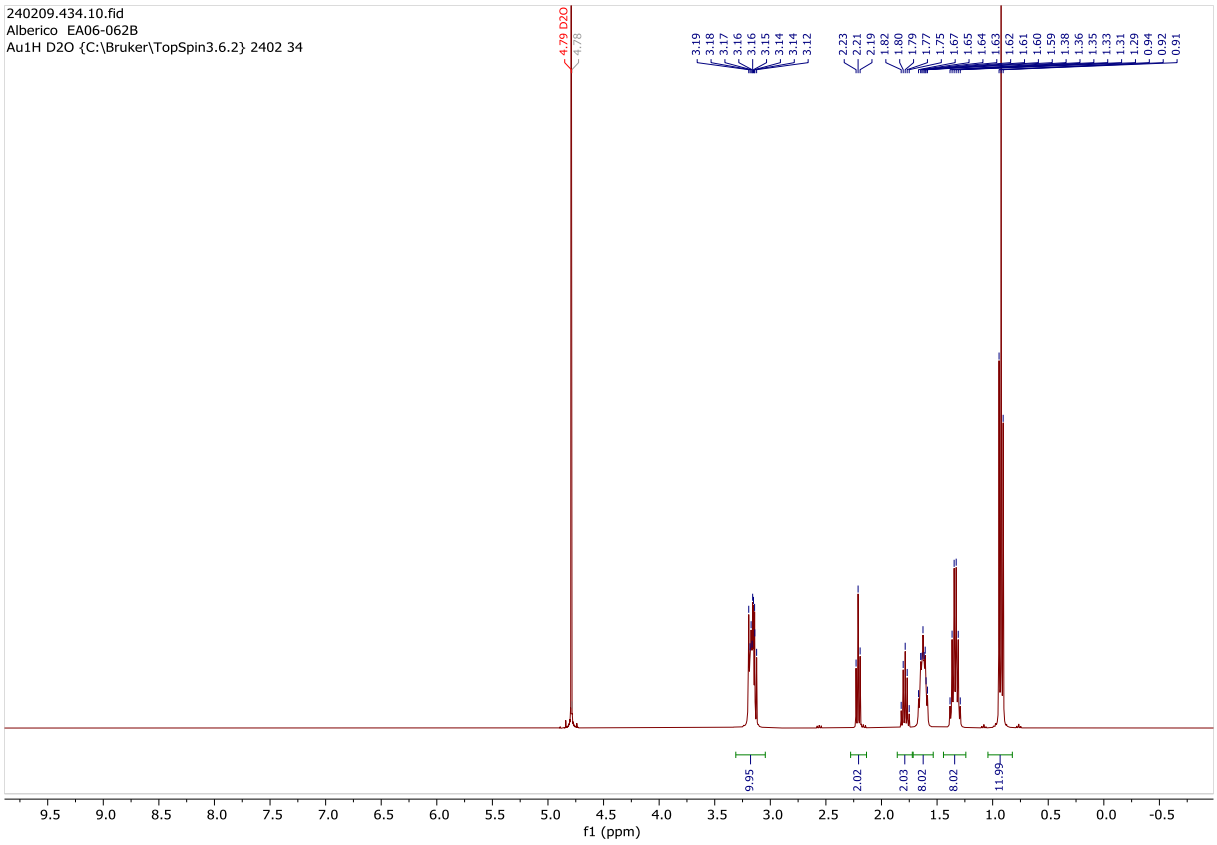


Figure A-13. ^{13}C NMR of [TBA][GB] in D_2O. Reproduced from ref.[177]

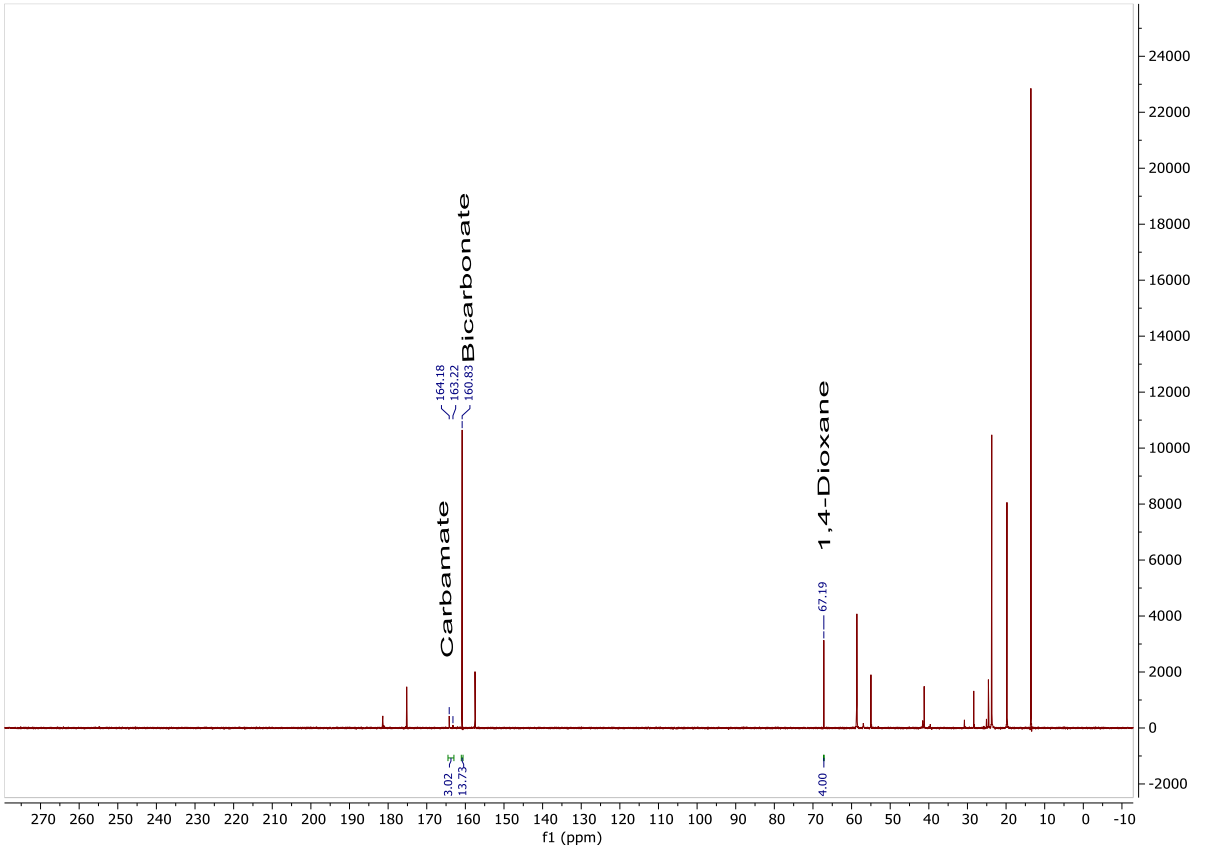


Figure A-14. ^{13}C NMR-quant in D_2O of CO_2 capture under 2 bars of CO_2 (18 h) with 5.0 mmol [TBA][Arg]. Reproduced from ref.[177]

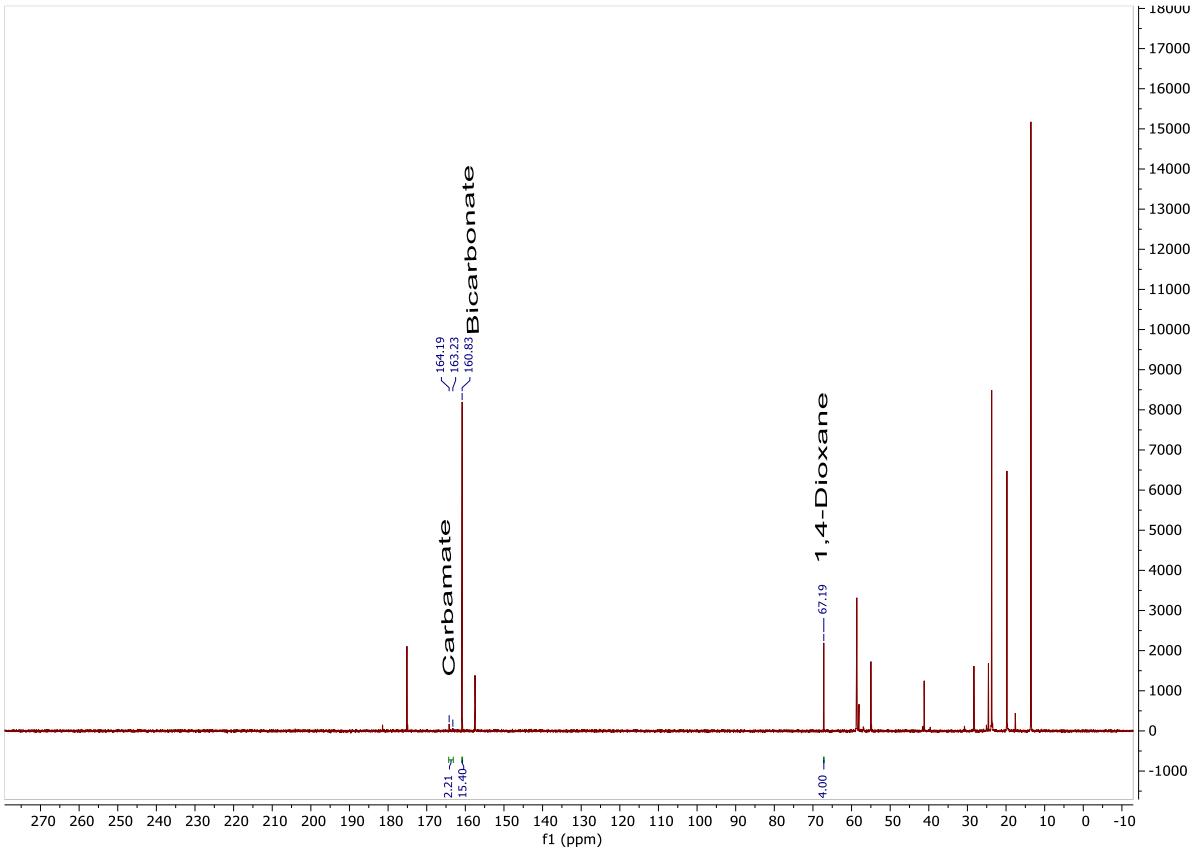


Figure A-15. ^{13}C NMR-quant in D_2O of CO_2 capture under 20 bars of CO_2 (6 h) with 5.0 mmol [TBA][Arg]. Reproduced from ref.[133]

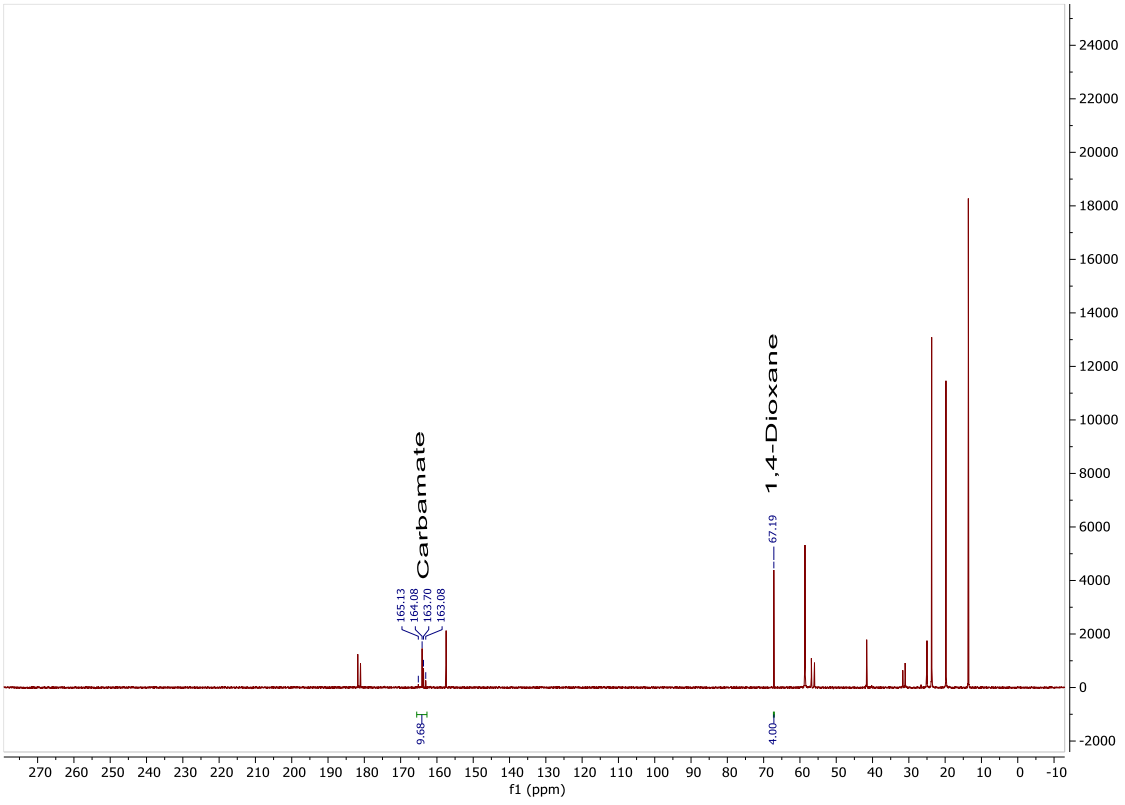


Figure A-16. ^{13}C NMR-quant in D_2O of CO_2 capture with air bubbling (1 L/min. 5 days) with 5.0 mmol [TBA][Arg]. Reproduced from ref.[133]

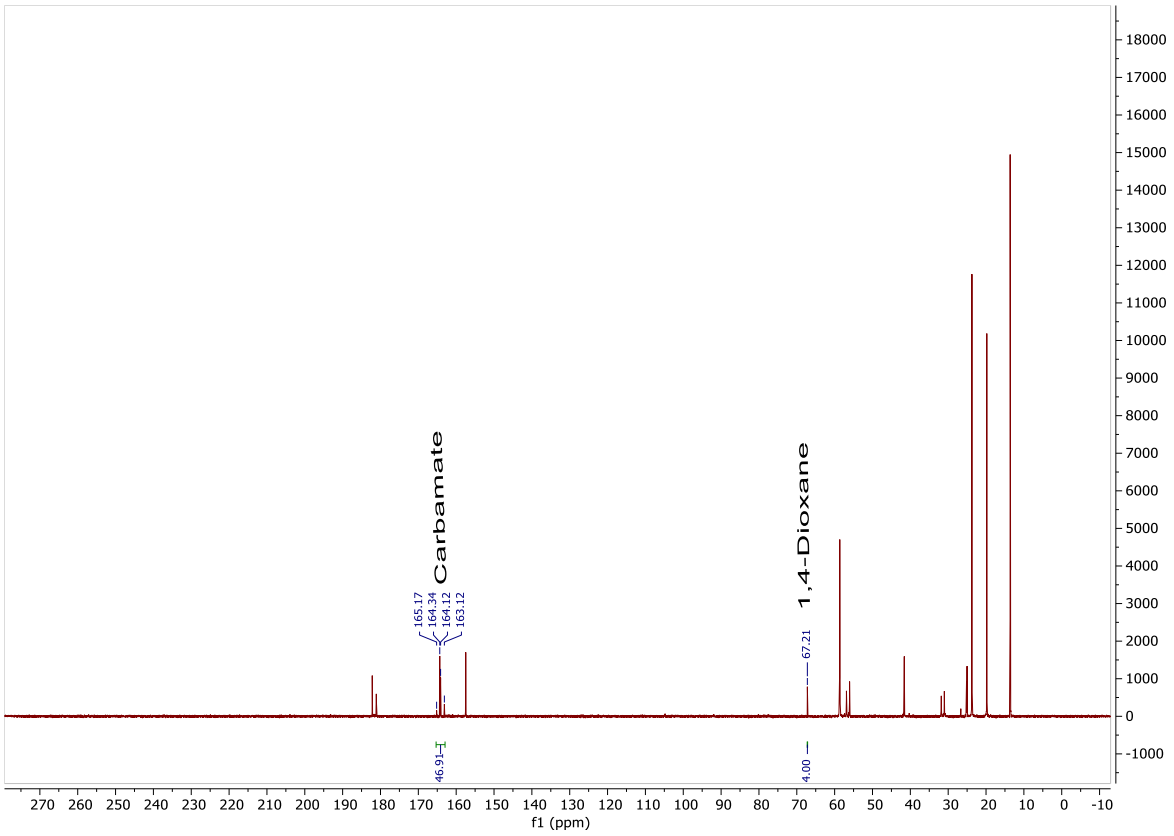


Figure A-17. ^{13}C NMR-quant in D_2O of CO_2 capture with air bubbling (1 L/min. 10 days) with 25.0 mmol [TBA][Arg]. Reproduced from ref.[133]

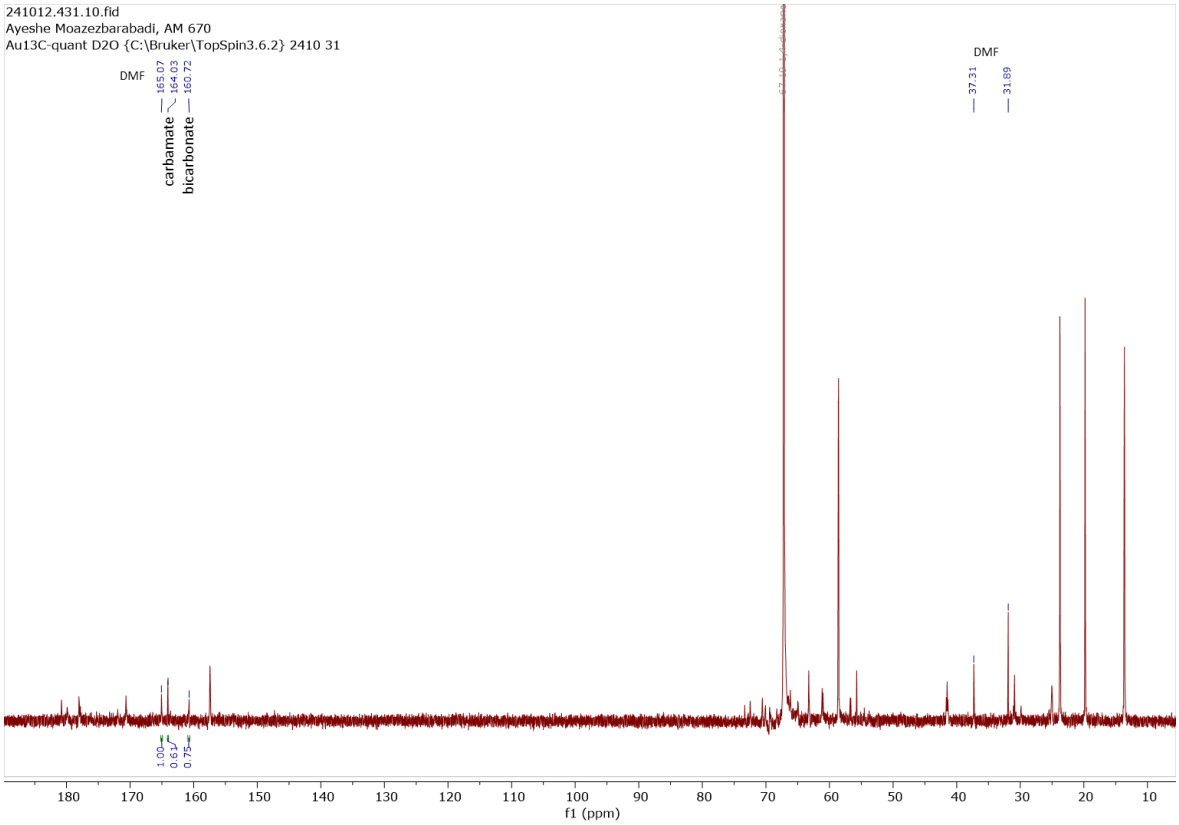


Figure A-18. ^{13}C NMR-quant in D_2O of CO_2 capture with air bubbling (450 mL/min. 10 days) with 5.0 mmol [TBA][Arg] suspended in 20 mL 1,4-dioxane. Reproduced from ref.[133]

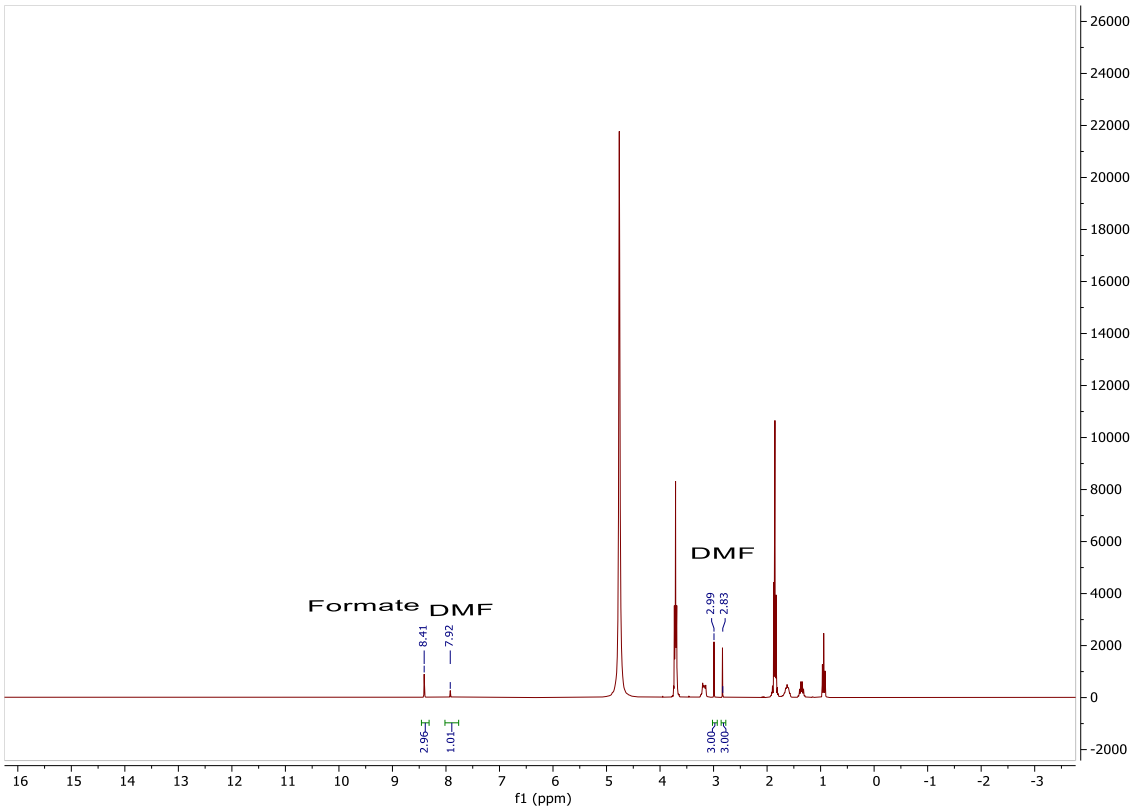


Figure A-19. Representative ^{1}H NMR spectrum (in D_2O) obtained after hydrogenation of gaseous CO_2 to formate using [TBA][Arg]. Reproduced from ref.[133]

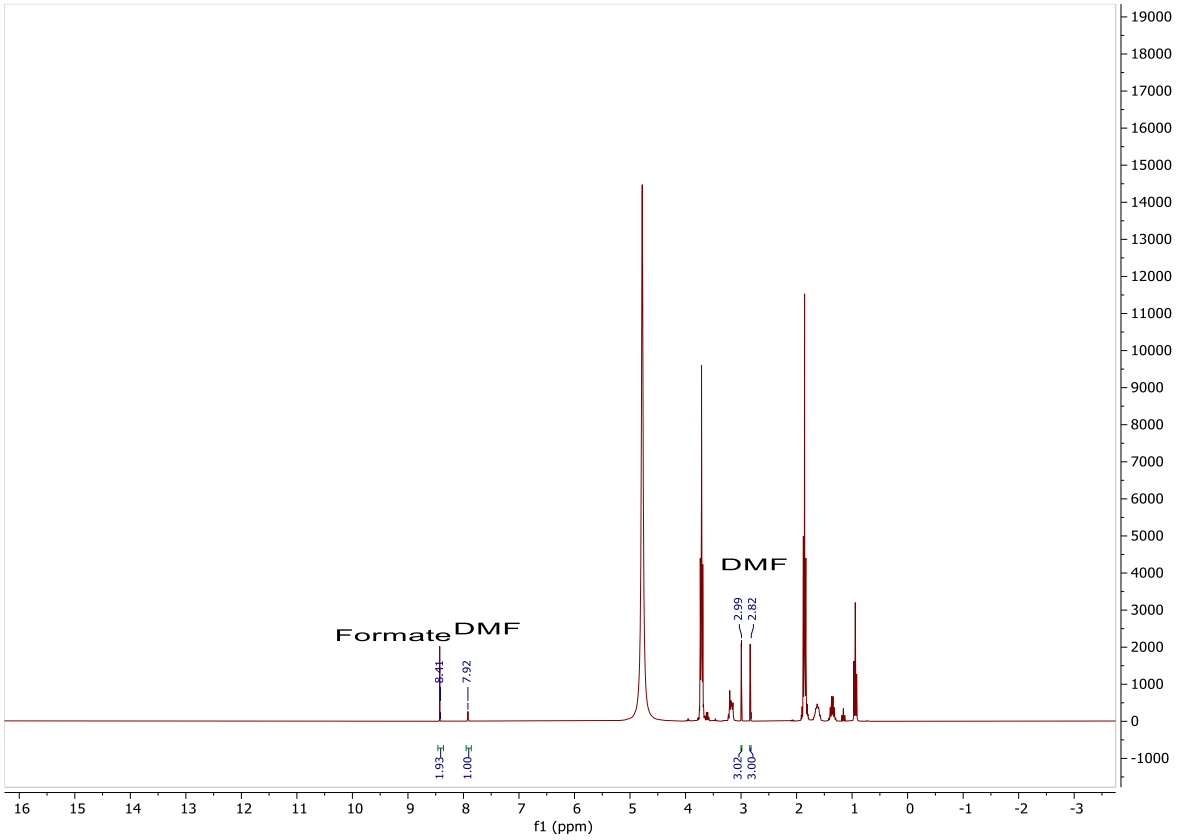
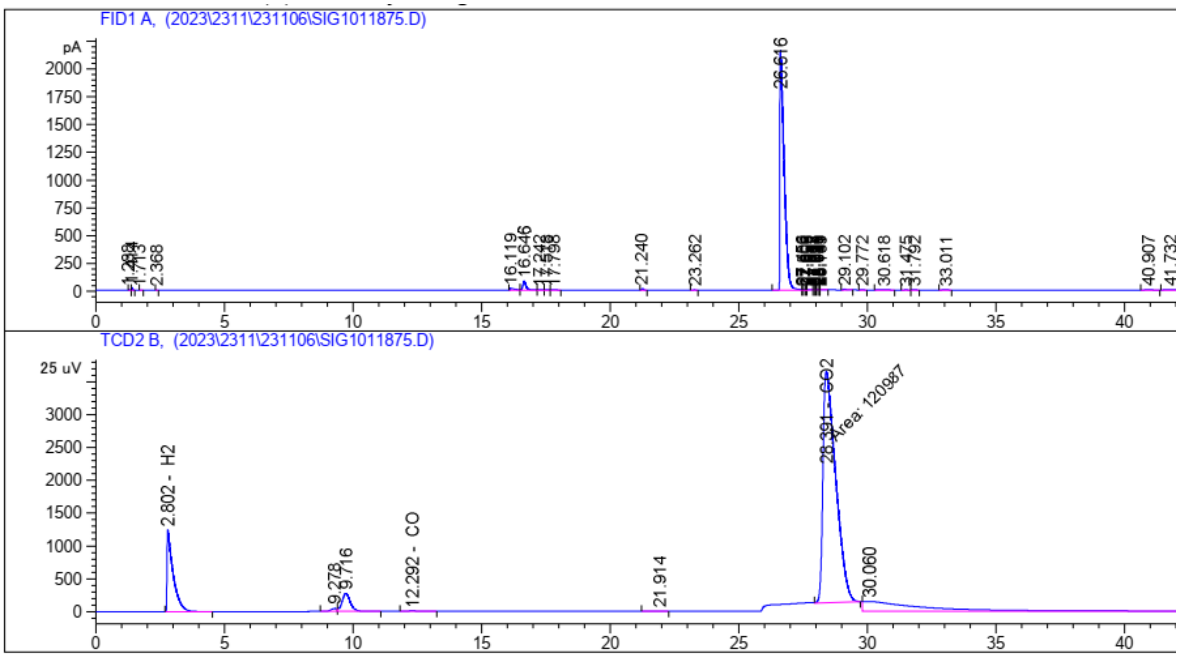


Figure A-20. Representative ^{1}H NMR spectrum (in D_2O) obtained after hydrogenation of captured CO_2 to formate. Reproduced from ref.[133]



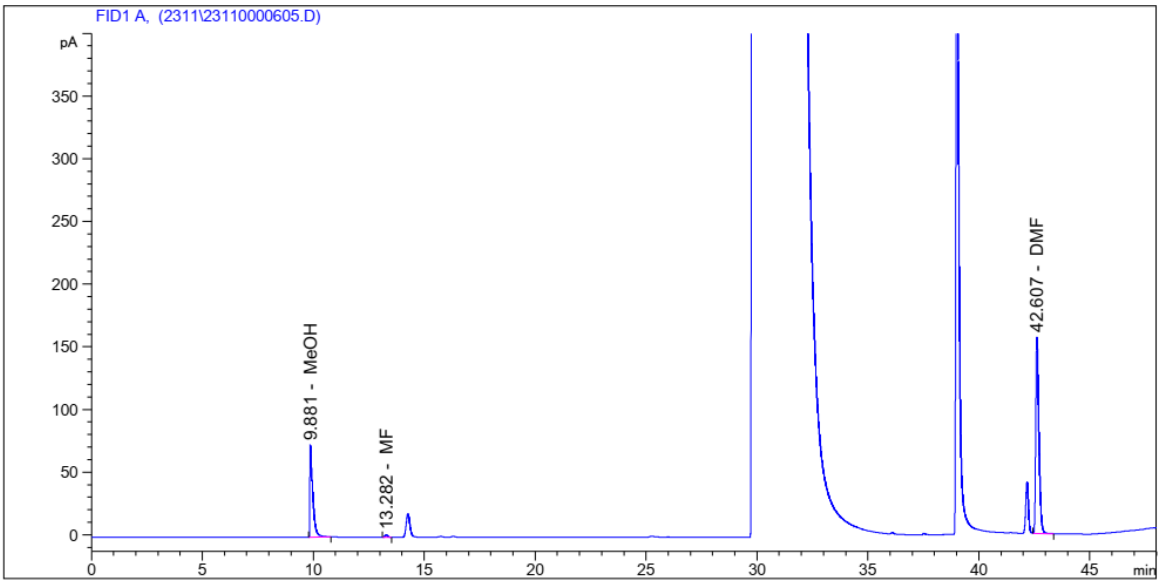

```
=====================================================================
                    External Standard Report
=====================================================================

Sorted By             :      Retention Time
Calib. Data Modified  :      11/16/2023 3:03:57 PM
Multiplier            :      1.0000
Dilution              :      1.0000
Use Multiplier & Dilution Factor with ISTDs

Signal 1: FID1 A,
Signal 2: TCD2 B,

RetTime Sig Type     Area      Amt/Area    Amount   Grp   Name
 [min]                                    [vol%]
-------|--|------|----------|----------|----------|--|---------------
  2.802  2 BB     2.01722e4  4.26053e-3   85.94439    H2
  8.050  2           -          -          -         Ar
 12.292  2 BB      218.22815 1.96302e-4 4.28386e-2    CO
 21.000  2           -          -          -         CH4
 28.391  2 MM     1.20987e5  1.51298e-4   18.30513    CO2
```

Figure A-21. Typical GC chromatogram of a gaseous sample for gas content quantification. Reproduced from ref.[177]




```
======================================================================
                    Internal Standard Report
======================================================================

Sorted By             :      Signal
Calib. Data Modified  :      11/2/2023 9:35:49 AM
Multiplier            :      1.0000
Dilution              :      1.0000
Use Multiplier & Dilution Factor with ISTDs
Sample ISTD Information:
ISTD  ISTD Amount   Name
  #     [µmol]
----|-------------|-------------------------
  1   2600.00000   DMF

Signal 1: FID1 A,

RetTime  Type  ISTD    Area     Amt/Area    Amount   Grp   Name
 [min]         used  [pA*s]      ratio      [µmol]
-------|------|----|----------|----------|----------|--|------------------
  9.881 BB        1  610.41888    2.34367 2414.88726    MeOH
 13.282 BB        1   17.58698    1.84273   54.70498    MF
 42.607 VB   I    1 1540.28333    1.00000 2600.00000    DMF

Totals without ISTD(s) :            2469.59224


======================================================================
                         *** End of Report ***
```

Figure A-22. GC of liquid organic part after hydrogenation of CO_2. Reproduced from ref.[177]

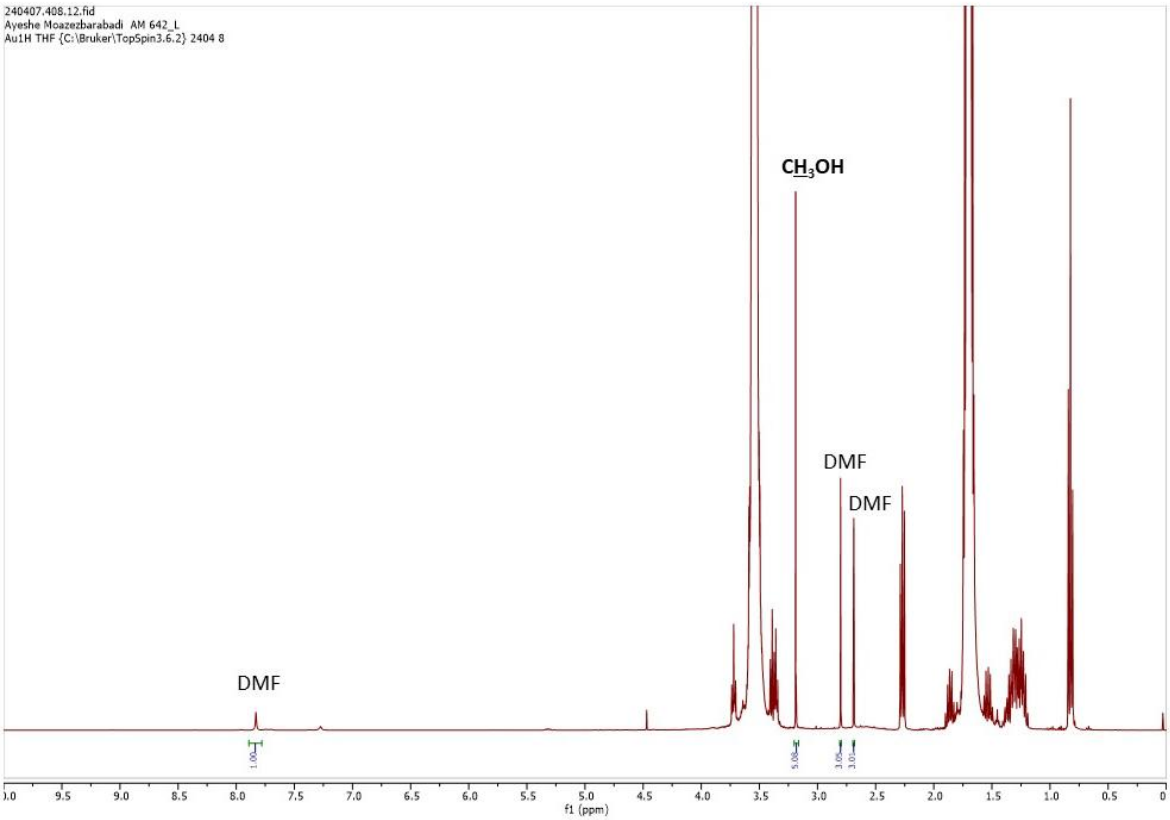


Figure A-23. Representative ^{1}H NMR spectrum of the post-reaction organic solution. Reproduced from ref.[177]

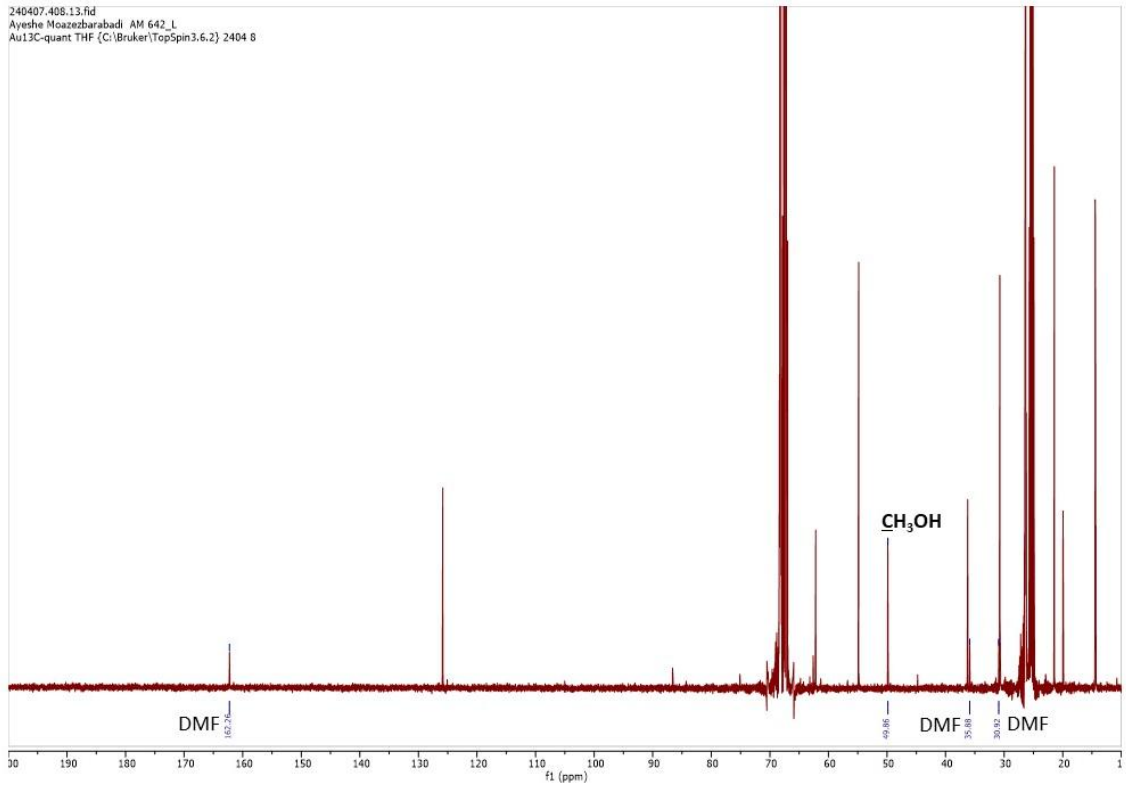


Figure A-24. Representative ^{13}C NMR spectrum of the post-reaction organic solution. Reproduced from ref.[177]

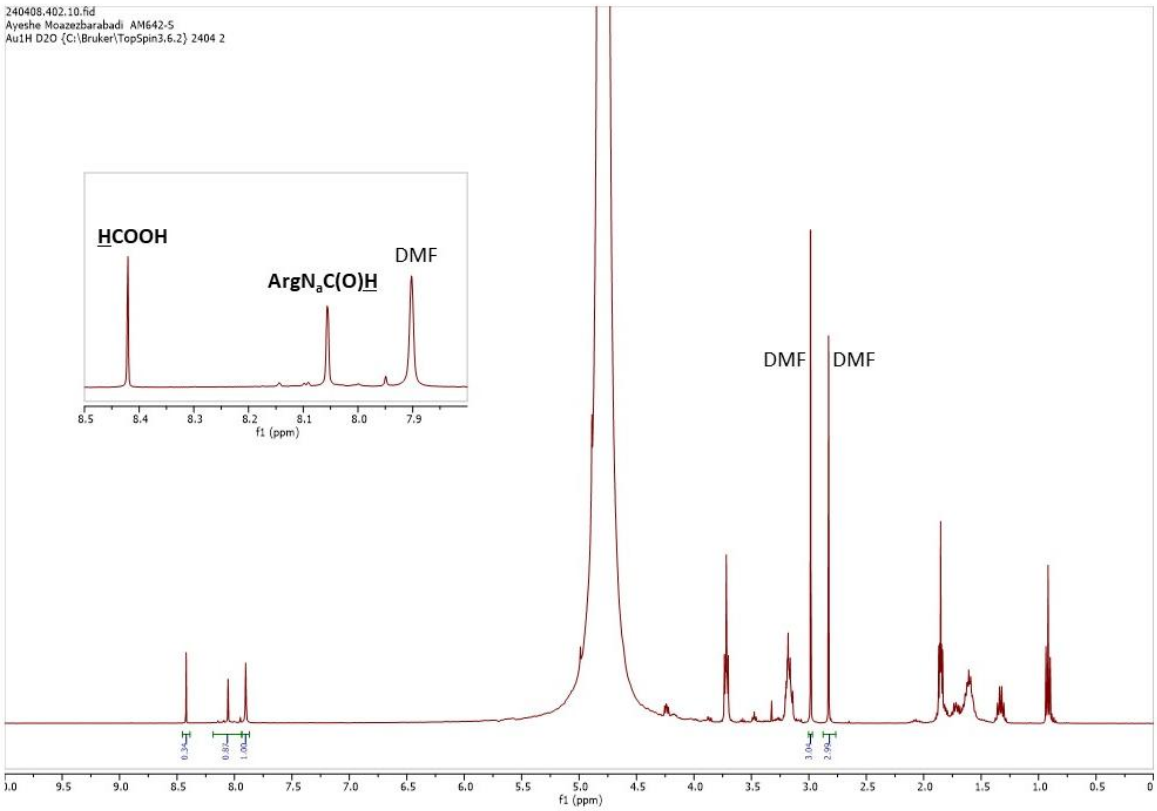


Figure A-25. Representative ^{1}H NMR spectrum of the post-reaction water-soluble residue.Reproduced from ref.[177]

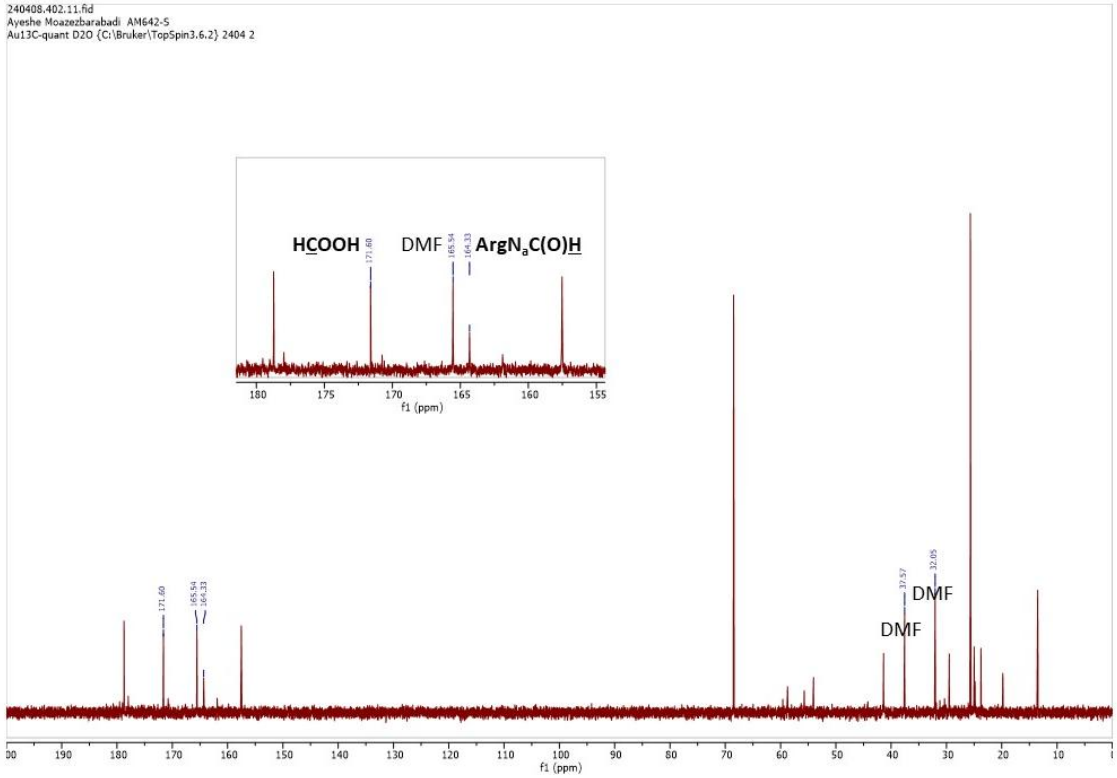


Figure A-26. Representative ^{13}C NMR spectrum of the post-reaction water-soluble residue. Reproduced from ref.[177]

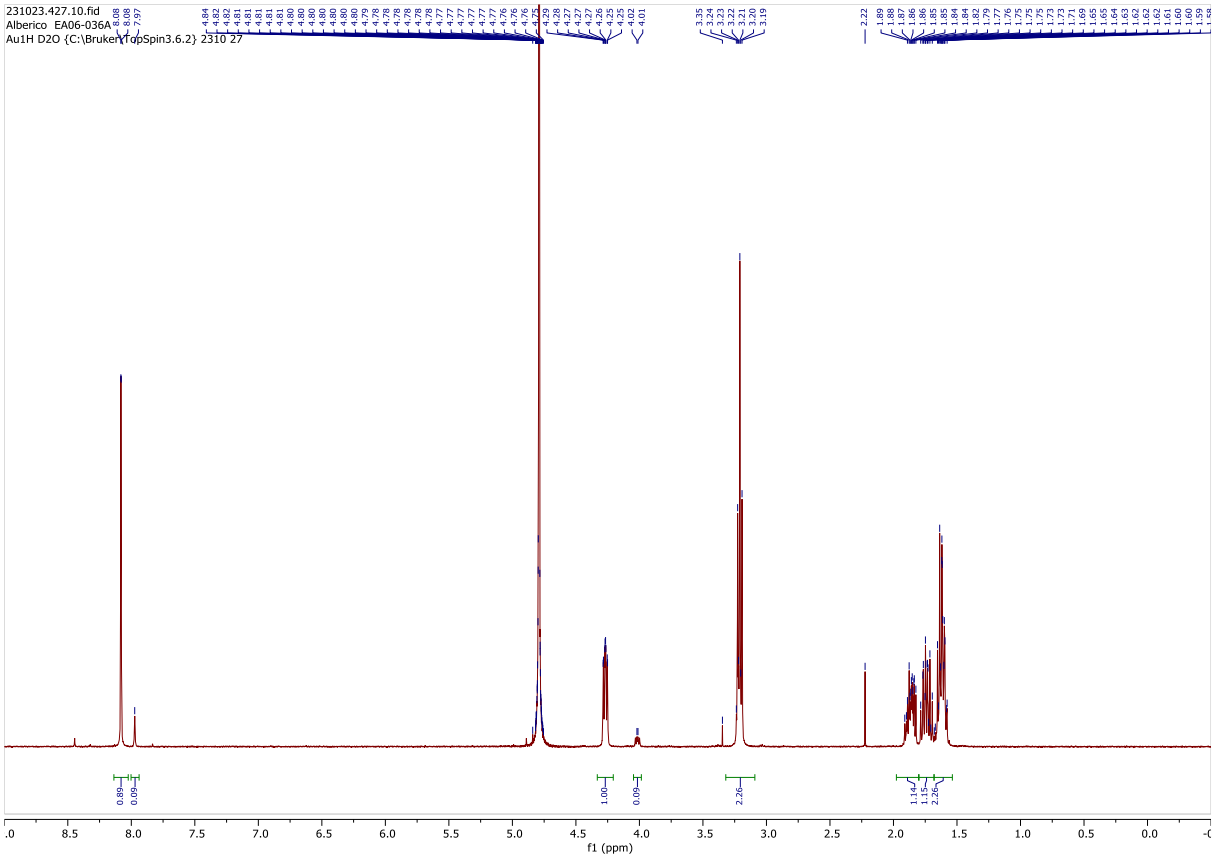


Figure A-27. ^{1}H NMR of N-α-formyl-L-Arginine in D_2O. Reproduced from ref.[177]

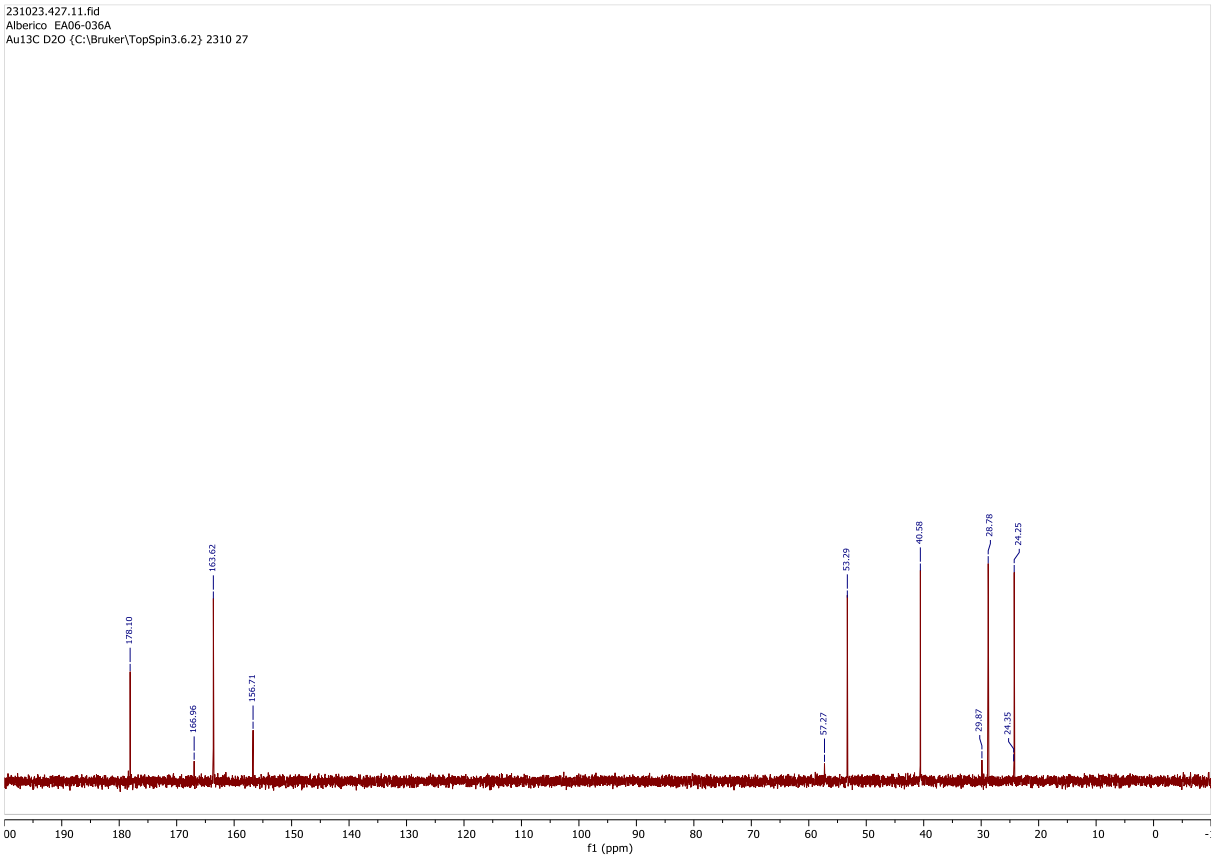


Figure A-28. ^{13}CNMR of N-α-formyl-L-Arginine in D_2O. Reproduced from ref.[177]

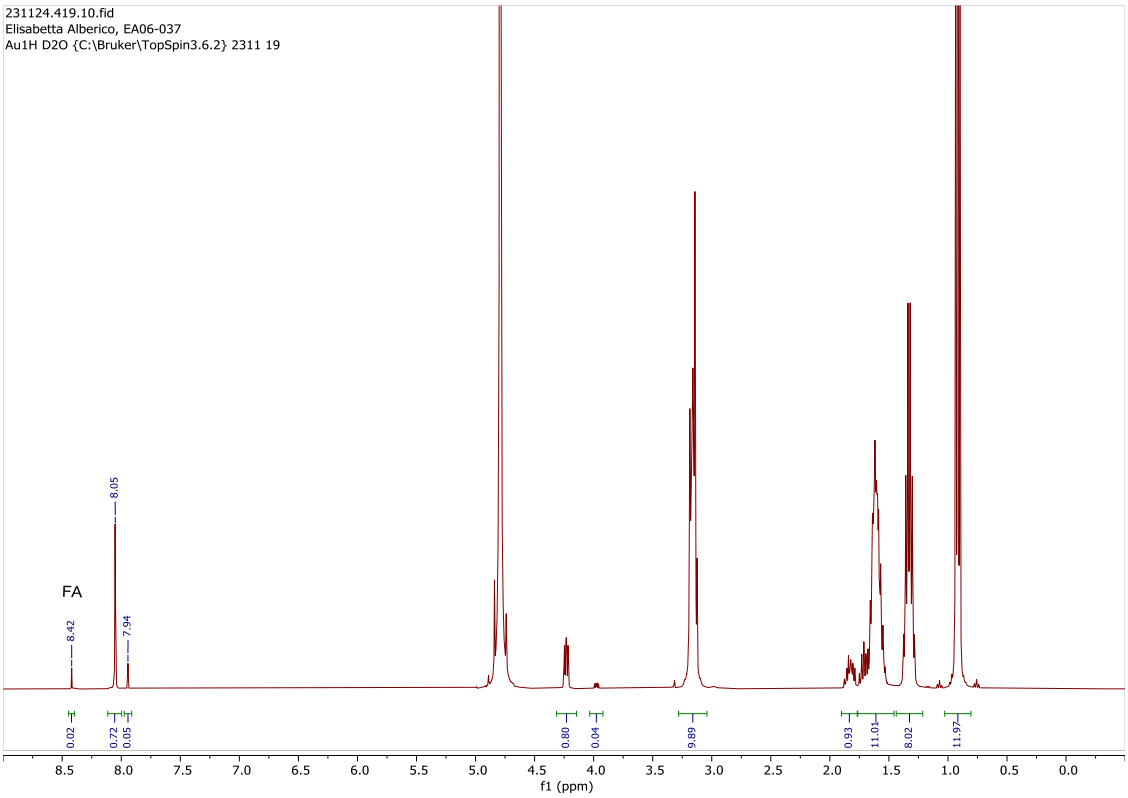


Figure A-29. ^{1}H NMR of N-α-formyl-L-Arginine NBu_4 in D_2O. Reproduced from ref.[177]

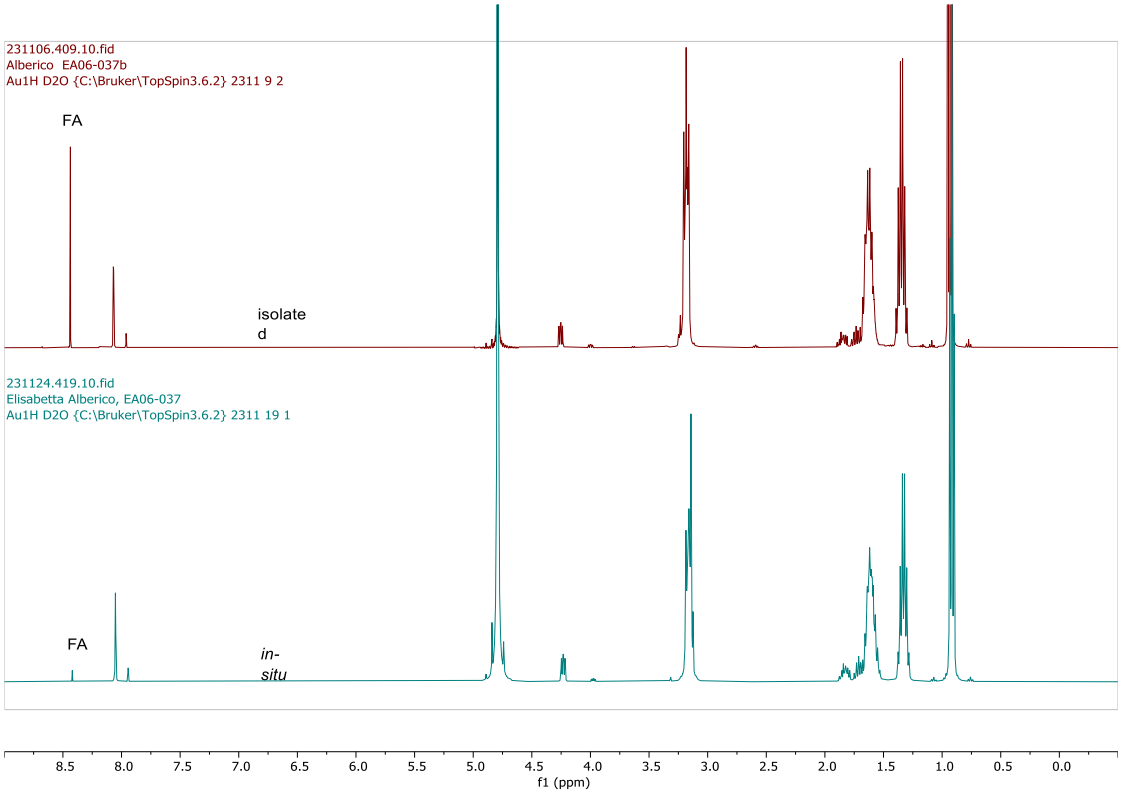


Figure A-30. Comparison of the ^{1}H spectra of the *in situ* (non-isolated) N-α-formyl-L-arginine·NBu_4 with the isolated product, recorded in D_2O. Reproduced from ref.[177]

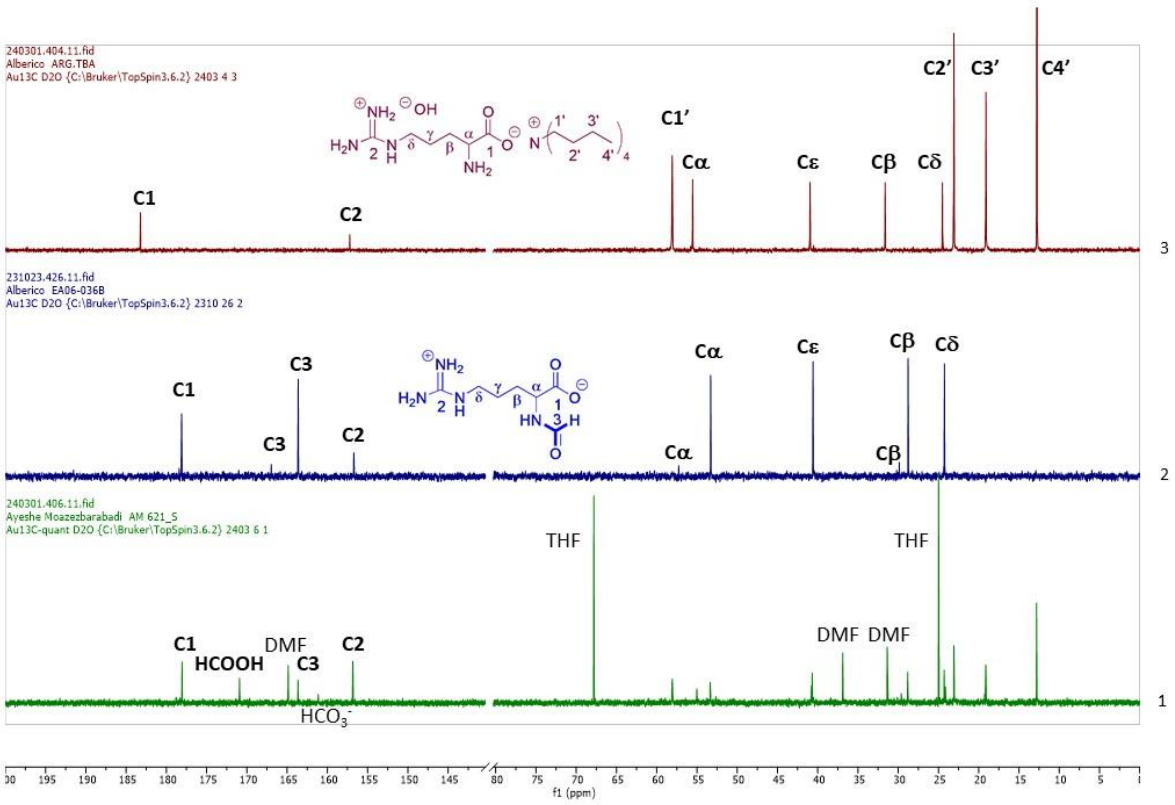


Figure A-31. Comparison of ^{13}C NMR spectrum of TBA·Arg. (spectrum 3) with N-α-formyl-L-arginine (spectrum 2) and the water soluble residue (spectrum 1) obtained after **Ru-1** catalyzed CO_2 hydrogenation in the presence of TBA·Arg. Reproduced from ref.[177]

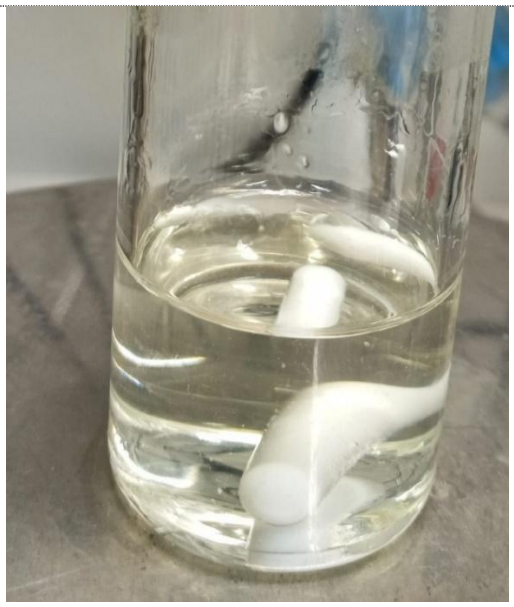
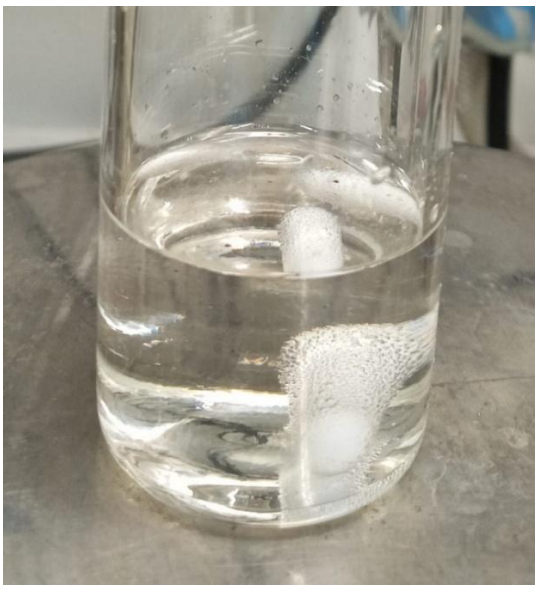
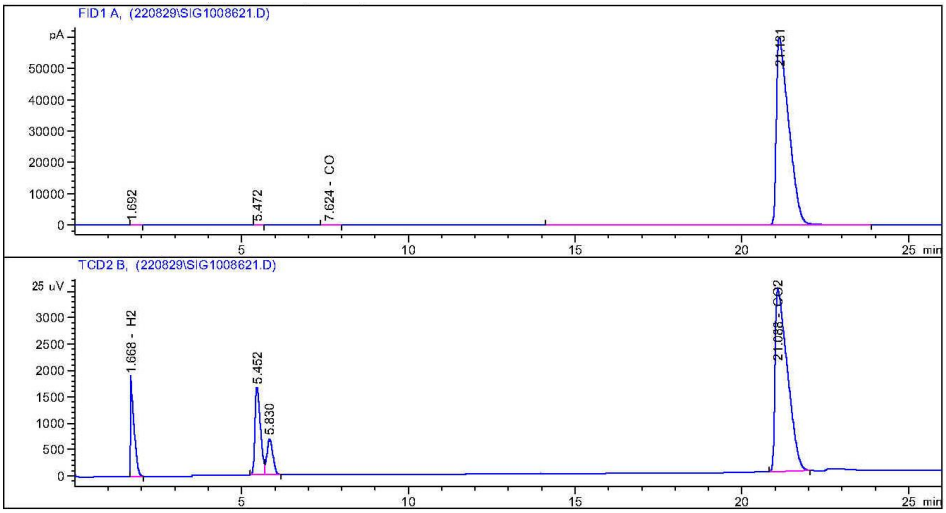
Before reaction (one-phase)	After reaction (one-phase)
	

Figure A-32. Representative appearance of the reaction mixture before and after CO_2 hydrogenation to formate using [TBA][Arg] as absorbent.Reproduced from ref.[133]




```
======================================================================
          External Standard Report (Sample Amount is 0!)
======================================================================

Sorted By             :      Signal
Calib. Data Modified  :      Monday, July 11, 2022 4:03:58 PM
Multiplier            :      1.0000
Dilution              :      1.0000
Use Multiplier & Dilution Factor with ISTDs

Signal 1: FID1 A,

RetTime  Type     Area     Amt/Area    Amount   Grp   Name
 [min]          [pA*s]                [Vol. %]
-------|------|----------|----------|----------|--|------------------
  7.624 BB        6.78681 1.45690e-5 9.88767e-5    CO
 14.496            -          -          -         CH4
 21.674            -          -          -         CO2

Totals :                              9.88767e-5



 Data File C:\CHEM32\1\DATA\220829\SIG1008621.D
 Sample Name: am368


     Signal 2: TCD2 B,

     RetTime  Type     Area     Amt/Area    Amount   Grp   Name
      [min]         [25 uV*s]              [Vol. %]
     -------|------|----------|----------|----------|--|------------------
       1.668 BB S   1.37790e4  4.74460e-3   65.37577    H2
       4.878            -          -          -         Ar/N2+O2
       7.644            -          -          -         CO
      14.476            -          -          -         CH4
      21.088 BB     8.87016e4  2.50409e-4   22.21166    CO2

     Totals :                              87.58743

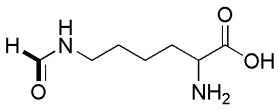

     1 Warnings or Errors :

     Warning : Calibrated compound(s) not found

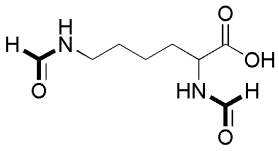
     ======================================================================
                              *** End of Report ***
```

Figure A-33. Typical GC chromatogram of a gaseous sample obtained from the hydrogenation of CO_2 to formate in the presence of [TBA][Arg] at 80 °C. The analysis was carried out using a system equipped with a Carboxen column, TCD, methanizer, and FID, with helium as the carrier gas. Gas quantification was calibrated using certified gas mixtures from Linde and Air

Liquide. The detected CO amount (< 1 µmol) is attributed to minor catalyst degradation or side reactions. Reproduced from ref.[133]



$[M-H]^-$	173.09262
[M]	174.10044
$[M+H]^+$	175.10827



$[M-H]^-$	201.08753
[M]	202.09536
$[M+H]^+$	203.10318

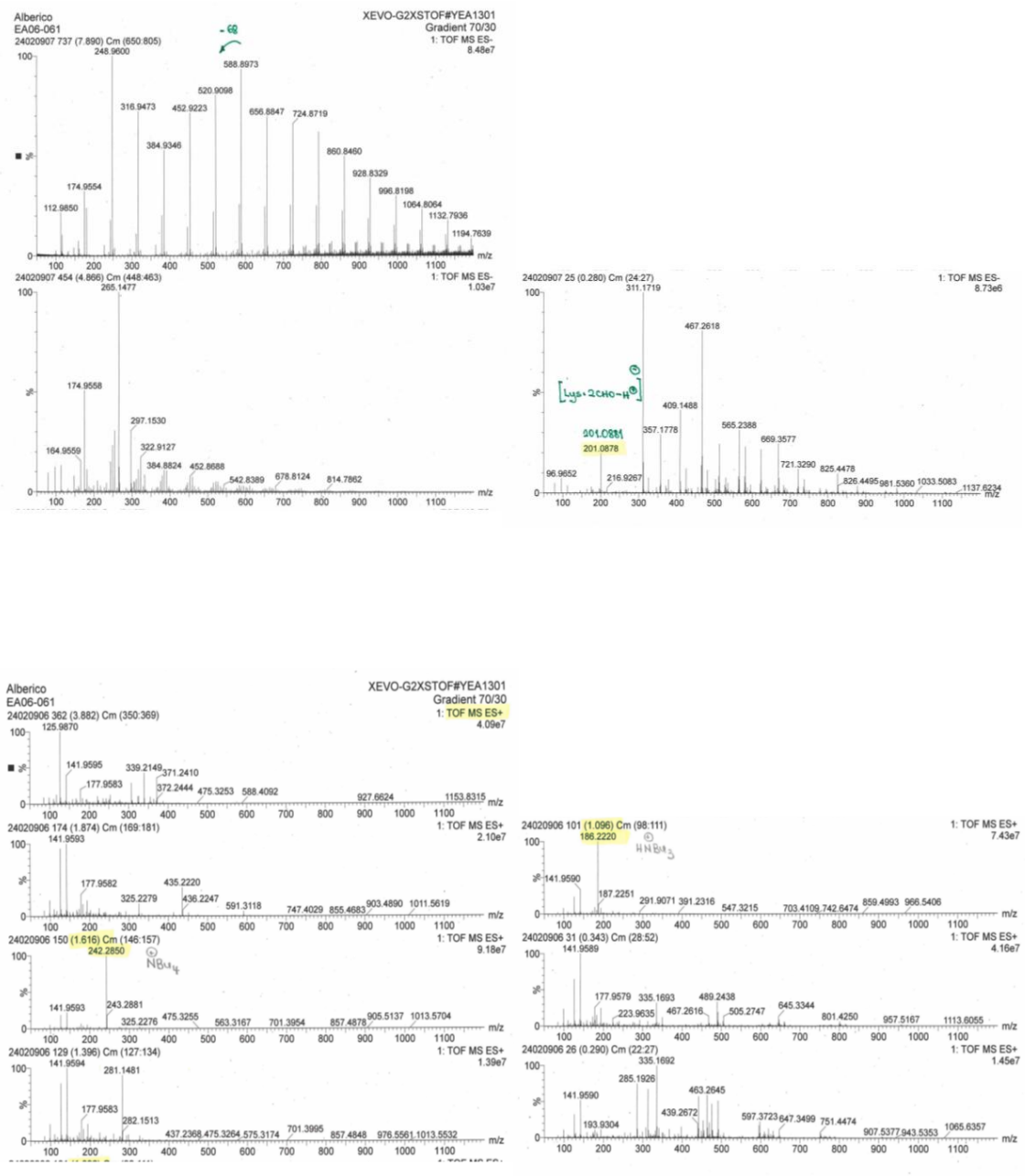
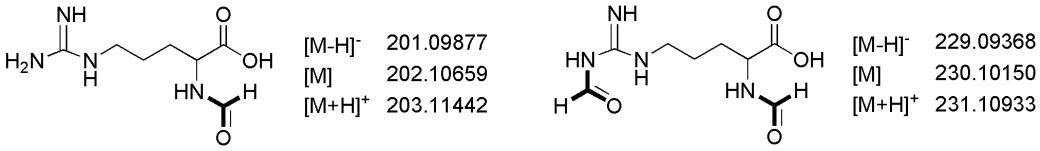


Figure A-34. High-resolution mass spectrum (HRMS) of the post-reaction water-soluble residue obtained after CO_2 hydrogenation in the presence of [TBA][Lys].Reproduced from ref.[177]



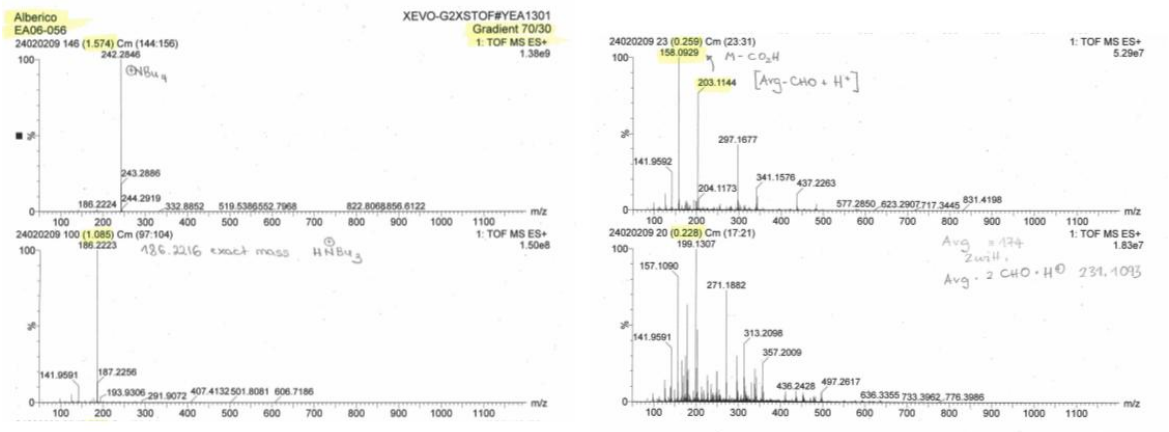


Figure A-35. HRMS of the post-reaction water-soluble residue obtained from CO_2 hydrogenation hydrogenation in the presence of TBA·Arg. Reproduced from ref.[177]

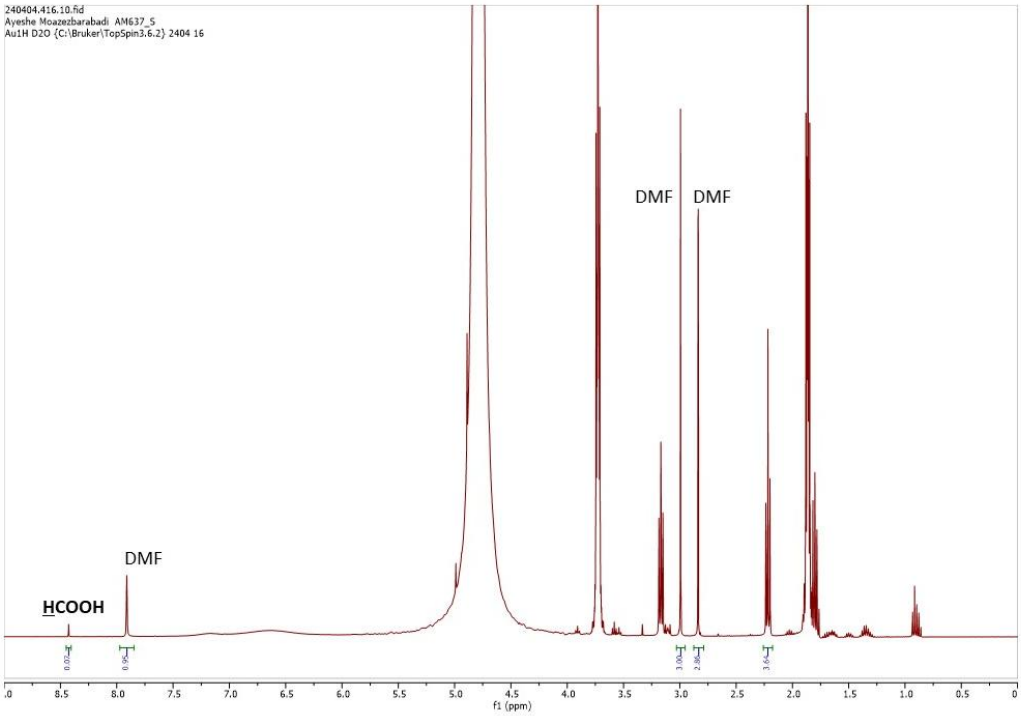


Figure A-36. ^{1}H NMR spectrum of the water-soluble residue obtained after Ru-1–catalyzed CO_2 hydrogenation in the presence of [TBA][GB].Reproduced from ref.[177]

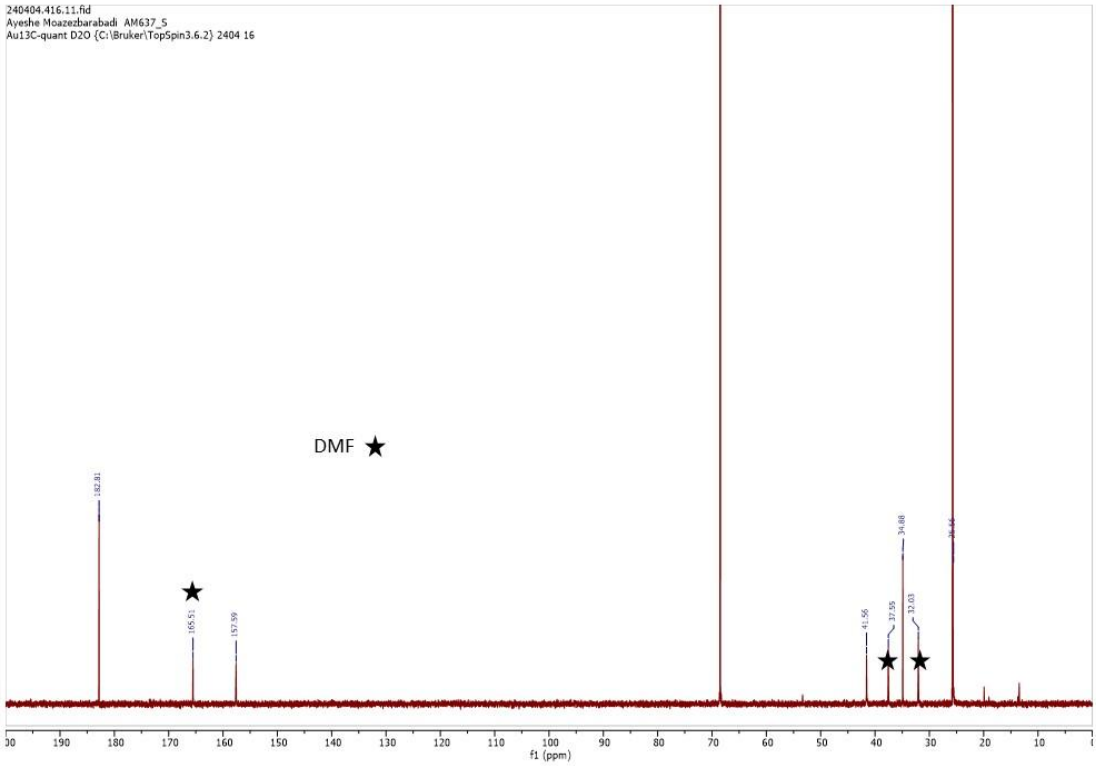


Figure A-37. ^{13}C NMR spectrum of the water soluble residue obtained after **Ru-1** catalyzed CO_2 hydrogenation in the presence of TBA·GB. Reproduced from ref.[177]

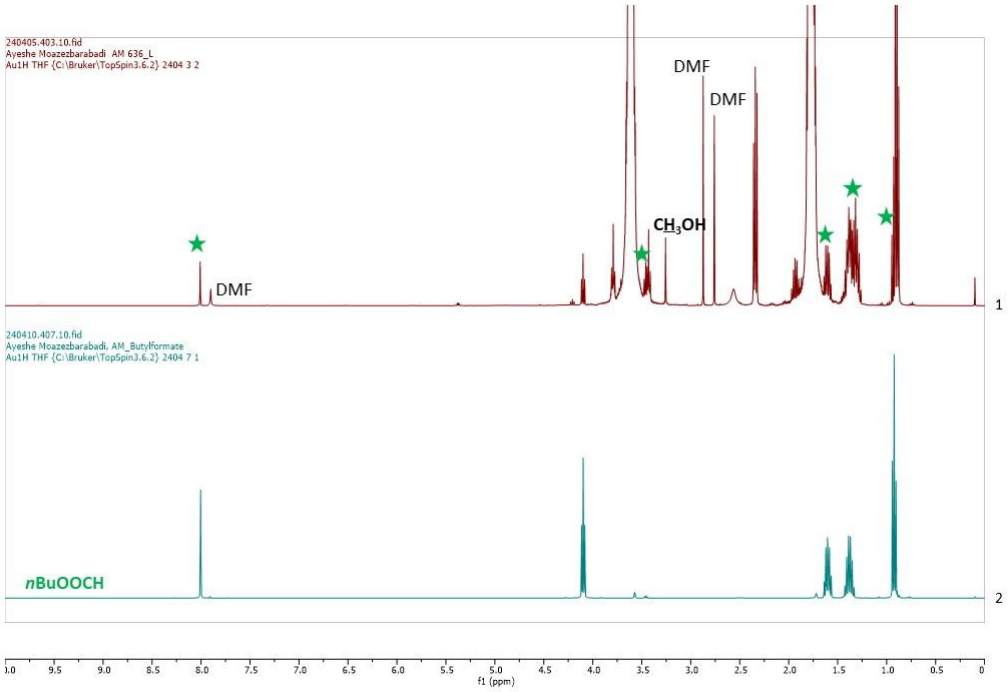


Figure A-38. ^{1}H NMR spectrum of the THF post-reaction solution (1) obtained after Ru-1–catalyzed CO_2 hydrogenation in the presence of [TBA][GB]. Comparison with the reference

spectrum of n-butyl formate (2) confirms that this compound was also formed during the reaction.Reproduced from ref.[177]

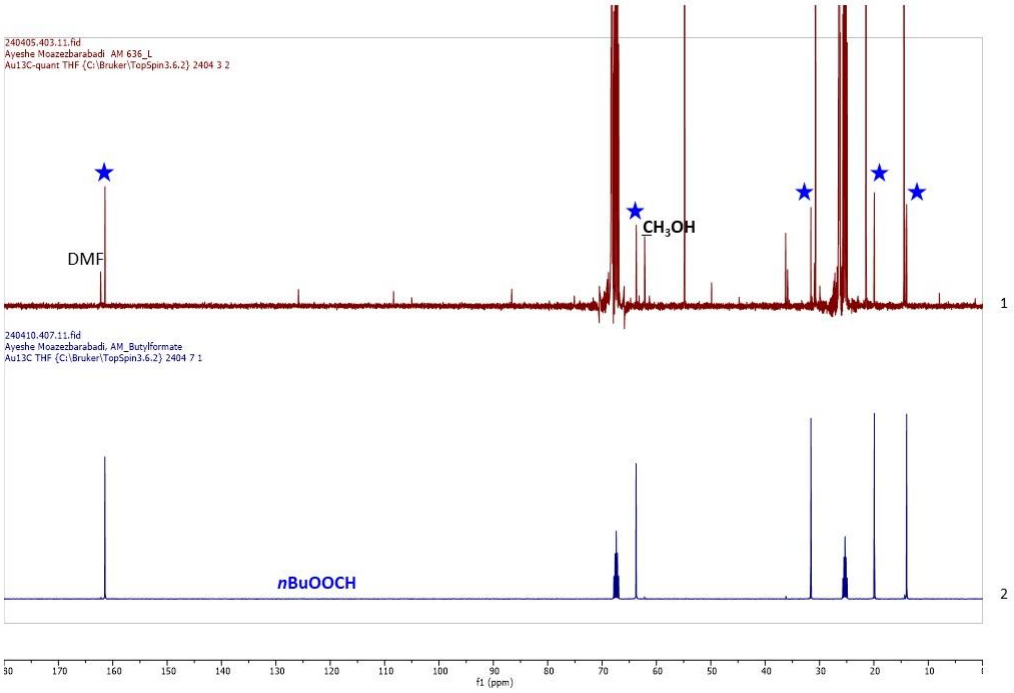


Figure A-39. ^{13}C NMR spectrum of the THF post-reaction solution (1) obtained after Ru-1-catalyzed CO_2 hydrogenation in the presence of [TBA][GB]. The comparison with the reference spectrum of *n*-butyl formate (2) confirms that this compound was also generated during the reaction. Reproduced from ref.[177]

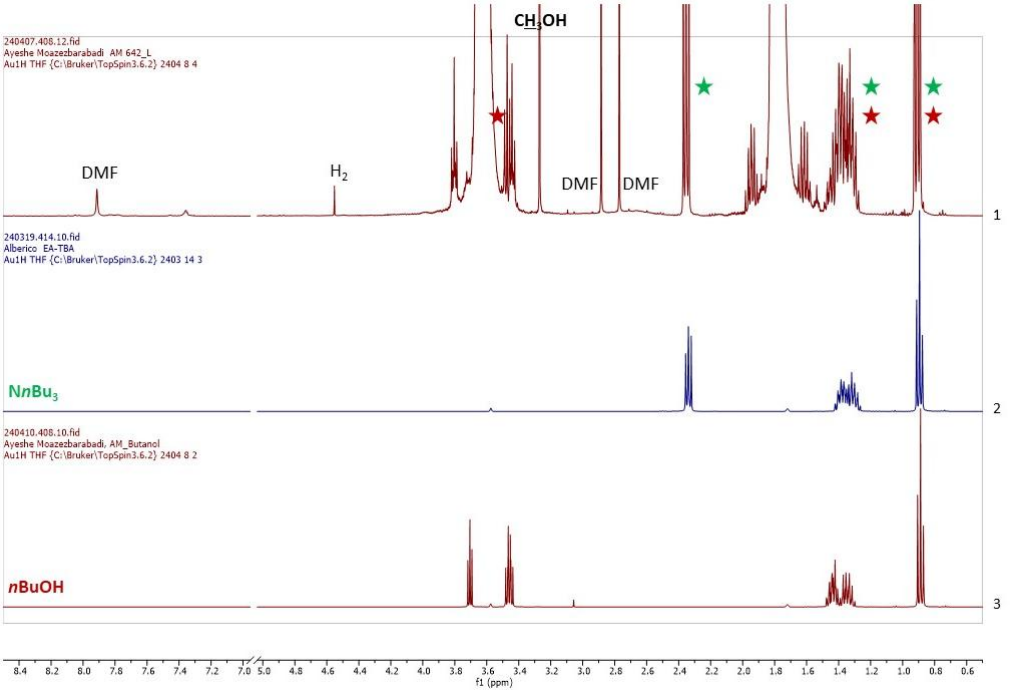


Figure A-40. ^{1}H NMR representative spectrum of the post-reaction THF solution (1) obtained after CO_2 hydrogenation to methanol in the presence of [TBA][Arg], and comparison with the spectra of $NnBu_3$ (2) and nBuOH (3) in THF-d_8.Reproduced from ref.[177]

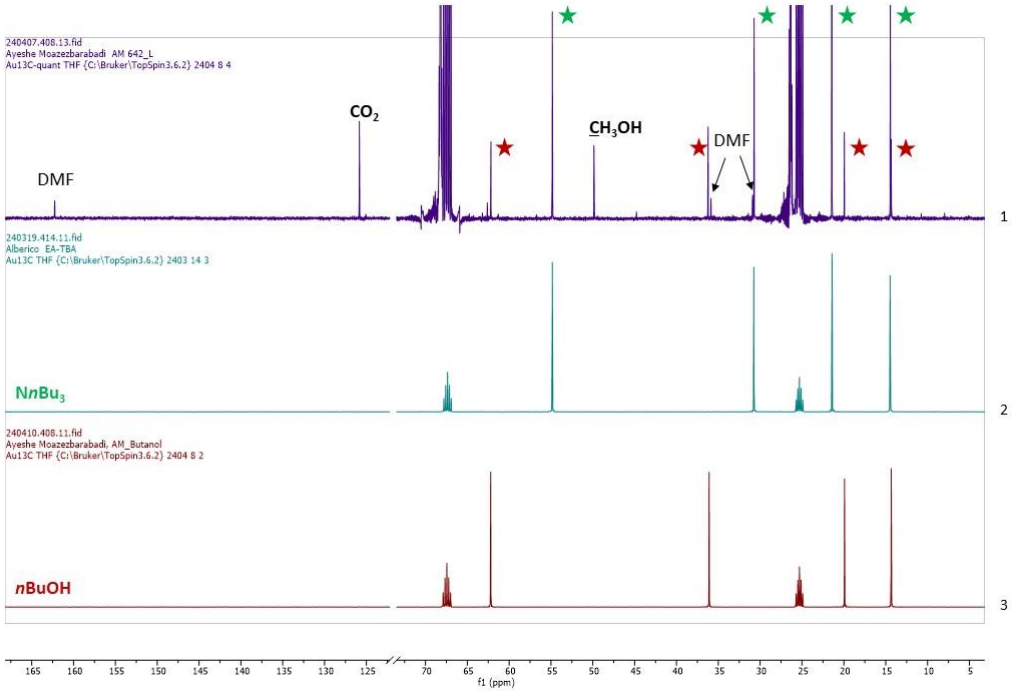


Figure A-41. ^{13}C NMR representative spectrum of the post-reaction THF solution (1) obtained after CO_2 hydrogenation to methanol in the presence of [TBA][Arg], and comparison with the spectra of $NnBu_3$ (2) and nBuOH (3) in THF-d_8. Reproduced from ref.[177]

8. Publications

Publications based on the work of this thesis:

1. Moazezbarabadi, A., Wei, D., Junge, H., & Beller, M. (**2022**). Improved CO_2 capture and catalytic hydrogenation using amino acid based ionic liquids. *ChemSusChem*, *15*(23), e202201502.
   DOI: https://doi.org/10.1002/cssc.202201502

2. Moazezbarabadi, A., Kammer, A., Alberico, E., Junge, H., & Beller, M. (**2024).** Amino Acid-Based Ionic Liquids-Aided CO_2 Hydrogenation to Methanol. *ChemSusChem*, e202401813.
   DOI: https://doi.org/10.1002/cssc.202401813

Further publications:

1. Wei, D., Sang, R., Moazezbarabadi, A., Junge, H., & Beller, M. (**2022**). Homogeneous carbon capture and catalytic hydrogenation: toward a chemical hydrogen battery system. *JACS Au*, *2*(5), 1020-1031.

   DOI: https://doi.org/10.1021/jacsau.1c00489

2. Wei, D., Kotwica, D., Nardi, G., Moazezbarabadi, A., Spannenberg, A., Ludwig, R.& Beller, M. (**2023**). A lysine-based system for CO_2 capture and catalytic utilization to produce formates: irreproducibility and conflicting reactivity. *ChemistrySelect*, *8*(32), e202302307.

   DOI: https://doi.org/10.1002/slct.20230230

3. Moazezbarabadi, A., Junge, H., & Beller, M. (**2025**). Formic Acid and Formates as CO_2-Based Green Intermediates: Production via CO_2 hydrogenation and their applications in organic synthesis (a mini-review). Manuscript in preparation.

9. Curriculum Vitae

Ayeshe Moazezbarabadi

Contact Information

Personal address: Wismarsche Strasse 72, 18057. Rostock
Work Address: Leibniz-Institut für Katalyse e. V.
Albert-Einstein-Straße 29a, 18059, Rostock
Mobile number: +49 (0)15118689449
E-mail address: ayeshe.moazez71@gmail.com
Date of Birth: February 4th 1991



Education

2021-present. Ph.D. (CO_2 capture and subsequent conversion), LIKAT, Rostock, Germany
Topic: "CO_2 capture using Amino Acid-based ionic liquids and subsequent hydrogenation to Formate and Methanol"

2015-2018 M. Sc. (Inorganic Chemistry), Universisty of Tehran, Iran.
GPA: 3.86 / 4
Graduation date: October 10th 2018
M. Sc. Thesis: "Synthesis of Carboxamide (Cu(II), Ni(II)) complexes using Green chemistry method and study of their electrocatalysis activity in CO_2 Reduction ; study of Spectroscopic and flourimetric properties of unsymmetrical imine ligands"

2012-2016 B. S. (Pure Chemistry), University of Zabol. Iran.
GPA: 3.74 /4.
Graduation date: June 30 2015

Work Experience

- Ph.D. position in the group Applied Homogeneous Catalysis. Research topic: CO_2 capture using Amino Acid-based ionic liquids and subsequent hydrogenation to Formate and Methanol. Leibniz Institute for Catalysis, Rostock, Germany, 2021-2024.
- Bicarbonate Hydrogenation to formate using heterogeneous catalysis. Apex Energy GmbH, Rostock, Germany, June 2024-October 2024
- Synthesis of M(II) and M(III) metal complexes driven by imine, carboxamide ligands and the study of their electrochemical and electrocatalytic activity in CO_2 reduction. Universisty of Tehran, Iran. 2015-2018.

Conferences and presentations

2023. Poster Presentation **57. Jahrestreffen Deutscher Katalytiker.** Weimar, 14th–16th March. “Improved CO_2 capture and catalytic hydrogenation using amino acid based ionic liquids”

2017. Seminar, Topics in Inorganic Chemistry: University of Tehran, “Single-molecule magnetism” Tehran, Iran, Feb. 2017

Academic activities

- Teaching spectroscopy application in organic chemistry for chemistry major, Zabol, Iran. 2014-2015
- Teaching advanced inorganic chemistry for inorganic chemistry major,Tehran, Iran. 2016-2017

Languages

- Persian (native)
- English (Advanced)
- Deutsch (B2 level): I am upgrading the language.

Publications

- Improved CO_2 capture and catalytic hydrogenation using amino acid based ionic liquids." ChemSusChem (2022).
- “Homogeneous Carbon Capture and Catalytic Hydrogenation: Toward a Chemical Hydrogen Battery System ”. JACS Au 2022.
- “A Lysine-Based System for CO_2 Capture and Catalytic Utilization to Produce Formates: Irreproducibility and Conflicting Reactivity“. Chemistry Select 2023.
- “Amino Acid-Based Ionic Liquids-Aided CO_2 Hydrogenation to Methanol “. ChemSusChem, 2024.
- Formic Acid and Formates as CO_2-Based Green Intermediates: Production via CO_2 hydrogenation and their applications in organic synthesis (a mini-review). Manuscript in preparation.